

AD-A128 497

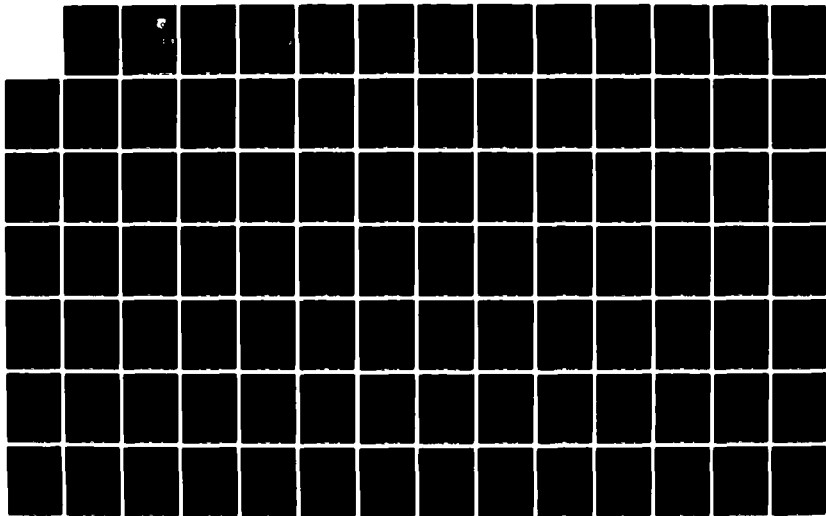
ELEMENTS OF SIMULATION ERROR ANALYSIS(U) SYSTEMS
TECHNOLOGY INC HAWTHORNE CA R F WHITBECK JUN 82
TR-1173-1 AFWAL-TR-82-3022 F33615-81-C-3606

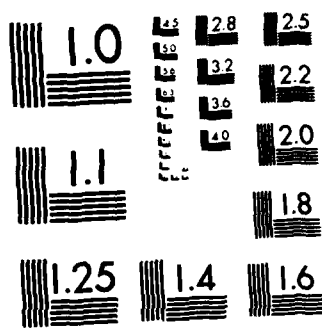
1/2

UNCLASSIFIED

F/G 12/1

NL





MICROCOPY RESOLUTION TEST CHART
NATIONAL BUREAU OF STANDARDS-1963-A

2

AFWAL-TR-82-3022

ELEMENTS OF SIMULATION ERROR ANALYSIS



Richard F. Whitbeck

Systems Technology, Inc.
1377 S. Hawthorne Blvd.
Hawthorne, CA 90250

June 1982

Final Report for Period 2 Mar 1981-22 Feb 1982

DTIC
ELECTE
MAY 25 1983
S H D

Approved for public release; distribution unlimited.

FLIGHT DYNAMICS LABORATORY
AIR FORCE WRIGHT AERONAUTICAL LABORATORIES
AIR FORCE SYSTEMS COMMAND
WRIGHT-PATTERSON AIR FORCE BASE, OHIO 45433

83 05 25 027

AD A128497

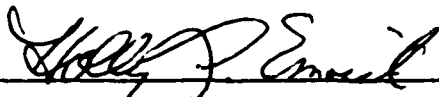
DTIC FILE COPY

NOTICE

When Government drawings, specifications, or other data are used for any purpose other than in connection with a definitely related Government procurement operation, the United States Government thereby incurs no responsibility nor any obligation whatsoever; and the fact that the government may have formulated, furnished, or in any way supplied the said drawings, specifications, or other data, is not to be regarded by implication or otherwise as in any manner licensing the holder or any other person or corporation, or conveying any rights or permission to manufacture use, or sell any patented invention that may in any way be related thereto.

This report has been reviewed by the Office of Public Affairs (ASD/PA) and is releasable to the National Technical Information Service (NTIS). At NTIS, it will be available to the general public, including foreign nations.

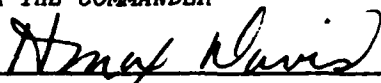
This technical report has been reviewed and is approved for publication.



HOLLY L. EMRICK, 1Lt, USAF
Project Engineer
Control Dynamics Branch
FOR THE COMMANDER



RONALD O. ANDERSON, Chief
Control Dynamics Branch
Flight Control Division



H. MAX DAVIS
Assistant Chief
Flight Control Division

"If your address has changed, if you wish to be removed from our mailing list, or if the addressee is no longer employed by your organization please notify AFWAL/FIGC, W-PAFB, OH 45433 to help us maintain a current mailing list".

Copies of this report should not be returned unless return is required by security considerations, contractual obligations, or notice on a specific document.

REPORT DOCUMENTATION PAGE		READ INSTRUCTIONS BEFORE COMPLETING FORM
1. REPORT NUMBER AFWAL-TR-82-3022	2. GOVT ACCESSION NO. A128497	3. RECIPIENT'S CATALOG NUMBER
4. TITLE (and Subtitle) Elements of Simulation Error Analysis	5. TYPE OF REPORT & PERIOD COVERED Final Report 2 Mar 81 - 22 Feb 82	
7. AUTHOR(s) Richard F. Whitbeck	6. PERFORMING ORG. REPORT NUMBER TR-1173-1	
9. PERFORMING ORGANIZATION NAME AND ADDRESS Systems Technology, Inc. 13766 S. Hawthorne Blvd. Hawthorne, CA 90250	8. CONTRACT OR GRANT NUMBER(s) F33615-81-C-3606	
11. CONTROLLING OFFICE NAME AND ADDRESS Flight Dynamics Laboratory, (AFWAL/FIGC) AF Wright Aeronautical Laboratories, AFSC Wright-Patterson Air Force Base, OH 45433	10. PROGRAM ELEMENT, PROJECT, TASK AREA & WORK UNIT NUMBERS PE 61102F, Project 2304, Math. Task N3, Math of Flt Control WU 18	
14. MONITORING AGENCY NAME & ADDRESS (if different from Controlling Office)	12. REPORT DATE June 1982	
	13. NUMBER OF PAGES	
	15. SECURITY CLASS. (of this report) Unclassified	
	15a. DECLASSIFICATION DOWNGRADING SCHEDULE	
16. DISTRIBUTION STATEMENT (of this Report) Approved for public release; distribution unlimited.		
17. DISTRIBUTION STATEMENT (of the abstract entered in Block 20, if different from Report)		
18. SUPPLEMENTARY NOTES The algorithms contained in this technical report are theoretical and in no way reflects any Air Force owned software programs.		
19. KEY WORDS (Continue on reverse side if necessary and identify by block number) Digital Control Systems Switch Decomposition Aliasing Sampled Data Linear Systems z-Transforms Simulation Error Analysis Multi-Rate Sampling Sklansky's Identity Frequency Response Data Holds		
20. ABSTRACT (Continue on reverse side if necessary and identify by block number) The past decade has seen an order-of-magnitude increase in reliance on fixed and moving based digital simulation for research and training in all types of aircraft. Along with this increase there has been a growing need to identify and analyze those anomalies introduced by digital computation which can adversely affect the fidelity of a simulation. Those anomalies arise for a variety of reasons, the most important being: 1) two or more computers required in a large simulation, each working in its own frametime, 2) serial processing (continued)		

DTIC
C O U N T E
MAY 25 1983
D
H

Unclassified

SECURITY CLASSIFICATION OF THIS PAGE (When Data Entered)

(calling) of subroutines which can cause skewed or stale data effects, 3) throughput delays, and 4) effects of various integration algorithms.

This report develops several key tools useful for the analysis of computer algorithms working in a skewed data, multi-rate environment and thus makes it possible to analytically investigate the anomalies mentioned above. Toward this end, numerous case studies, based upon existing computer simulations, are presented which specifically treat the independent processor problem and the unintentional filtering introduced by the serial call of subroutines.

Accession For	
NTIS	<input checked="checked" type="checkbox"/>
DTIC	<input type="checkbox"/>
Uncl	<input type="checkbox"/>
Just	<input type="checkbox"/>
By _____	
Distribution/	
Avail	ality Cards
	and/or
Dist	erial
A	

DTIC
COPY
DELETED
2

Unclassified

SECURITY CLASSIFICATION OF THIS PAGE(When Data Entered)

FOREWORD

The research described in this report was performed by Systems Technology, Inc., Hawthorne, California, under Air Force Contract F33615-81-C-3606. The Task Number N3, Mathematics of Flight Control, was under Project Number 2304, Mathematics. This work was directed by the Control Dynamics Branch, Flight Control Division, Flight Dynamics Laboratory, Air Force Wright Aeronautical Laboratories, Air Force Systems Command, Wright-Patterson Air Force Base, Ohio. The work was administered by Lt. Holly Emrick.

Richard F. Whitbeck was the Systems Technology Project Engineer, under the direction of Duane McRuer.

The author wishes to express his appreciation to the Systems Technology publication staff for their efforts in preparing this lengthy report.

The author also wishes to express his thanks to Dr. James C. Smith of Systems Technology for his appreciable efforts on the refinement of root-finding algorithms as they pertain to z -plane zeros clustered close to the unit circle.

This report covers work performed from March 1981 through 22 February 1982. The report was submitted by the authors in February 1982.

TABLE OF CONTENTS

	<u>Page</u>
I. INTRODUCTION.....	1
II. DISTINCTIONS IN "FREQUENCY RESPONSE".....	6
A. Introduction.....	6
B. Frequency Response of a Sampled System.....	8
C. Continuous System Bode Plots.....	9
D. Mathematical Preliminaries.....	10
E. Open-Loop Frequency Response -- Finite N.....	13
F. Open Loop Frequency Response -- Continuous Output.....	22
G. Input Signal with Phase Shift.....	24
H. Single-Rate Closed-Loop Frequency.....	26
I. A Particular Two-Rate Configuration.....	31
J. Section Summary.....	38
III. VECTOR SWITCH DECOMPOSITION AND A "SCALAR" APPROACH.....	39
A. Introduction.....	39
B. Review of Switch Decomposition.....	39
C. Extension to the Vector Case.....	42
D. Nonsynchronous Sampling.....	47
E. Special Case.....	49
F. A Particular Three-Rate Closed-Loop System.....	51
G. Section Summary.....	54
IV. A USEFUL ALGORITHM FOR THE ANALYSIS OF MULTI-RATE CONTROLLERS.....	55
A. Introduction.....	55
B. An Important Identity.....	55
C. Outline of a New Procedure.....	58
D. Impulse Response Matching.....	59
E. Section Summary.....	65

	<u>Page</u>
V. MULTI-RATE FREQUENCY RESPONSE: SWITCH DECOMPOSITION CONTRASTED WITH SCALAR ANALYSIS.....	67
A. Introduction.....	67
B. Review of Multi-Rate Frequency Response, Switch Decomposition Model.....	67
C. A Closed-Loop Application.....	73
D. A Direct Approach.....	74
E. Section Summary.....	79
VI. SIMULATION MODELS.....	80
A. Introduction.....	80
B. Modeling a Buffer Register.....	80
C. Modeling Throughput Delay.....	82
D. Switch Decomposition Model.....	84
E. Time-Advanced Digital Filters.....	86
F. Difference Equations for Modeling an Integrator.....	89
G. Section Summary.....	90
VII. A T/2, T/3 CLOSED-LOOP SIMULATION CASE STUDY.....	92
A. Introduction.....	92
B. Problem Description.....	92
C. Decomposition of $G_1^{T/2}$ and $G_2^{T/3}$	98
D. Results.....	103
E. Introduction of Lightly Damped Modes.....	106
F. Section Summary.....	111
VIII. INTERPRETATION OF MULTI-RATE FREQUENCY RESPONSE.....	113
A. Introduction.....	113
B. A T/2 Input, T/3 Output Simulation Example.....	113
C. Switch Decomposition Development.....	120
D. Section Summary.....	121

	<u>Page</u>
IX. A THREE-RATE SIMULATOR CASE STUDY.....	122
A. Introduction.....	122
B. A Simplified Three-Rate Study and Associated Dimensional Difficulties.....	122
C. The A-10, Displayed Pitch to Pilot Stick Force Case Study.....	134
D. A-10 Switch Decomposition Model.....	139
E. Algebraic Manipulations.....	142
F. Comparison with Baseline.....	143
G. Summary and Conclusions.....	145
X. AN ORDER-OF-CALL CASE STUDY.....	146
A. Introduction.....	146
B. Description of Washout Computation.....	146
C. Third-Order Washout Case Study.....	148
D. Sixth-Order Washout Example.....	152
E. Summary and Conclusions.....	157
APPENDIX A. EXAMPLES DEMONSTRATING THE SETUP OF THE GENERALIZED SKIP-SAMPLING THEOREM.....	A-1
APPENDIX B. SKIP-SAMPLING THEOREM.....	B-1
APPENDIX C. A DIMENSIONALITY PROBLEM.....	C-1
APPENDIX D. s- AND z-DOMAIN A-10 TRANSFER FUNCTIONS.....	D-1
REFERENCES	R-1

LIST OF FIGURES

	<u>Page</u>
1. Single-Rate Digitally Controlled System.....	7
2. Step Response and Bode Plot.....	7
3. Continuous System.....	9
4. Open-Loop Case.....	13
5. Magnitude Plot for $N = 1, 2, 4$	18
6. Two Continuous Sine Waves Which Match the Sample Points.....	19
7. Frequency Response and Spectral Components of Output.....	25
8. "Steady-State" Transient Response.....	26
9. Illustrative Vector Closed-Loop Configuration.....	27
10. Transient Response, $a = 10$, ZOH, $\sin(\pi/2)t$ Input.....	30
11. Steady-State Sinusoidal Components, $N = 1$	30
12. Steady-State Sinusoidal Components, $N = 2$	32
13. Steady-State Sinusoidal Components, $N = 10$, Half Period.....	33
14. A Specific Two-Rate Closed-Loop Configuration.....	35
15. Decomposition of a Sample Sequence.....	41
16. Vector Block Diagrams for Multi-Rate Sampling Operations.....	44
17. A Multi-Rate Closed-Loop System.....	46
18. A Set on Non-Synchronously Sampled Signals.....	48
19. Sampling Notation.....	48
20. Advance, Sample, Delay.....	48
21. An Open-Loop Configuration.....	50
22. A Closed-Loop Configuration.....	50
23. A Three-Rate Configuration; $T, T/2, T/4$	52

	<u>Page</u>
24. A Phantom Sampler Formulation of a T/N, T/M Sampling Format.....	56
25. Example 5 (and 1) Block Diagram.....	64
26. Multi-Rate/Multiple-Order Open-Loop System.....	68
27. Open-Loop System with Switch Decomposition.....	68
28. Closed-Loop System with Switch Decomposition.....	73
29. A Three-Rate Scalar Configuration.....	74
30. Illustrative Example #1.....	76
31. Fast Output, Slow Input Example.....	77
32. Three Rate Example.....	77
33. Model of a Buffer Register.....	81
34. A Particular Serial Operation.....	82
35. Buffer Register Model with Throughput Delay.....	84
36. Timing Diagram.....	84
37. Example Two-Rate Open-Loop System.....	85
38. Switch Decomposition Formulation for Figure 35.....	85
39. A "Time Advanced" Filter Section.....	87
40. A Vector Switch Decomposition Simulation Case Study.....	93
41. Case IV, Switch Decomposition Model.....	95
42. Magnitude Plot; Case I, Case II.....	104
43. Magnitude Plot; Case I, Case III.....	105
44. Comparison; Case II and Case III.....	107
45. Magnitude Plot; Case I, Case IV.....	108
46. Comparison, Case II and Case IV.....	109
47. Comparison, All Cases.....	110

	<u>Page</u>
48. A Phantom Sampler Formulation of a T/N, T/M Sampling Format.....	111
49. Response of a T/2 Input Sampled, T/3 Output Sampled System.....	112
50. A Two Rate Experiment.....	114
51. $C^{T/3}$ Versus Time.....	116
52. Switch Decomposition Model for Figure 48.....	120
53. A Three Rate Example.....	123
54. A-10 Like Example.....	135
55. A-10 Case Study - Original Representation.....	137
56. A-10 Case Study - Models of Buffer Registers Added.....	138
57. A-10 Case Study-Simplified Block Diagram.....	140
58. Switch Decomposition Block Diagram.....	140
59. Equivalent Models.....	141
60. Display Pitch Angle to Stick Force Input.....	144
61. Washout Analog Block Diagrams.....	149
62. Discrete Integrator.....	150
63. A More Complex "Sway/Roll" Example.....	156

LIST OF TABLES

	<u>Page</u>
1. Component Coefficients $N = 1, 2, 4$	34
2. Classical Integrators.....	91
3. Coefficients for $C^{T/3}$	116
4. Spectral Coefficients for Equation 277.....	118
5. Comparison of Steady-State Transient Responses.....	119
6. The "a" Vector, Step I.....	125
7. The "a" and "c" Vectors, Step III.....	129
8. a, b, and c Vectors, Part III.....	132
9. Third, Sixth Model Data.....	152
10. Some Representative Bode Data.....	153
11. Impulse Responses.....	154
12. Coefficients for 6th Order Washout.....	156
13. Frequency Response Data, 6th Order Washout.....	159
14. s-, z-Plane A-10 Transfer Functions.....	D-2

SECTION I

INTRODUCTION

The past decade has seen an order-of-magnitude increase in reliance on fixed- and moving-base simulation for research and training in all types of aircraft. The reasons for this increase are numerous, ranging from the development of vehicles which must be completely design-validated before flight test (e.g., the Space Shuttle) to the increased use of simulation for training purposes (for reasons of safety, repeatability, and reduction of fuel costs). As a result, simulation facilities are in widespread use throughout the Air Force as well as other government agencies and private industry.

Accompanying this increased use of simulation has been a dramatic increase in simulator complexity. This particular development manifests itself most noticeably as digital computers replace analog equipment. While digital implementations provide better reliability and maintenance, increased static accuracy, and greater flexibility, they also introduce an array of simulation artifacts heretofore unconsidered. These anomalies impact the new generation of simulators in two areas:

- Hardware/software procurement. Techniques used to specify analog systems will no longer suffice in a digital environment. Critical concerns such as frame time, word length, integration algorithms, data skewness, order of subroutine call, etc., are presently the heuristic choice of the contractor, since the contracting agency has no analytical means by which to specify these items.
- Research/training on existing equipment. Often digital simulation artifacts creep into a simulation facility as a result of upgrading existing equipment with digital computers. As a result, experiments and training sessions may be contaminated with extraneous simulation errors. These errors are difficult to detect and assess without the aid of analytical tools.

The anomalies themselves are many but can be roughly described as frequency aliasing effects (another term is folded power). They arise for a variety of reasons:

- 1) Two or more computers required in a large simulation, each working in its own frame time (the so-called independent processor problem
- 2) Serial processing (calling) of subroutines. The first subroutine called may work with different input data than those called later (skewed data, "stale" input data).
- 3) Throughput delay factors.
- 4) Staircasing (zero-order-hold effects) when the digital computer output is used to drive the actuators of motion-base cabins.

A set of recently developed concepts provides the basis for identifying potentially critical simulation anomalies at the design stage in an organized and rational way. Moreover, a method exists which can be used to implement given computer code (integration algorithms) into a multi-rate, time delayed, skewed data analytical model, and predict the impact of these digital effects on the proposed simulation. To date these new methods have been demonstrated on low-order models with only limited demonstration of the theory. It is necessary to demonstrate all features of the new theory in a joint fashion on higher-order problems.

The methodology embodies three concepts. The first, which will be illustrated in Section II, is the continuous frequency response of a digitally controlled system. Using techniques developed in References 1 and 2, it is possible to compute the group of N sinusoids which fit the response of a digitally controlled system not only at the sample points but at the $(N - 1)$ inter-sample points as well. In the limit, as N approaches infinity, one obtains the "continuous" frequency response of a digitally controlled system. This section will clarify the term "frequency response" in the content of this report; it will be demonstrated that there is a truly significant difference between the frequency response of a digitally controlled continuous system and the discrete spectrum of sampled data control theory. It is convenient to review the

theory of the single-rate frequency response since it affords the opportunity to present several clarifying comments on the frequency response concept suggested by various readers of Reference 1*. Thus, Section II is also an "update" of the frequency response concept for digitally controlled systems and provides a link with newer developments.

The second component of this simulation analysis method is vector switch decomposition, a technique for analyzing simulations with two or more sample rates, data skewness, throughput delays, etc. As described in Section III, this technique is conceptually quite simple. All samplers in a given system are replaced by equivalent samplers whose periods are the least common sampling period, and the appropriate time delay vectors. One practical problem with this method is the accompanying increase in dimensionality for the "decomposed" vector. Vector switch decomposition is not a particularly workable tool for pencil and paper design, although it is quite amenable to computerization, since the matrix manipulations are routine.

We then develop from switch decomposition an algebra that circumvents, for a limited class of problems, the dimensional complexities introduced by the decomposition itself. In effect, a scalar problem will remain, in the framework of this algebra, a completely scalar problem. This "limited class of problems" is important since it encompasses the open-loop analysis of particular elements of a simulation as well as closed-loop multi-rate systems wherein the sample rates are related as powers of 2. This latter case covers both the Space Shuttle (25, 50, 100 Hz) and the F-18 (20, 40, and 80 Hz) digital control systems.

An important computational aspect of this scalar algebra is discussed extensively in Section IV. Specifically, an algorithm is described for transforming from a T/N time frame to a T/M time frame, N and M being arbitrary but rational. For example, sets of (M, N) such as

*In particular, the comments of Dr. Hsi-Han Yeh of the University of Kentucky provided an excellent interpretation of the limiting results as $N \rightarrow \text{infinity}$.

(3, 2), (2, 3), (7.8, 1), etc., are permissible. The algorithm is of particular importance as it permits the user to circumvent certain dimensionality constraints introduced by multi-rate methods based on residue theory. The nature of these constraints will be made clear in the case studies of Sections VII through IX.

In Section V, the application of the scalar algebraic approach to multi-rate frequency response is compared with the more general switch decomposition approach of Reference 2.

The third component of the simulation analysis method was developed in Reference 2. It is primarily a technique to incorporate, within the switch decomposition framework, a specified computer code. For example, there are a variety of methods available for modeling a low-pass filter section on a digital computer. One can use the Tustin transform, a rectangular integration algorithm, Adams-Bashforth, etc. Clearly, in analyzing a given simulation there must be a capability for incorporating the given difference equations into the analysis, without any particular regard (or prejudice) as to what the originator intended the code to represent. It is the task of the analysis to show the originator how successful his digital model is in representing the principal features of the continuous system. Facets of this problem are discussed in Section VI.

In Section VII, a first effort is made to bring all of the key elements together into a two-rate simulation case study. The ratio between the two frame times forces the use of the switch decomposition format and furnishes insight into the dimensionality problems encountered. This case study also demonstrates how a two rate format can introduce unintended lightly damped modes into a simulation.

In Section VIII, another case study is described which does not require the use of switch decomposition. The primary purpose of this study is to gain insight into the multi-rate frequency response. Suppose the output is sampled in a $T/3$ time frame but other rates are involved in preceding portions of the system. How many sine waves are required to exactly match the steady state $T/3$ output samples?

In Section IX the analysis of an existing three rate simulation is attempted. It was in this high-order simulation study, where the ratios between frame times were very large, that shortcomings in our computational tools proved to be more critical than previously suspected. For instance, in moving from one time frame to another, a fourteenth-order system becomes a system of order 112! The "invention" of the algorithm of Section IV was a direct result of these difficulties. Subsequently, we were able to proceed through the case study with relative ease and achieve important results. Thus Section IX, as it now stands, will give little insight into the numerical and dimensional difficulties first encountered.

The multi-rate simulation studies of Sections VII through IX have a primary goal of providing insight into the spectral characteristics of the output steady-state waveform in terms of the number of sinusoids required to match the output (sampled) data points. A secondary objective is to call attention to some observed anomalies (such as extraneous lightly damped modes introduced by the multi-rate structure) which can be identified and quantified using the analytical tools described in the earlier sections of the report.

Section X treats a single-rate case study which investigates the effective and unintended filtering introduced when subroutines are called in a serial manner. Specifically, it is shown that the z-domain analytical model of the computer code used in the implementation of a washout filter for a large moving-base simulator is twice the order of the intended s-domain transfer function.

The report is a lengthy one, attributable in a large part to a desire to pull together under one cover the key elements of References 1 and 2 which have application to simulation error analysis. Those readers familiar with the concepts of References 1 and 2 are therefore in a position to selectively read the present report.

2

SECTION II

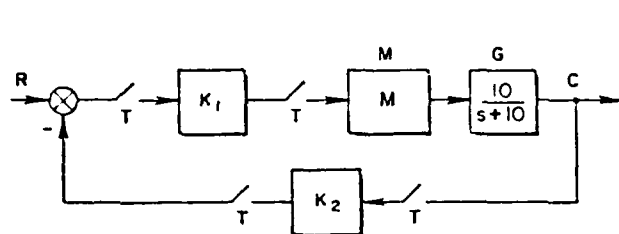
DISTINCTIONS IN "FREQUENCY RESPONSE"

A. INTRODUCTION

The term "frequency response" for discrete systems refers to the process of selecting the magnitude and phase of a single frequency sine wave to fit sample points at the sampling instants. In contrast, the concept of "frequency response" for the continuous variables of a discretely (digitally) controlled system defines the infinite set of sine waves (in terms of a fundamental and aliased frequencies) which add together to exactly reproduce the continuous output steady state waveform.

A simple but illuminating example, defined by Figure 1, illustrates the distinction. Suppose the system is forced by a step input and the continuous output C is recorded — both as a continuous analog quantity and also sampled at a rate of $1/T$ Hz. Furthermore, let the open-loop plant, $10/(s + 10)$, be subject to two different control laws, one implemented with a zero-order hold (ZOH), the other with the "slewer" data hold. The control laws were synthesized with the objective of forcing the output to be the same at the sampling instants, regardless of the control law/coupler being used. These responses are shown in Figure 2. Note the smoothness of the slewer-controlled response and the roughness of the ZOH response. However, an observer who is shown only the $1/T$ Hz sampled output would be unable to detect any differences in the transient responses, even though the continuous responses are very different.

Next force each system with a sine wave and record both the continuous and discrete output waveforms. The observer who is only interested in matching the sample points uses the discrete frequency response and picks the magnitude and phase from a Bode plot, such as the one labeled "discrete," in Figure 2b. Again, this observer is unaware of any distinction between the two systems (ZOH or slewer) as the same sine wave



$$M = \text{ZOH} = \frac{1 - e^{-sT}}{s}$$

$$M = \text{Slewer} = \frac{(1 - e^{-sT})^2}{s^2 T}$$

Design objective: reduce
open-loop dynamics $(s + 10)$
to $(s + 0.5)$

Figure 1. Single-Rate Digitally Controlled System

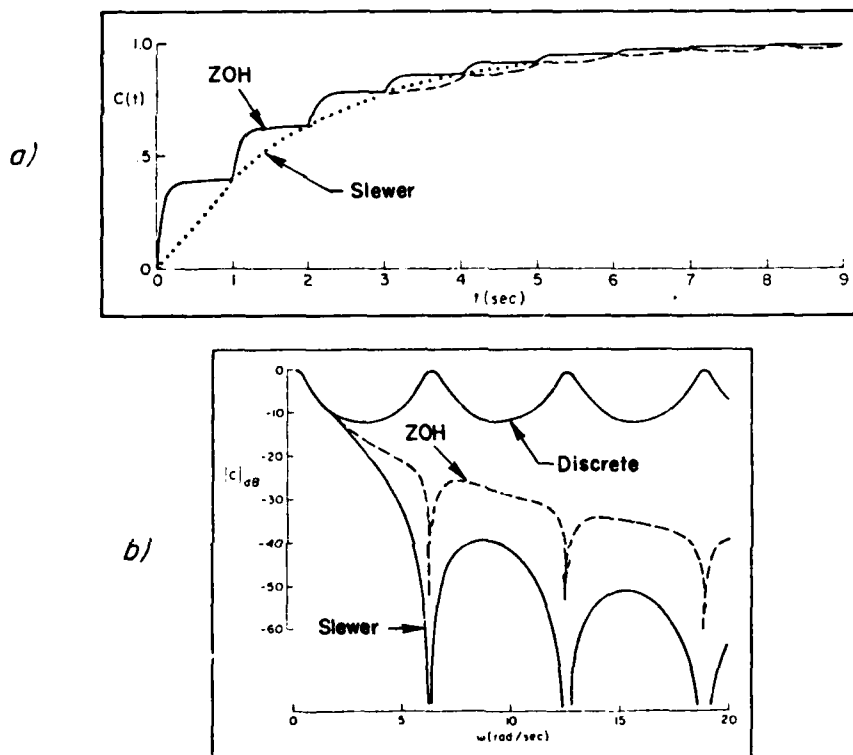


Figure 2. Step Response and Bode Plot

fits the sampled points of either output waveform. The "continuous" frequency response magnitude plots for the ZOH and slewer designs are also shown in Figure 2b. Here the observer must know how to reproduce the output waveform as the sum of a fundamental and its aliased frequencies -- a point discussed next. We merely observe that the "continuous" Bode plots show a truly significant difference between the two systems -- differences which the discrete frequency response of classical sample data control theory is incapable of detecting.

In the analysis of multi-rate simulations, one is often more interested in the finite set of sine waves that fits an output sequence sampled in, for example, a T/M time frame when the input is sampled in a T/N time frame. It is therefore appropriate to review the "finite N case" and the subsequent extension to the continuous frequency response of a discretely excited system.

B. FREQUENCY RESPONSE OF A SAMPLED SYSTEM

When a continuous, stable, linear system is excited by a sine wave, the steady-state waveform is comprised of a single wave at the same frequency as the input. It differs from the input wave only by a phase angle and a magnitude factor. Moreover, it is unnecessary to compute the actual transient response of the system when the behavior for large values of time is of interest, since both the magnitude factor and phase angle can be read from a Bode plot.

The analysis of a continuous system which is discretely controlled is more complex. Given that the system is stable, the continuous output waveform will contain more than just a wave at the fundamental frequency. It will consist of the fundamental and all of its aliases. Thus, if the system is forced with $1 \sin bt$, the output will contain terms at frequencies b , $[b + (2\pi/T)]$, $[b - (2\pi/T)]$, The relative amplitudes and phase angles will depend on the data hold employed as well as the system transfer function. Nevertheless, given a data hold and transfer function, the magnitude and phase angle of each component can be read from a particular Bode plot. This concept of frequency response is more comprehensive than the traditional concept of the

"sampled spectrum," which is limited to determining the single sinusoid that fits the system output samples at the sampling instants.

In the subsections to follow the Bode plot concept for a continuous system is reviewed and then extended to the frequency response of a discretely excited open-loop system.

C. CONTINUOUS SYSTEM BODE PLOTS

It will be helpful to first review the Bode plot concept for continuous systems. Let R in Figure 3 be a unit input sine wave with frequency ω_0 rad/sec. The output, in the frequency domain, is:

$$C(s) = G(s)R(s) = G(s) \frac{\omega_0}{s^2 + \omega_0^2} \quad (1)$$

Equation 1 can be expanded in partial fractions as:

$$C(s) = \frac{A\omega_0}{s^2 + \omega_0^2} + \frac{Bs}{s^2 + \omega_0^2} + \left[\begin{array}{l} \text{Terms associated} \\ \text{with characteristic} \\ \text{polynomial of } G(s) \end{array} \right] \quad (2)$$

Given that all poles of $G(s)$ are in the left half plane, the bracketed term in Equation 1 represents time functions that vanish as $t \rightarrow \infty$. Thus, the steady-state behavior is completely determined by the partial fraction coefficients A and B , and once they are known the steady-state time response can be written directly as:

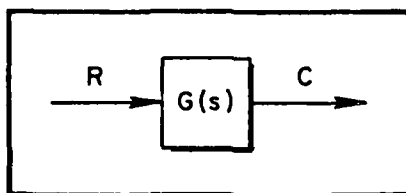


Figure 3. Continuous System

$$\begin{aligned}
C(t) \Big|_{\lim_{t \rightarrow \infty}} &= A \sin \omega_0 t + B \cos \omega_0 t \\
&= \sqrt{A^2 + B^2} \sin (\omega_0 t + \phi)
\end{aligned} \tag{3}$$

where $\phi = \tan^{-1} (B/A)$.

The details of solving for A and B show the relationship between the Bode plot and the steady-state waveform. To solve for A and B, multiply Equation 2 by $[s^2 + \omega_0^2]$ and evaluate the result for $s = j\omega_0$:

$$G(s)\omega_0 \Big|_{s=j\omega_0} = (A\omega_0 + Bs) \Big|_{s=j\omega_0} + \left[\begin{array}{l} \text{Terms associated} \\ \text{with characteristic} \\ \text{polynomial of } G(s) \end{array} \right] (s^2 + \omega_0^2) \Big|_{s=j\omega_0} \tag{4}$$

or

$$G(s) \Big|_{s=j\omega_0} \omega_0 = A + jB = \sqrt{A^2 + B^2} e^{j \tan^{-1} B/A} \tag{5}$$

To summarize, a sinusoidal input at frequency ω_0 produces a steady-state waveform of the same frequency. It differs from the input only by a magnitude factor and a phase shift. Both the magnitude factor and phase shift for any given input frequency, ω_0 , can be read directly from the Bode plot for $G(j\omega)$. That is, for any given input frequency ω_0 :

$$A + jB = G(s) \Big|_{s=j\omega_0} \tag{6}$$

This "frequency response" viewpoint is expanded to encompass discretely excited continuous systems.

D. MATHEMATICAL PRELIMINARIES

Let R be a sinusoid of unit amplitude with frequency b rad/sec ($R = 1 \sin bt$). If R is sampled at $1/T$ Hz and then described in terms of an N/T Hz model, we obtain

$$R^T = \frac{z^N \sin bT}{z^{2N} - (2 \cos bT)z^N + 1} ; \quad z = e^{sT/N} \quad (7)$$

where the superscript $[\cdot]^T$ is used to denote the frametime of the sampling operator. For later use, it is necessary to find the $2N$ factors of the denominator of Equation 7 in a form that will permit a partial fraction expansion containing terms for which corresponding time functions are known. For example, if $f(t) = \sin bt$, then

$$f^T(t) = [\sin bt]^T \Rightarrow F(z) = \frac{z \sin bT}{z^2 - (2 \cos bT)z + 1} \quad (8)$$

but we do not know the time function corresponding to

$$F(z) = \frac{z \sin bT}{z^2 + (2 \cos bT)z + 1} \quad (9)$$

which will also occur among the N factors of the denominator of Equation 7.

This problem can be examined in more detail by letting $z^N = X$ in Equation 7 and solving for the roots using exponential notation:

$$z^{2N} - (2 \cos bT)z^N + 1 = X^2 - 2(\cos bT)X + 1 \quad (10)$$

In turn,

$$X^2 - (2 \cos bT)X + 1 \equiv (X - \cos bT)^2 + (\sin bT)^2 \quad (11)$$

The N roots of Equation 11 can now be expressed as

$$(X - \cos bT)^2 = -(\sin bT)^2$$

$$X - \cos bT = \pm j \sin bT$$

$$X = \cos bT \pm j \sin bT = e^{\pm j bT}$$

Replacing X by z^N gives one of the many ways of describing the roots of Equation 7:

$$z = e^{\pm j(bT/N)} = e^{\pm j[(bT/N) + (2\pi n/N)]} = 1 \angle \pm [(bT/N) + (2\pi n/N)] \quad (12)$$

In a purely formal sense, the n in Equation 12 can take on both positive and negative integer values. The preferred format for defining the roots of Equation 12 is:

$$\frac{bT}{N} + \frac{2\pi n}{N} = \left[b + \left(\frac{2\pi n}{T} \right) \right] \frac{T}{N} = \omega_n \frac{T}{N}$$

As we have said, both positive and negative values of n are permitted. For example, if $N = 3$ there are three complex conjugate roots pertaining to the frequencies

$$b, \quad b + 2\pi/T, \quad b + 4\pi/T$$

However, the values

$$b, \quad b - (2\pi/T), \quad b + (2\pi/T)$$

are equally permissible. For the finite N case many readers will prefer the description in terms of the input frequency and the positive aliases, avoiding a description that contains negative frequencies.

E. OPEN-LOOP FREQUENCY RESPONSE — FINITE N

Consider the system of Figure 4 where $G(s)$ represents an arbitrary transfer function and M represents an arbitrary data hold. Suppose R is a unit amplitude sine wave and the output is sampled in a T/N frame time:

$$C^{T/N} = (GM)^{T/N} R^T = (GM)^{T/N} \frac{z^N \sin bT}{z^{2N} - (2 \cos bT)z^N + 1}, \quad z = e^{sT/N} \quad (13)$$

The superscript is used to call out the defining time frame and use is made of the identity $[A B^T]^{T/N} = A^{T/N} B^T$ (Reference 1).

Expand the right-hand side of Equation 13 in partial fractions:

$$C^{T/N} = \sum_{n=0}^{N-1} \frac{A_n z \sin \omega_n(T/N) + B_n z [z - \cos \omega_n(T/N)]}{z^2 - [2 \cos \omega_n(T/N)] z + 1} + [\text{Terms due to modes of } (GM)^{T/N}] \quad (14)$$

Assume that responses in the modes of $(GM)^{T/N}$ approach zero as $t \rightarrow \infty$, i.e., that all modes are stable. In Equation 14,

$$\omega_n = b + \frac{2\pi n}{T}, \quad n = 0, 1, 2, \dots, N-1$$

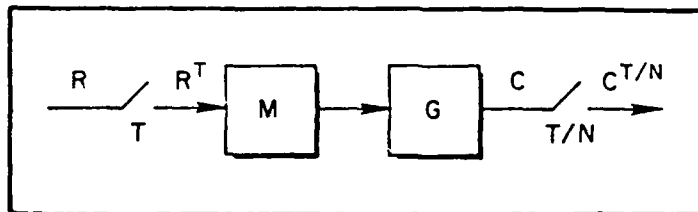


Figure 4. Open-Loop Case

For the present, we assume that $b \leq 2\pi T$. The steady-state waveform, at the sampling instants, can be written as:

$$[C(t)]^T = \left[\sum_{n=0}^{N-1} (A_n \sin \omega_n t + B_n \cos \omega_n t) \right]^T \quad (15)$$

To solve for A_n and B_n , multiply each side of Equation 14 by

$$[z^2 - [2 \cos \omega_k (T/N)]z + 1] \quad , \quad 0 \leq k \leq (N-1)$$

and evaluate for $z = e^{j\omega_k (T/N)}$. The only term that can survive on the right-hand side occurs when $n = k$ (the k notation can then be changed to n). To illustrate,

$$\begin{aligned} & (GM)^{T/N} \frac{z^N \sin bT}{z^{2N} - (2 \cos bT)z^N + 1} [z^2 - 2 \cos \omega_k (T/N)z + 1] \Big|_{z=e^{j\omega_k (T/N)}} \\ & = \sum_{n=0}^{N-1} \frac{[A_n z \sin \omega_n (T/N)] + B_n z [z - \cos \omega_n (T/N)]}{z^2 - [2 \cos \omega_n (T/N)]z + 1} [z^2 - [2 \cos \omega_k (T/N)]z + 1] \Big|_{z=e^{j\omega_k (T/N)}} \end{aligned} \quad (16)$$

For any $n \neq k$, the right-hand side of Equation 16 is identically zero since

$$z^2 - [2 \cos \omega_k (T/N)]z + 1 = [z - \cos \omega_k (T/N)]^2 + [\sin \omega_k (T/N)]^2 \quad (17)$$

vanishes when

$$z = e^{j\omega_k (T/N)} = \cos \omega_k (T/N) + j \sin \omega_k (T/N) \quad (18)$$

Specifically, we obtain

$$[\cos \omega_k(T/N) + j \sin \omega_k(T/N) - \cos \omega_k(T/N)]^2 + [\sin \omega_k(T/N)]^2 \equiv 0 \quad (19)$$

For $n = k$, the cancellation of the common factor guarantees the survival of an $n = k$ term. Factoring out a common z gives

$$\begin{aligned} z[A_k \sin \omega_n(T/N) + B_k[\cos \omega_n(T/N) - \cos \omega_n(T/N) + j \sin \omega_n(T/N)]] \\ = (A_k + jB_k)z \sin \omega_k(T/N) \Big|_{z=1 \pm j\omega_k(T/N)} \end{aligned} \quad (20)$$

Therefore, Equation 16 becomes

$$z \sin \omega_k(T/N)(A_k + jB_k) = \frac{(G/M)^{T/N} (z^N \sin bT) \{z^2 - [2 \cos \omega_k(T/N)]z + 1\}}{z^{2N} - [2 \cos bT]z^N + 1} \Big|_{z=1 \pm j\omega_k(T/N)} \quad (21)$$

At this point, let k revert to n .

$$A_n + jB_n = (GM)^{T/N} \Big|_{z=1 \pm j\omega_n(T/N)} \cdot \frac{z^{N-1} \sin bT}{\sin \omega_n(T/N)} \cdot \frac{\{z^2 - [2 \cos \omega_n(T/N)]z + 1\}}{z^{2N} - (2 \cos bT)z^N + 1} \Big|_{z=1 \pm j\omega_n(T/N)} \quad (22)$$

The last term on the right-hand side of Equation 22 is indeterminate (0/0) when $z = 1 \pm j\omega_n(T/N)$. Therefore, apply L'Hôpital's rule once and obtain

$$A_n + jB_n = (GM)^{T/N} \Big|_{z=1 \pm j\omega_n(T/N)} \cdot \frac{z^{N-1} 2[z - \cos \omega_n(T/N)]}{2Nz^{N-1}(z^N - \cos bT)} \cdot \frac{\sin bT}{\sin \omega_n(T/N)} \Big|_{z=1 \pm j\omega_n(T/N)} \quad (23)$$

$$A_n + jB_n = \frac{1}{N} (GM)^{T/N} \Big|_{z=14\omega_n(T/N)} \cdot \frac{[\cos \omega_n(T/N) + j \sin \omega_n(T/N) - \cos \omega_n(T/N)]}{[\cos \omega_n T + j \sin \omega_n T - \cos bT]} \frac{\sin bT}{\sin \omega_n(T/N)} \quad (24)$$

A direct substitution for $\omega_n = b + (2\pi n/T)$ quickly shows that the last part of the product in Equation 24 is unity. Therefore,

$$A_n + jB_n = \frac{1}{N} (GM)^{T/N} \Big|_{z=14\omega_n(T/N)} z^{\frac{1}{2}} e^{sT/N} \quad (25)$$

The superscript notation in Equation 25 is for the purpose of calling out the definition of z being used in the evaluation.

To review the situation, the system is forced with the $\sin bt$. The steady-state output waveform, sampled with a T/N frametime, has the form

$$c^{T/N}(t) = \left[\sum_{n=0}^{N-1} (A_n \sin \omega_n t + B_n \cos \omega_n t) \right]^{T/N} \quad (26)$$

where

$$\omega_n = b + \frac{2\pi n}{T}, \quad n = 0, 1, 2, \dots, N-1 \quad (27)$$

As an alternative, one may use

$$c^{T/N} = \left[\sum_{n=-(N-1)/2}^{(N-1)/2} (A_n \sin \omega_n t + B_n \cos \omega_n t) \right]^{T/N}, \quad N \text{ odd} \quad (28)$$

or

$$c^{T/N} \left[\sum_{n=-N/2}^{(N/2)-1} (A_n \sin \omega_n t + B_n \cos \omega_n t) \right]^{T/N}, \quad N \text{ even} \quad (29)$$

The coefficients A_n and B_n are computed using Equation 25.

For example, let

$$M = \frac{1 - e^{-sT}}{s}, \quad G(s) = \frac{a}{s + a} \quad (30)$$

so that

$$\frac{1}{N} (GM)^{T/N} = \frac{1 - e^{-aT/N}}{N(z - e^{-aT/N})} \frac{(1 - z^{-N})}{(1 - z^{-1})} \quad (31)$$

It is instructive to plot the Bode plot for Equation 31 using N as a parameter. For the sake of clarity, we will plot versus ω rather than $\log \omega$ and omit the phase angle plot. Also, for reasons of clarity, the ordinate scales will be displaced for the different values of N (refer to Figure 5). Over the plotted range of 8π , the $N = 1$ case repeats itself 4 times. In a like manner, the $N = 2$ case repeats twice, whereas $N = 4$ goes through one cycle.

Using $[1 \sin (\pi/2)t]$ as an input, in the $N = 1$ case our only interest is matching the sampling points with a single sine wave. The magnitude and phase angle (not shown in Figure 5) could be read from this plot at $\omega = \pi/2, \pi/2 + 2\pi, \pi/2 + 4\pi, \pi/2 + 6\pi, \dots$; giving the correct values for each point. Assume next that the input has a frequency $b = (\pi/2 + 4\pi)$. Clearly, if the objective is to match the sample points with a single sinusoid, the frequency of the output could be b plus any $2\pi/T$ multiple as the sampler cannot tell the difference. In fact, the "sub" aliases at $b - 2\pi/T, b - 4\pi/T$ will also work. These "sub" aliases are the difference terms so prominent in modulation theory.

Figure 6 depicts this situation for a steady-state response given an input frequency of $b = \pi/2$ rad/sec, assuming the system in Equation 31.

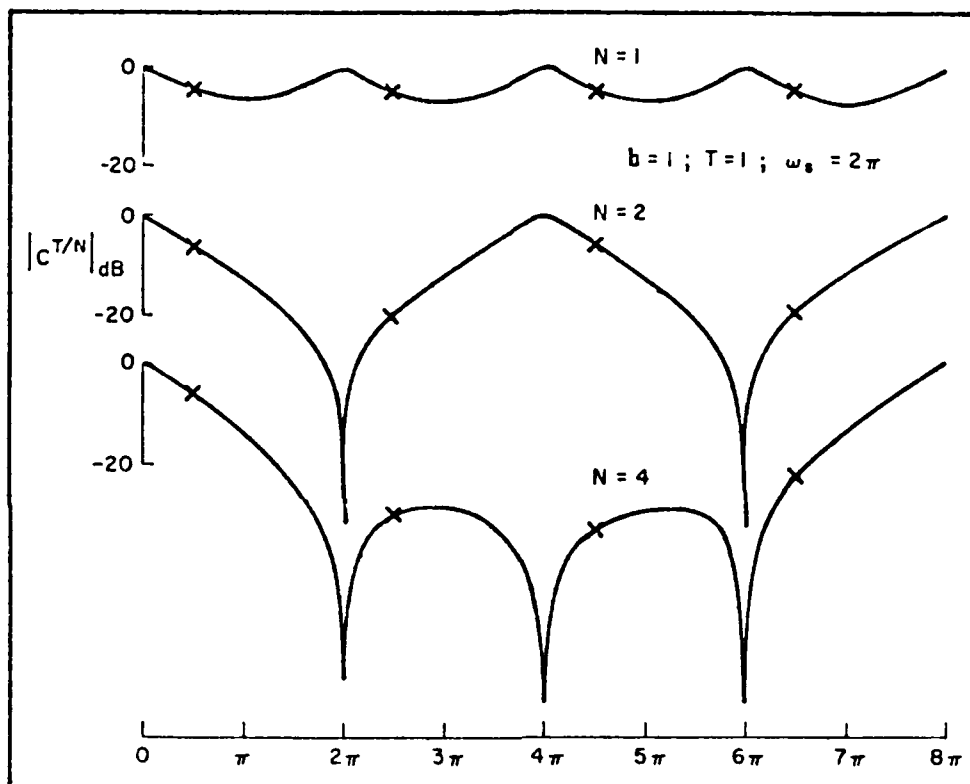


Figure 5. Magnitude Plot for $N = 1, 2, 4$

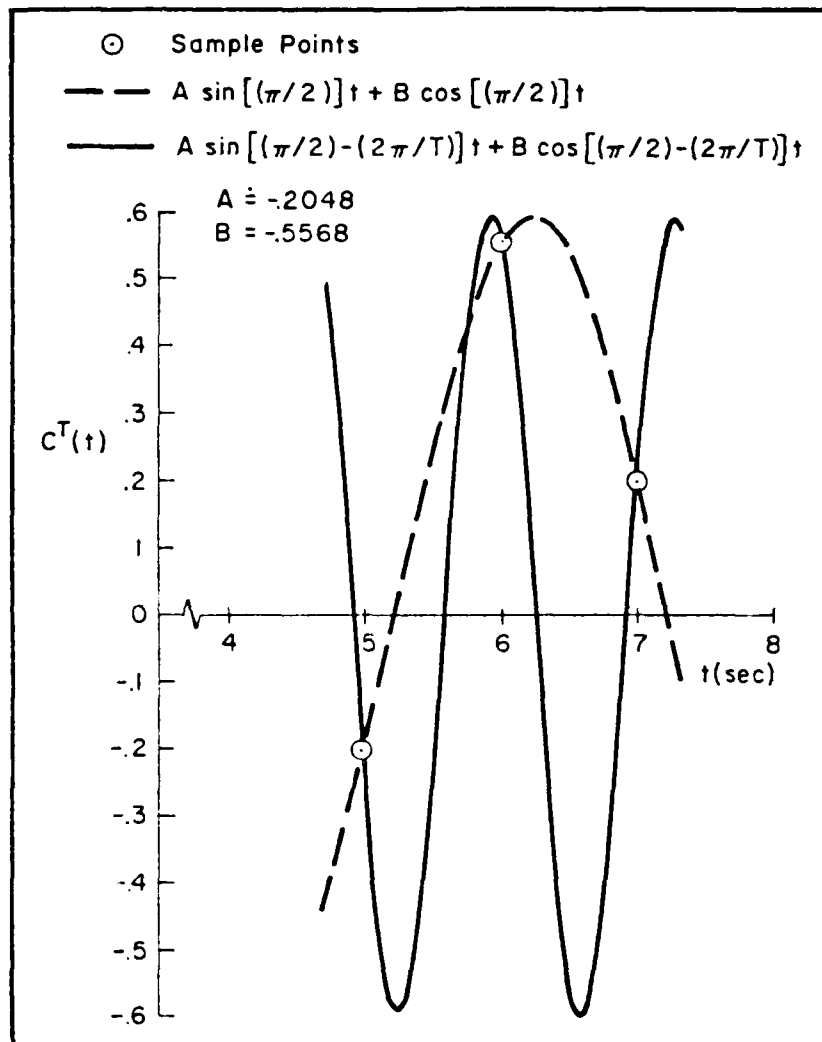


Figure 6. Two Continuous Sine Waves Which Match the Sample Points

For the sake of clarity, only two of the many waves which fit the sample points are shown — one at $\pi/2$ rad/sec, the other at $[(\pi/2) - (2\pi/T)]$ rad/sec.

The $N = 1$ plot in Figure 5 corresponds to the "sampled spectrum" of sampled data control theory. Turn now to the $N = 2$ case wherein the objective is to match one inter-sample point as well as the sample points. Let the input frequency be $\pi/2$ and note that the points at $\omega = \pi/2$, $\pi/2 + 2\pi$ give the correct answers, as would the points $\pi/2 + 4\pi$, $\pi/2 + 6\pi$. Suppose next that the input frequency is $b = \pi/2 + 2\pi$. Clearly, the second required component could be read from the "first alias" at $b + 2\pi/T$ or the first sub-alias at $b - 2\pi/T$ [or, for that matter, all the frequencies $\omega = (\pi/2) + 2n\pi$ where n is an integer].

In the $N = 4$ case, four sine waves are required to fit three inter-sample points as well as the sampled points. If the input frequency were $b = \pi/2 + 6\pi$, and if the plot of Figure 5 with its limited range of 8π were the only one available, clearly it would be to our advantage to use the "difference" frequency points at $\omega = b - 2\pi/T$, $b - 4\pi/T$, and $b - 6\pi/T$ to establish the magnitude and relative phase of the three remaining sine waves.

This brief discussion serves to point out that the aliases and sub-aliases can be associated with the sum and difference frequencies of modulation theory. One should not, however, think that both sum and difference components must be simultaneously present in the output. Clearly, only N components are needed. We can now remove the earlier constraint that $b < 2\pi/T$. If b is less than $2\pi/T$, it is certainly true that

$$\omega_n = b + \frac{2\pi n}{T}, \quad n = 0, 1, 2, \dots, N-1 \quad (32)$$

However, if $b > 2\pi/T$, let $\omega_s = 2\pi/T$ and use

$$n_0 = - \left(\frac{b}{\omega_s} \right)_{\text{INT}} \quad (33)$$

to restate Equation 32 as

$$\omega_n = b + \frac{2\pi n}{T}, \quad n = n_0, n_0 + 1, \dots, 0, 1, 2, \dots, N - n_0 - 1 \quad (34)$$

For our previous example where $N = 4$, suppose $b = 6\pi + \pi/2$. Then

$$n_0 = -\left(\frac{6\pi + (\pi/2)}{2\pi}\right)_{\text{INT}} = -3 \quad (35)$$

Thus,

$$\omega_n = b + \frac{2\pi n}{T}, \quad n = -3, -2, -1, 0 \quad (36)$$

and we use three sub aliases. If $b = \pi/2$, then

$$n_0 = -\left(\frac{\pi/2}{2\pi}\right)_{\text{INT}} = 0$$

and we use

$$\omega_n = \frac{2\pi n}{T}, \quad n = 0, 1, 2, 3$$

the "positive" aliases.

Keep in mind that all this represents a convention which the reader may not necessarily elect to follow. What is important is a clear understanding which will permit one to pick a consistent set of N points from the Bode plot. In this regard, the reader should note that the use of Equation 28 (or Equation 29) instead of Equation 27 eliminates the need for the definition of n_0 .

Of interest is the case where N is extremely large. In fact, let $N \rightarrow \infty$ after evaluating Equation 31 at $z = 1 \pm \omega_n(T/N)$:

$$\left. \frac{1 - e^{-sT/N}}{N(z - e^{-sT/N})} \frac{1 - z^{-N}}{1 - z^{-1}} \right|_{z = 1 \pm j\omega_n(T/N)} = \frac{(1 - e^{-sT/N})(1 - 1 \pm j\omega_n T)}{N[1 \pm j\omega_n(T/N) - e^{-sT/N}][1 - 1 \pm j\omega_n(T/N)]} \bigg|_{\lim_{N \rightarrow \infty}} \quad (37)$$

An indeterminate form is obtained. Therefore, use L'Hôpital's rule twice (substitute $1 \pm j\omega_n(T/N) = \cos \omega_n(T/N) + j \sin \omega_n(T/N)$, etc.) and obtain:

$$\left. \frac{1}{N} \left(\frac{1 - e^{-sT}}{s(s+1)} \right) \right|_{z = 1 \pm j\omega_n(T/N)} \bigg|_{\lim_{N \rightarrow \infty}} = \frac{1 - e^{-j\omega_n T}}{j\omega_n T} \frac{1}{1 + j\omega_n} = \frac{1 - e^{-sT}}{sT} \frac{1}{s+1} \bigg|_{s = j\omega_n} \quad (38)$$

That is, as $N \rightarrow \infty$, one simply divides GM by T and evaluates the coefficients at $s = j\omega_n$. This is representative of the general result discussed in the next subsection. A word of caution is in order on ω_n . As N approaches infinity, the definition of Equation 28 (or Equation 29) should be adhered to in order to properly incorporate the sub-aliases into the spectrum.

F. OPEN LOOP FREQUENCY RESPONSE — CONTINUOUS OUTPUT

The next development uses an approach suggested by Professor Hsi-Han Yeh (University of Kentucky). This approach more clearly shows the dependence of the spectrum on both positive and negative aliases. That is, for finite N, there is a choice in the makeup of the sinusoidal components which exactly match the steady-state sample points. The finite N case is therefore not unique — in sharp contrast to the infinite N results which require (as will be shown) the use of all the sub-aliases as well as all of the aliased components.

In the previous section it was shown that

$$A_n + jB_n = \frac{1}{N} (GM)T/N \left| \begin{array}{l} z = e^{sT/N} \\ z = 1 + j\omega_n(T/N) \end{array} \right. \quad (39)$$

To deduce the behavior for infinite N, use an alternative description of Figure 4 which describes the sine wave input directly in the s-domain:

$$C(s) = G(s)M(s) \left[\frac{1}{T} \sum_{n=-\infty}^{\infty} \frac{\omega_n}{s^2 + \omega_n^2} \right] \quad (40)$$

where $\omega_n = b + 2\pi n/T$.

The partial fraction expansion of Equation 40 may be written as

$$C(s) = \left[\sum_{n=-\infty}^{\infty} \frac{A_n(\omega_n)}{s^2 + \omega_n^2} + \frac{B_n s}{s^2 + \omega_n^2} \right] + [\text{Transient modes of GM}] \quad (41)$$

Multiply each side of Equation 41 by $s^2 + \omega_n^2$ and evaluate at $s = j\omega_n$:

$$\begin{aligned} C(s)(s^2 + \omega_n^2) &= A_n \omega_n + B_n j\omega_n \\ &= G(s)M(s)(1/T)\omega_n \end{aligned}$$

$$A_n + jB_n = (1/T)G(s)M(s) \Big|_{s=j\omega_n}, \quad n = 0, \pm 1, \pm 2, \dots \quad (42)$$

Thus the continuous spectrum contains, because of the summation from $-\infty$ to $+\infty$, both positive and negative aliased frequencies.

The finite N example of the previous section can now be studied for the case of infinite N. Thus

$$A_n + jB_n = \frac{1 - e^{-sT}}{sT} \cdot \frac{1}{s + 1} \Big|_{s=j\omega_n} \quad (43)$$

produces the Bode plot of Figure 7.

The interpretation of Figure 7 is as follows. Suppose a unit sine wave at 1 rad/sec is input to the sampler. Then, if sine waves at 1, $1 + 2\pi/T$, $1 - 2\pi/T$, $1 + 4\pi/T$, $1 - 4\pi/T$, ... are added together, the resultant waveform will be an exact match of the actual steady-state output waveform. In Figure 7, one may plot the sub aliases (the negative frequency components) on a "positive frequency" Bode plot by taking advantage of the fact that the magnitude is an even function of frequency and the phase is an odd function of frequency.

One would expect this waveform to be relatively clean, since the first alias is 30 dB lower than the input component. However, the transient response itself does not bear out this conjecture, as can be seen in Figure 8. The reason is that the higher terms are important. They do not represent "harmonic" terms but are rather modulation components which must add together properly in order to match conditions at the T transition points. It can be seen that the "steady state" does not necessarily take on the additional attribute of periodicity. This occurs only when the input frequency and the sampling frequency bear an integer relationship with respect to one another.

G. INPUT SIGNAL WITH PHASE SHIFT

If the input signal has the form

$$r(t) = k_1 \sin bt + k_2 \cos bt \quad (44)$$

the results of the previous section are changed only by a complex constant. Following exactly the procedures of Subsection E, except for using the more general input given in Equation 44, gives (Reference 1):

$$A_n + jB_n = \frac{1}{N} (GM)^{T/N} \left| \begin{matrix} z = e^{sT/N} \\ z = 1 + j\omega_n(T/N) \end{matrix} \right| \cdot (k_1 + jk_2) \quad (45)$$

Given that the limit $N \rightarrow \infty$:

$$A_n + jB_n = \frac{1}{T} GM \left| \begin{matrix} s = j\omega_n \end{matrix} \right| \cdot (k_1 + jk_2) \quad (46)$$

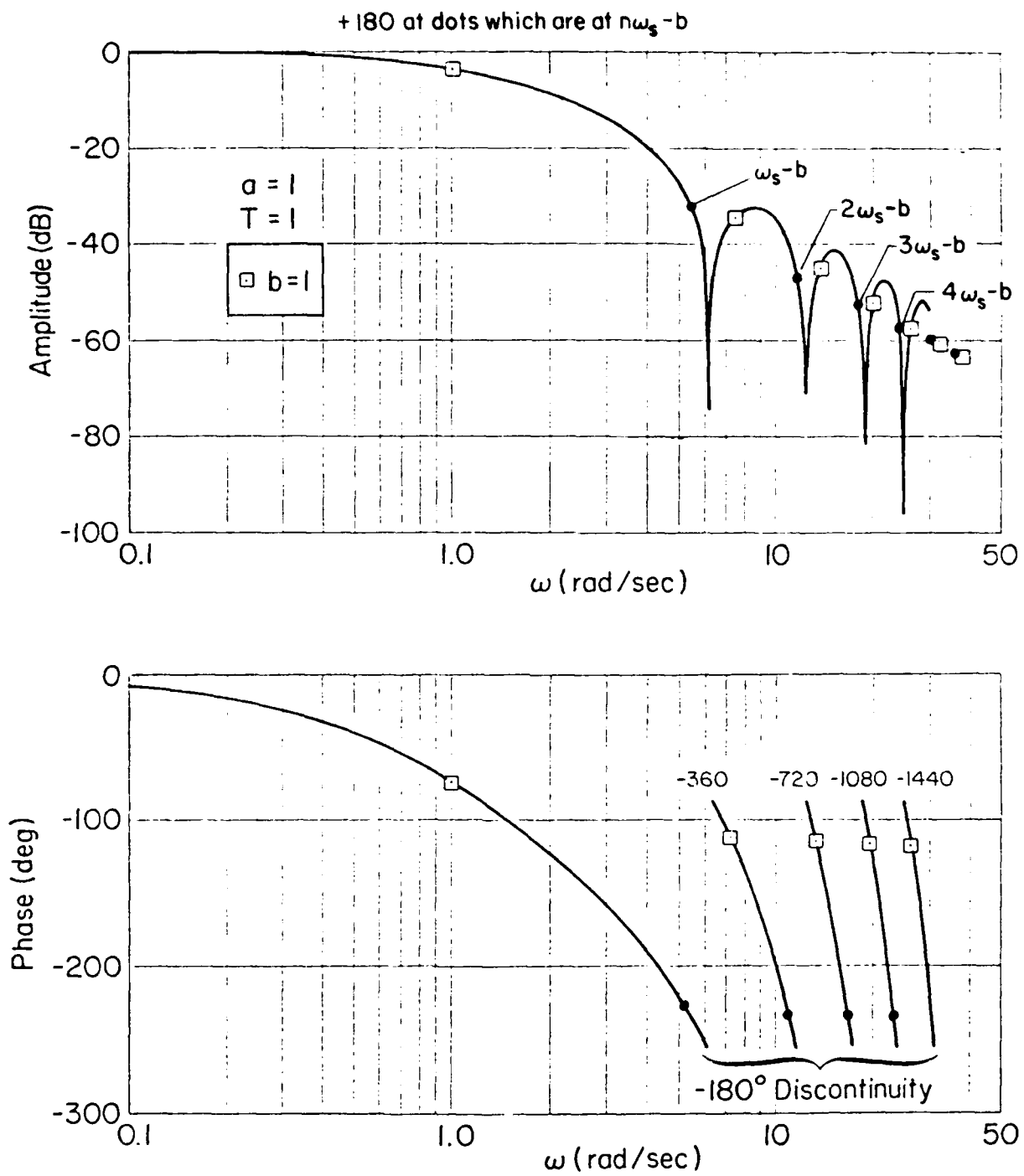


Figure 7. Frequency Response and Spectral Components of Output

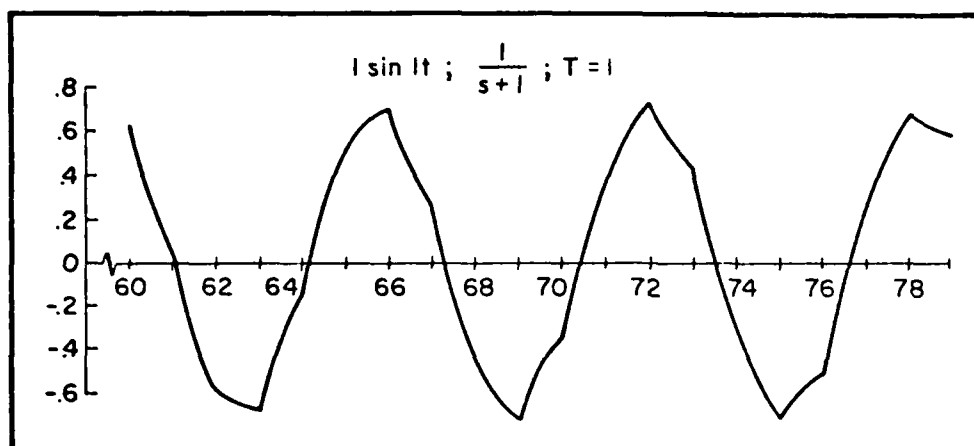


Figure 8. "Steady-State" Transient Response

The choice of the N frequencies for the finite N case is at the discretion of the user. However, both "negative" and "positive" frequencies are required as $N \rightarrow \infty$ (Equations 28 and 29).

H. SINGLE-RATE CLOSED-LOOP FREQUENCY RESPONSE

The closed-loop results will be configuration dependent. However, the mathematics remains tractable and can be followed through on a case-by-case basis. It is important to have an insight into the mathematical structure and the particular simplifications that surface in a closed-loop analysis.

Consider the (vector) system shown in Figure 9. The procedure we now follow will be typical. First, solve for the vector component at the input of the data holds.

$$E^T = G_1^T R^T - G_1^T G_2^T (GM)^T E^T \quad (47)$$

Therefore

$$E^T = [I + G_1^T G_2^T (GM)^T]^{-1} G_1^T R^T \quad (48)$$

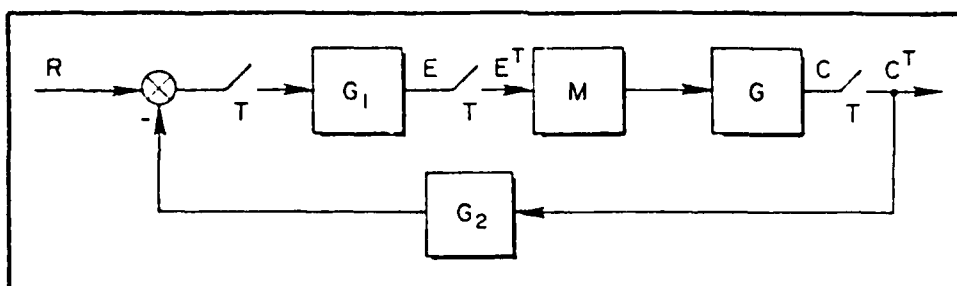


Figure 9. Illustrative Vector Closed-Loop Configuration

Next, solve for $C(s)$:

$$C = (GM)[I + G_1^T G_2^T (GM)^T]^{-1} G_1^T R^T \quad (49)$$

The spectrum of $C(s)$ is of interest; we seek it by finding first the spectrum of $C^{T/N}$ and going to the limiting case of $N \rightarrow \infty$.

Let the input be a sine wave at frequency b rad/sec and let the delay operator be

$$z^{-1} = e^{-sT/N} \quad (50)$$

so that

$$R^T = \frac{z^N \sin bT}{z^{2N} - 2(\cos bT)z^N + 1} \quad (51)$$

Therefore

$$\begin{aligned} C^{T/N} &= [(GM)[I + G_1^T G_2^T (GM)^T]^{-1} G_1^T R^T]^{T/N} \\ C^{T/N} &= (GM)^{T/N} [I + G_1^T G_2^T (GM)^T]^{-1} G_1^T R^T \end{aligned} \quad (52)$$

For the sake of brevity write Equation 52 as

$$C^{T/N} = G_A^{T/N} G_B^T R^T \quad (53)$$

Note that Equation 53 is exactly the same as Equation 13, except $(GM)^{T/N}$ has been replaced by $G_A^{T/N} G_B^T$. Hence we can write a key result using Equation 25:

$$A_n + jB_n = \frac{1}{N} G_A^{T/N} G_B^T \Big|_{z=14\omega_n(T/N)} \quad (54)$$

But

$$G_B^T \triangleq G_B(z^N)$$

Therefore, using

$$\begin{aligned} [14\omega_n(T/N)]^N &= 14\omega_n T \\ &= \cos \omega_n T + j \sin \omega_n T \\ &= \cos [b + (2\pi n/T)]T \\ &\quad + j \sin [b + (2\pi n/T)]T \\ &= \cos bT + j \sin bT \end{aligned} \quad (55)$$

we obtain

$$\begin{aligned} G_B^T \Big|_{14\omega_n(T/N)} &\equiv G[14\omega_n(T/N)]^N \\ &\equiv G[14\omega_n T] = G[14bT] \end{aligned} \quad (56)$$

It is permissible to replace z^N in G_B^T with z and evaluate it at $z = 14bT$. At this point we have

$$A_n + jB_n = \left(\left[\frac{1}{N} G_A^{T/N}(z) \right]_{z=14\omega_n(T/N)}^{z^N e^{sT/N}} \right) \left(\left[G_B^T(z) \right]_{z=14bT}^{z^N e^{sT}} \right) \quad (57)$$

Equation 57 is the basic result for the finite N case. To reiterate, to find the coefficients of the N sine waves for the T/N sampled output of C , compute the normal "T" transfer functions for

$$G_B^T = [I + G_1^T G_2^T (GM)^T]^{-1} G_1^T \quad (58)$$

and evaluate it for

$$z = l_4 b T \quad (59)$$

Next, compute the normal T/N pulsed transfer function for G_A and evaluate it at $z = l_4 \omega_n(T/N)$ where $\omega_n = b + (2\pi n/T)$.

Thus, G_B^T is periodic in $(2\pi n/T)$ and it suffices to use bT instead of $\omega_n(T/N)$. Moreover, only the $G_A^{T/N}$ is a function of N ; this simplifies the procedure involved in the limiting case tremendously. For the case of $N \rightarrow \infty$, the continuous case, we obtain:

$$A_n + jB_n = \left(\left| \frac{M(s)G(s)}{T} \right|_{s=j\omega_n} \right) \left(\left| G_B^T(z) \right|_{z=l_4 b T} z^{\frac{a}{2}} e^{sT} \right), \quad n = 0, \pm 1, \pm 2, \dots \quad (60)$$

Equation 60 is the desired result for the given closed-loop configuration.* However, the mathematical ideas are what count; one can follow the details through for other configurations with relative ease.

With this development, one is in a position to plot the Bode plots for the closed-loop system of Figure 1 and verify the results given in Fig. 2. We will also use that example to solidify the meaning of the frequency response for the finite N case. Suppose the continuous transient response for a unit amplitude sine wave, with a frequency of $\pi/2$, is available (see Fig. 10). According to theory, one should be able to set $N = 1$ and from the Bode plot read the magnitude and phase of the single sinusoid that fits the sample points at the sample instant. This indeed proves to be the case and is shown in Figure 11. In Figure 11 a section of the transient response has been "copied" and

*Accurate numerical determination of $G_B^T|_{l_4 b T}$ may prove difficult at high sampling rates. This is the result of small differences between large numbers which occur in the computations as poles and zeros approach the unit circle. In this event, one is well advised to carry out equivalent computations in a domain where numerical conditioning is much improved (e.g., in terms of w' or w).

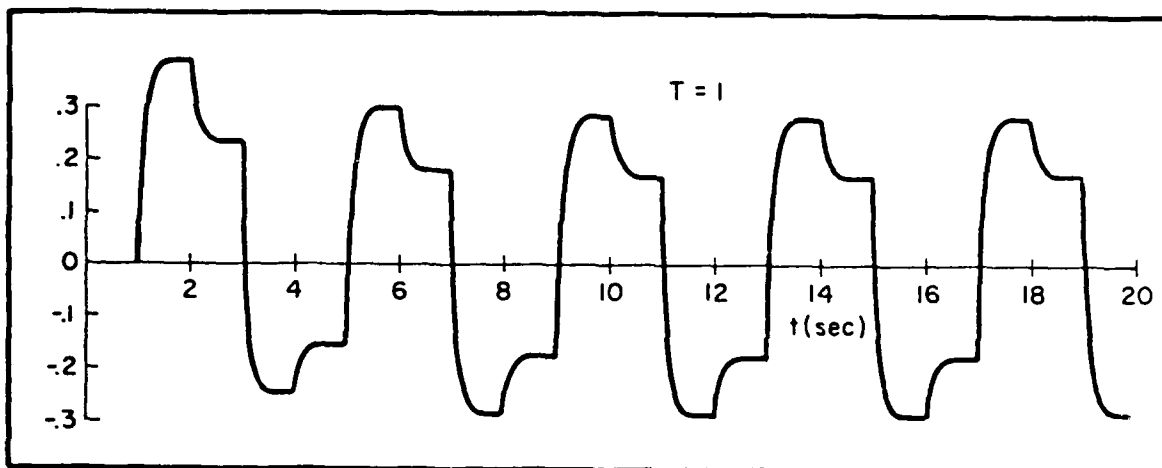


Figure 10. Transient Response, $a = 10$, ZOH, $\sin(\pi/2)t$ Input

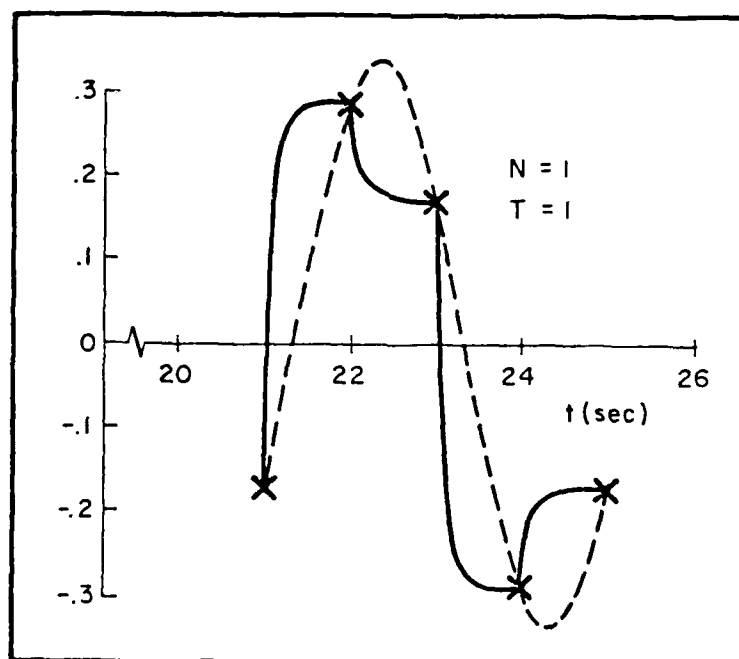


Figure 11. Steady-State Sinusoidal Components, $N = 1$

overlaid with the sine wave which results from the $N = 1$ computation, namely

$$[C(t)]^T = \left(a_0 \sin \frac{\pi}{2} t + b_0 \cos \frac{\pi}{2} t \right)^T \quad (61)$$

Equation 61 indicates that the value of the wave at the sampling instants is of interest. However, for expository purposes, a complete cycle has been shown.

Next, consider the $N = 2$ case where the desire is to fit not only the sample point but one inter-sample point as well. This case is shown in Figure 12. The $T/2$ response equation is

$$C(t) \Big|_{ss}^{T/2} = \left[a_0 \sin \frac{\pi}{2} t + b_0 \cos \frac{\pi}{2} t + a_1 \sin \left(\frac{\pi}{2} + \frac{2\pi}{T} \right) t + b_1 \cos \left(\frac{\pi}{2} + \frac{2\pi}{T} \right) t \right]^{T/2} \quad (62)$$

Again, for expository reasons, the continuous waveform is shown which results from sines and cosines at $\omega = \pi/2$ and its first alias at $\omega = (\pi/2) + (2\pi/T)$. A half period for the $N = 10$ case is shown in Figure 13. The steady-state wave of this example is periodic and free of modulation effects simply because the selected input frequency bears an integer relationship to the sampling frequency.

It is also important to bear in mind when "matching" sample points that the a_0 term for $N = 1$ will be unequal to the a_0 term for $N = 2$. This is demonstrated in Table 1 for $N = 1, 2$, and 4 and $b = \pi/2$.

I. A PARTICULAR TWO-RATE CONFIGURATION

As with the analysis of closed-loop single-rate systems, the analysis of the multi-rate closed-loop case is configuration dependent. Here we treat a particularly simple two-rate configuration which can be analyzed without resorting to a switch decomposition format. A more complex example, which requires the use of vector switch decomposition, will be treated after the fundamentals of that technique have been reviewed in Section III.

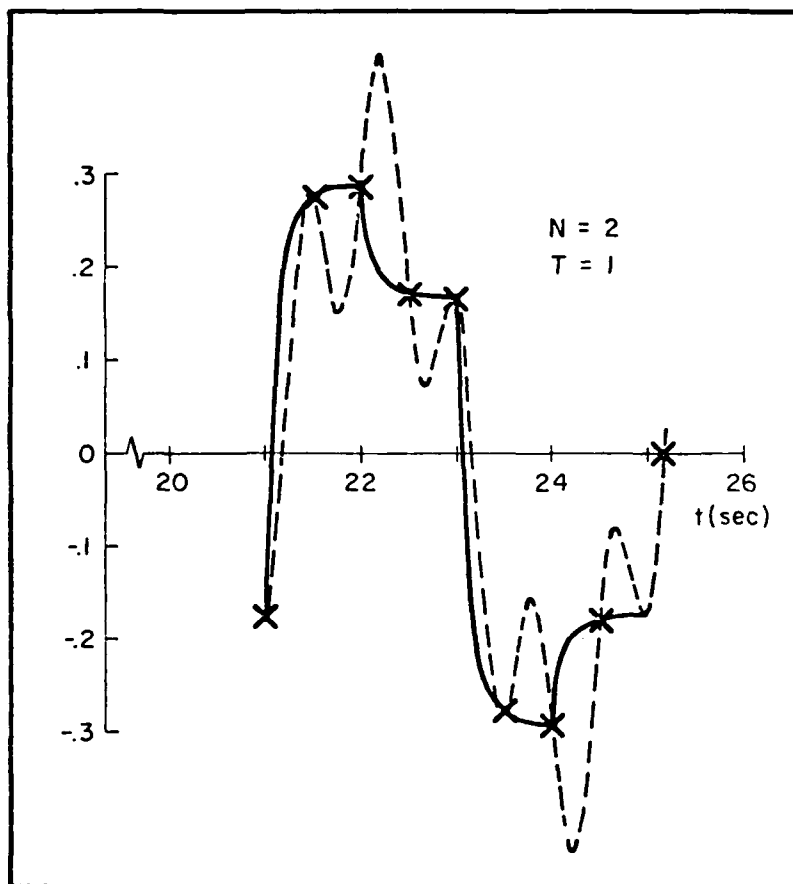


Figure 12. Steady-State Sinusoidal Components, $N = 2$

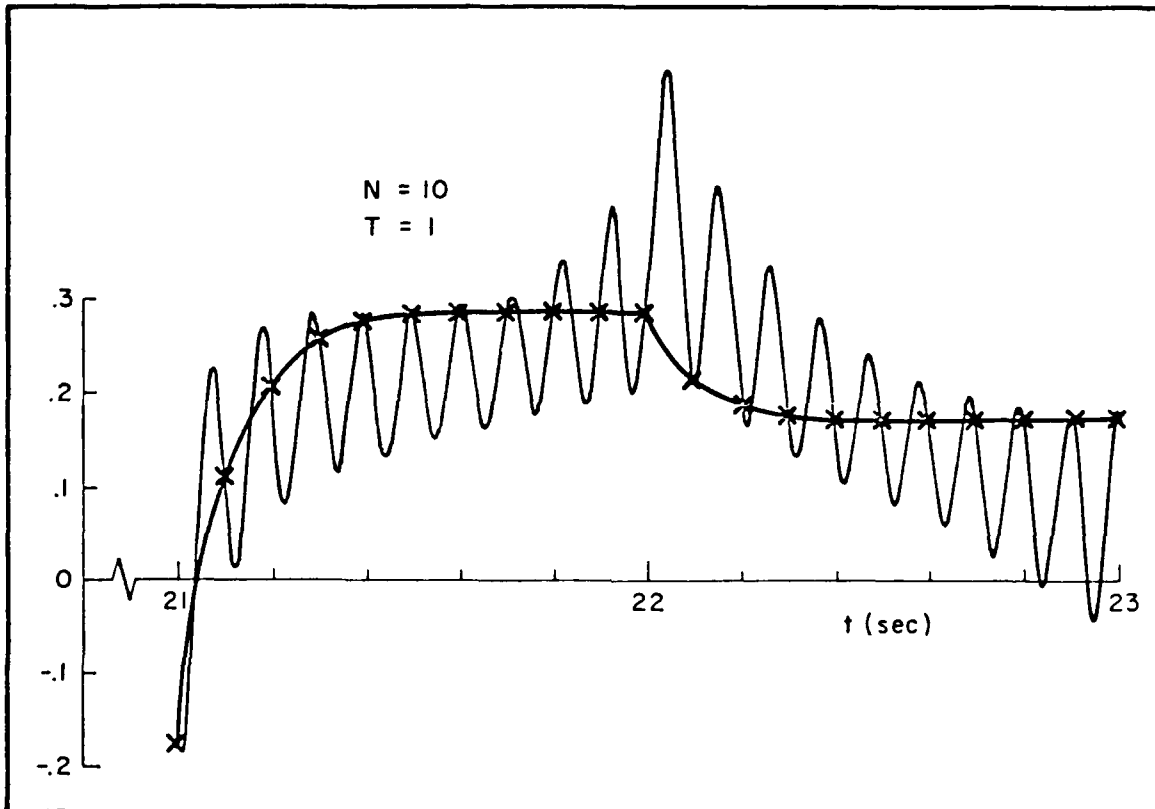


Figure 13. Steady-State Sinusoidal Components, $N = 10$, Half Period

TABLE 1. COMPONENT COEFFICIENTS $N = 1, 2, 4$

	$N = 1$	$N = 2$	$N = 4$
b	a_0 -0.174468021	a_0 -0.048579760	a_0 0.002998683
	b_0 -0.287649137	b_0 -0.306381976	b_0 -0.302606086
$b + \frac{2\pi}{T}$		a_1 -0.125888261	a_1 -0.046197029
		b_1 0.018732839	b_1 -0.043548018
$b + \frac{4\pi}{T}$			a_2 -0.051578443
			b_2 -0.003775889
$b + \frac{6\pi}{T}$			a_3 -0.079691232
			b_3 0.062280857

Consider the two-rate system shown in Figure 14. In Figure 14, W_1 and W_2 are compensation networks, M is a data hold, and G represents the open-loop system dynamics (consider these to be matrices of the proper dimensions).

The objective is to find the "frequency response" for the output vector C . As in the single-rate case, assume that C undergoes a phantom T/N sampling operation and then seek the limit as $N \rightarrow \infty$. From Figure 14:

$$C = GME^T/M \quad (63)$$

or

$$C^{T/N} = (GM)^T/N E^T/M, \quad N/M \text{ an integer} \quad (64)$$

The first task is to solve for $E^{T/M}$. This is non-trivial; the details must be followed with care.

$$E = W_1 R^T - W_1 W_2^T (GME^T/M)^T \quad (65)$$

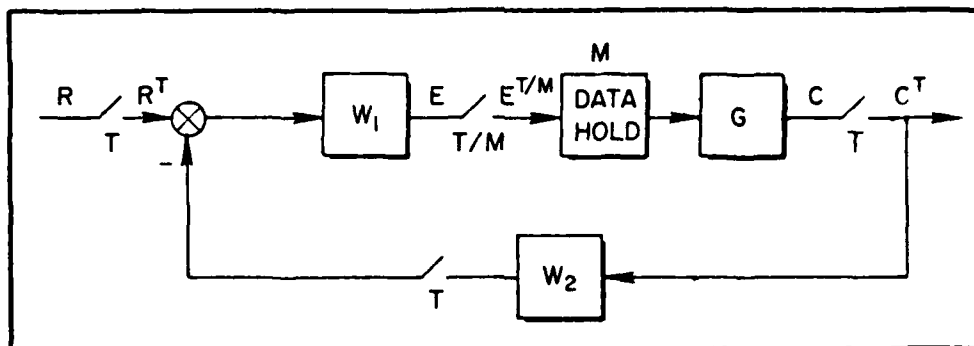


Figure 14. A Specific Two-Rate Closed-Loop Configuration

Therefore,

$$E^{T/M} = W_1^{T/M} R^T - W_1^{T/M} W_2^T (GME^{T/M})^T \quad (66)$$

Pre-multiply Equation 66 by GM and sample at a T interval.

$$(GME^{T/M})^T = (GMW_1^{T/M})^T R^T - (GMW_1^{T/M})^T W_2^T (GME^{T/M})^T \quad (67)$$

Solve Equation 67 for $(GME^{T/M})^T$:

$$(GME^{T/M})^T = [I + (GMW_1^{T/M})^T W_2^T]^{-1} (GMW_1^{T/M})^T R^T \quad (68)$$

Substitute Equation 68 into Equation 66 and clear through. The result is:

$$E^{T/M} = W_1^{T/M} \{ I - W_2^T [I + (GMW_1^{T/M})^T W_2^T]^{-1} (GMW_1^{T/M})^T \} R^T \quad (69)$$

For brevity, let

$$E^{T/M} = W_1^{T/M} G_A^T R^T \quad (70)$$

The evaluation of G_A^T is not elementary. For example, the $(GMW_1^{T/M})^T$ element of G_A^T will have to be computed using either switch decomposition or

the phantom sampler (Reference 1 or see the development of Section IV).
Via the phantom sampler,

$$(GMW_1^{T/M})^T \equiv [(GM)^T/MW_1^{T/M}]^T \quad (71)$$

To this point, the two-rate example yields

$$C^{T/N} = (GM)^T/NW_1^{T/M}G_A^T \quad (72)$$

and we see that the only new element added over the single-rate case is the addition of a term sampled on a T/M interval together with a constraint that N/M be an integer.

Let

$$z = e^{sT/N} \quad (73)$$

so that a unit amplitude sinusoidal input at b rad/sec has the transform

$$R^T = \frac{z^N \sin bT}{z^{2N} - (2 \cos bT)z^N + 1} \quad (74)$$

As in the single-rate case, substitute Equation 74 into Equation 72:

$$C^{T/N} = (GM)^T/NW_1^{T/M}G_A^T \frac{z^N \sin bT}{z^{2N} - (2 \cos bT)z^N + 1} \quad (75)$$

Again, the problem is in a recognizable form and we may proceed directly to the answer.

$$A_n + jP_n = \frac{1}{N} (GM)^T/NW_1^{T/M}G_A^T \Big|_{14\omega_n(T/N)} \quad (76)$$

Next, since the local definition of $z = e^{sT/N}$ is in effect, express $e^{sT} = (e^{sT/N})^N$ and write

$$G_A^T = G_A(z^N)$$

Therefore,

$$\begin{aligned} G_A(z^N) \Big|_{l\Delta\omega_n(T/N)} &= G_A[l\Delta\omega_n(T/N)]^N \\ &= G_A(l\Delta\omega_n T) = G_A(l\Delta b T) \end{aligned} \quad (77)$$

That is, take the "T" z-transform of G_A , and evaluate at $z = l\Delta b T$. Now, the "new" element, $W_1^{T/M}$:

$$W_1^{T/M} \triangleq W_1(z^{N/M}) \quad (78)$$

Therefore,

$$W_1(z^{N/M}) \Big|_{l\Delta\omega_n(T/N)} = W_1[l\Delta\omega_n(T/N)]^{N/M} \quad (79)$$

$$= W_1[l\Delta\omega_n(T/M)] \quad (80)$$

taking the "T/M" z-transform of W_1 and evaluating it at $z = l\Delta\omega_n(T/M)$.

At this point, only GM depends on N and we can go to the limit of $N \rightarrow \infty$.

$$A_n + jB_n = \frac{1}{N} \left[(GM)^{T/N} \begin{matrix} z^{\Delta} e^{sT/N} \\ z=l\Delta\omega_n(T/N) \end{matrix} \right] \left[W_1^{T/M} \begin{matrix} z^{\Delta} e^{sT/M} \\ z=l\Delta\omega_n(T/M) \end{matrix} \right] \left[G_A^T \begin{matrix} z=e^{sT} \\ z=l\Delta b T \end{matrix} \right] \quad (81)$$

This is the desired result for finite N (remember $N = M, 2M$, etc.).

As $N \rightarrow \infty$, the coefficients of the continuous spectrum are given by

$$A_n + jB_n = \frac{1}{T} (GM)_{s=j\omega_n} \left[W_1^{T/M} \begin{matrix} z^{\Delta} e^{sT/M} \\ z=l\Delta\omega_n(T/M) \end{matrix} \right] \left[G_A^T \begin{matrix} z^{\Delta} e^{sT} \\ z=l\Delta b T \end{matrix} \right] \quad (82)$$

$$n = 0, \pm 1, \pm 2, \dots$$

The algebraic manipulations used in this example circumvented the need for the use of a switch decomposition model by using the classic concept of a phantom sampler. The limitations of this type of algebraic manipulation will be discussed in more detail in Section V.

J. SECTION SUMMARY

The "sampled spectrum" concept of sampled data control theory is concerned with determining the single sinusoid which fits the output samples of a single-rate system at the sampling instants. In this section, we have reviewed the extension which encompasses the continuous spectrum of the continuous variables in a discretely controlled system. Moreover, the theory considers the finite N case wherein one is concerned with the group of N sinusoids that matches the data not only at the sample points but at $N-1$ inter-sample points as well. This is an important aspect since bench validation of digital hardware is often specified in terms of an end-to-end "frequency response." Since output data are taken at a finite number of points, it will be important to compute finite N results; the coefficients may differ significantly from the continuous ($N \rightarrow \infty$) values.

The results for the closed-loop cases have been configuration dependent; however, the basic technique is relatively clear. One starts at the continuous state vector and writes the system equations back to the first input point. The next fundamental step is to convert that input into an equation which contains the sinusoidal input as the basic forcing function. At this point, the basic equations which apply to the open-loop case can be used. A closed-loop two-rate case was discussed which did not require the use of switch decomposition. The limitations of the algebraic manipulations will be discussed more fully in Section V.

SECTION III

VECTOR SWITCH DECOMPOSITION AND A "SCALAR" APPROACH

A. INTRODUCTION

This section reviews vector switch decomposition, noting the dimensionality problems introduced by multiple frame times. This is followed by a brief discussion pertaining to a class of multi-rate problems which can be treated without recourse to switch decomposition. Several examples are then used to demonstrate the scalar algebraic manipulation required, establish the relationship between the scalar algebra and switch decomposition, and motivate the need for an algorithm which can be used to evaluate the various expressions that result. The algorithm itself is discussed in Section IV.

B. REVIEW OF SWITCH DECOMPOSITION

In essence, switch decomposition is a procedure wherein systems having multiple sampling operations (occurring at fixed but unequal sampling intervals but with a sampling pattern which is repeated over a fixed, finite time interval) are converted into an equivalent single sample rate format. As originally introduced by Kranc (Reference 3), the method used a summing point methodology that proved to be extremely cumbersome when the ratios of the sampling periods become high. For this reason, and because evolving state transition methods were tending to push transform methods into the background, the method fell into disuse. However, there is much to recommend the switch decomposition concept for use in both time domain and transform domain analyses. In the subsection that follows we will review the basic concept and remove some earlier restrictions by recasting it in vector form. The vector form simplifies matrix block diagram manipulation for multiloop, multi-rate sampled systems.

An example reveals the key ideas. Consider the continuous signal, shown in Figure 15a, to be sampled at $T/3$ samples per second. This results in the sample sequence shown in Figure 15b. The sampled values have been numbered for easy reference. Suppose we now sample the continuous signal with a sampling period T . This results in the sample sequence consisting of sample numbers 1, 4, 7, 10, 13, ... shown in Figure 15c. Define this sample sequence to be R^T .

Next, advance the continuous signal R by $T/3$. Then sample the advanced signal with a sampling period T . This results in a sample sequence consisting of sample numbers 2, 5, 8, 11, 14, ... shown in Figure 15d. Define this sample sequence to be $(e^{sT/3} R)^T$. Finally, advance the continuous signal R by $2T/3$ and sample it with a sampling period T . This results in the sequence consisting of sample numbers 3, 6, 9, 12, 15, ... shown in Figure 15e. Define this signal sequence to be $(e^{2sT/3} R)^T$.

The significance of the switch decomposition concept resides in its ability to provide an alternative expression for the original sequence $R^{T/3}$ in terms of several quantities which are each sampled simultaneously every T seconds. This alternative expression for $R^{T/3}$ consists of the sum of R^T , $(e^{sT/3} R)^T$, and $(e^{2sT/3} R)^T$:

$$R^{T/3} = R^T + (e^{sT/3} R)^T e^{-sT/3} + (e^{2sT/3} R)^T e^{-2sT/3} \quad (83)$$

Equation 83 has a simple factored equivalent that is the product of two vectors and the scalar R ,

$$R^{T/3} = \begin{bmatrix} 1, & e^{-sT/3}, & e^{-2sT/3} \end{bmatrix} \left\{ \begin{bmatrix} 1 \\ e^{sT/3} \\ e^{2sT/3} \end{bmatrix} R \right\}^T \quad (84)$$

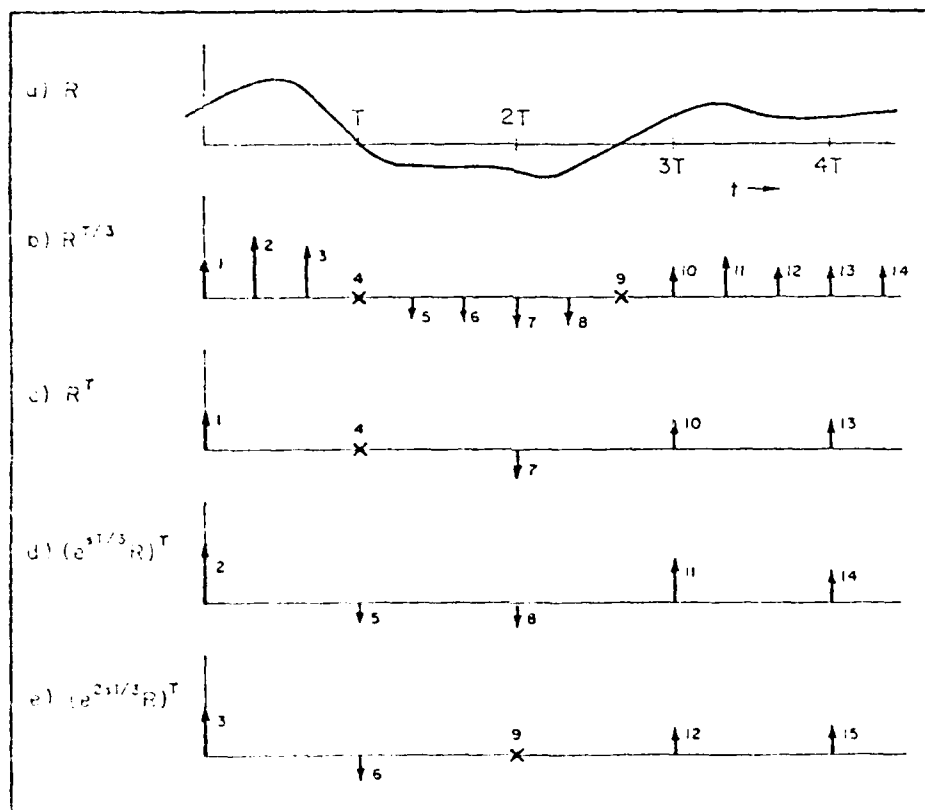


Figure 15. Decomposition of a Sample Sequence

Or, more compactly,

$$R^{T/3} = W(W_*R)^T \quad (85)$$

where

$$W = [1, e^{-sT/3}, e^{-2sT/3}] \quad (86)$$

and

$$W_* = \begin{bmatrix} 1 \\ e^{sT/3} \\ e^{2sT/3} \end{bmatrix} \quad (87)$$

C. EXTENSION TO THE VECTOR CASE

Further generalization allows R to be a vector of continuous signals. It is necessary to define a least common sampling period, T , and a greatest common subinterval, T_0 , with respect to the R vector. The p elements of R may be sampled at different minor sampling periods: $T_1, \dots, T_2, \dots, T_p$, respectively. It is further assumed that the minor sampling periods are such that a finite positive T exists such that

$$T = N_1 T_1 \dots = N_i T_i \dots = N_p T_p \quad (88)$$

holds for a set of finite positive integers:

$$N_1, \dots, N_i, \dots, N_p$$

The minimum T for which Equation 88 holds is the least common sampling period (for R). A subinterval can be found for which

$$T = NT_0 \quad (89)$$

and N/N_i is an integer for all $i = 1, 2, \dots, p$. The largest value of T_0 satisfying these conditions is the greatest common subinterval (for R). Equation 89 defines N for the greatest common subinterval. Given values for N, N_i, p , and T , the $p \times \infty$ block diagonal matrix, W , is

$$W = W(s) = \begin{bmatrix} W_1 & & & 0 \\ & W_2 & & \\ & & \ddots & \\ & & & W_1 & \ddots \\ 0 & & & & & W_p \end{bmatrix} \quad (90)$$

where

$$W_1 = [1 \ e^{-sT/N_1} \ \dots \ e^{-s(j-1)T/N_1} \ \dots \ e^{-s(N_1-1)T/N_1}] \quad (91)$$

The operator matrices W and W^* can be used to represent multi-rate sampling operations in terms of a single-rate sampling operator in vector block diagrams. This is illustrated in Figure 16.

Consider an example. Let R be a vector with three components. Let the first component be sampled with period $T/6$, the second with period $T/3$, and the third with period $T/2$, i.e.,

$$R^* = \begin{bmatrix} R_1^{T/6}, & R_2^{T/3}, & R_3^{T/2} \end{bmatrix} \quad (92)$$

The objective is to compute W in order to obtain an explicit expression for R^* via Equations 90 and 91 (which is equivalent to Figure 16). For this example,

$$p = 3$$

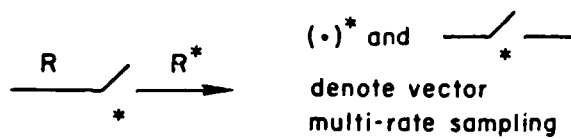
T is the least common sampling period

$$T_1 = T/6, \ T_2 = T/3, \ T_3 = T/2$$

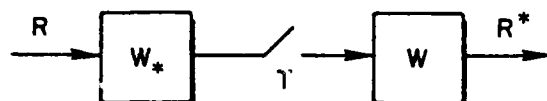
$$N_1 = 6, \ N_2 = 3, \ N_3 = 2$$

$T/6$ is the greatest common subinterval

$$N = 6$$



a) Vector Block Diagram for Multi-Rate Sampling



b) Equivalent Single Sample Rate Vector Block Diagram

Figure 16. Vector Block Diagrams for Multi-Rate Sampling Operations

Therefore

$$W = \begin{bmatrix} 1, e^{-sT/6}, e^{-2sT/6}, e^{-3sT/6}, & & \\ e^{-4sT/6}, e^{-5sT/6} & 0 & 0 \\ \hline 0 & 1, e^{-2sT/6}, e^{-4sT/6} & 0 \\ \hline 0 & 0 & 1, e^{-3sT/6} \end{bmatrix}$$

(93)

This example gives some insight as to how increased dimensionality can complicate problems in practical application. Consider the vectors R , R^* , and $(W \star R)^T$. These vectors have 3, 3, and 11 elements, respectively. The vector $(W \star R)^T$ will have pN_1 elements in general; whereas R and R^* will have only p elements each. This is significant in that analyses will tend to be conducted in terms of vectors like $(W \star R)^T$ in distinction to vectors like R^* . Consequently, the potential for expanded dimensionality in connection with analyses of multi-rate sampled problems is great. For example, consider a problem wherein there are two minor sampling periods, 39 ms and 40 ms. It is easy to verify that the dimensionality expansion factor, N , is 1560.

On the more positive side, matrix operations are routine. Consider the system shown in Figure 17. Once the vector multi-rate sampling operations in Figure 17a have been replaced by the switch decomposition equivalent (Figure 17b), analytical manipulations are routine:

$$E_1^T = (W_1 \star R)^T - (W_1 \star H W_2)^T (W_2 \star G W_1)^T E_1^T \quad (94)$$

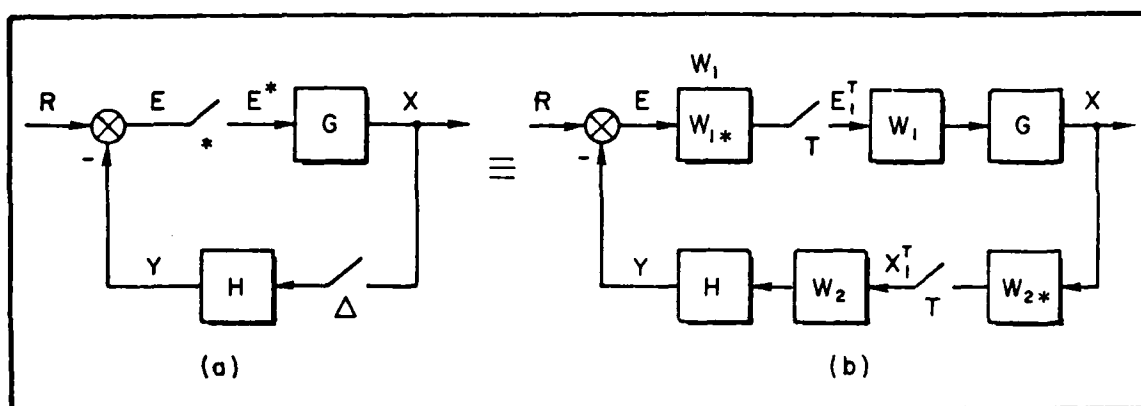


Figure 17. A Multi-Rate Closed-Loop System

Therefore

$$E_1^T = [I + (W_{1*}HW_2)^T(W_{2*}GW_1)^T]^{-1} (W_{1*}R)^T \quad (95)$$

and

$$X = GW_1 E_1^T \quad \text{or} \quad X^{T/N} = (GW_1)^{T/N} E_1^T \quad (96)$$

Notice that the dimension of the inverse in Equation 95 is determined by the column dimension of W_1 . If this dimensionality is high, and if the column dimension of W_2 is lower, then we can develop an alternate equation having lower dimension. The alternative equation is in terms of the X_1^T vector. The dimension in this case is determined by the column dimension of W_2 .

$$X_1^T = [I + (W_{2*}GW_1)^T(W_{1*}HW_2)^T]^{-1} (W_{2*}GW_1)^T(W_{1*}R)^T \quad (97)$$

$$X = GW_1 [(W_{1*}R)^T - (W_{1*}HW_2)^T X_1^T] \quad (98)$$

or

$$X^{T/N} = (GW_1)^{T/N} [(W_{1*}R)^T - (W_{1*}HW_2)^T X_1^T] \quad (99)$$

D. NONSYNCHRONOUS SAMPLING

Nonsynchronous sampling is a basic tool useful for modeling distributed computation architecture, data skewness in the A/D and D/A conversion processes as well as the internal computational delay of the digital computer. By definition, nonsynchronous sampling occurs when all the systems' sampling operations are repeated at the same rate but occur at different instants of time (refer to Figure 18).

In Figure 18 both continuous signals, x_1 and x_2 , are sampled at $1/T$ Hz, but the x_2 sampler is "out of sync" with the x_1 sampler by T_0 seconds. The sampling operation for x_1^T is shown symbolically in Figure 19a and for x_2^* in Figure 19b. (* notation on x_2 is used here to indicate an "unconventional" sampling operation.)

Figure 19b models the nonsynchronous sampler with a synchronous sampler by preceding the sampler with the operation W_* followed by the operator W , i.e.,

$$x_2^* = W(W_*x_2)^T \quad (100)$$

where

$$W = e^{-sT_0} \quad , \quad W_* = e^{sT_0} \quad (101)$$

Proceeding according to Equation 101, one advances x_2 by T_0 seconds, samples at the $1/T$ rate, and then delays $(W_*x_2)^T$ by T_0 seconds to obtain the time sequence (refer to Figure 20). Note how the nonsynchronous sampling operation on x_2 is modeled in terms of a scalar factor; thus the dimension of the equivalent single-rate sampled signal, $(W_*x_2)^T$, is not increased.

The model readily extends to the case where x is a vector.

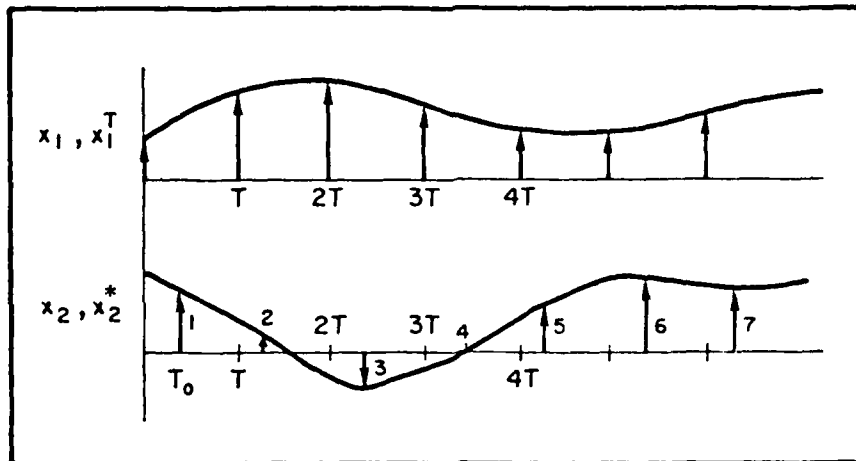


Figure 18. A Set on Non-Synchronously Sampled Signals

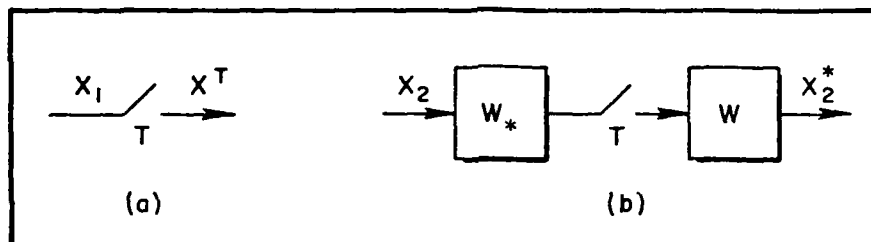


Figure 19. Sampling Notation

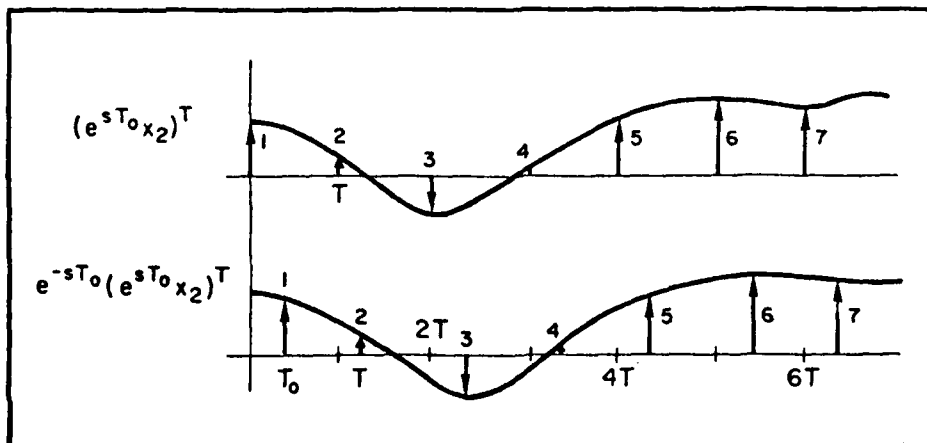


Figure 20. Advance, Sample, Delay

E. SPECIAL CASE

Consider Figure 21, a three-rate system without feedback.

$$C^{T/N_3} = [G_2(G_1 R^{T/N_1})^{T/N_2}]^{T/N_3} \quad (102)$$

$$= G_2^{T/N_3} G_1^{T/N_2} R^{T/N_1} \quad (103)$$

if N_3/N_2 and N_2/N_1 are integers. However, Equation 103 can, using the algorithm given in Section IV, be evaluated directly (for a given R) in the event that N_3/N_2 and N_2/N_1 do not satisfy the integer relationship. This is not the case for the feedback system of Figure 22.

$$E = R - G_2 [G_1 E^{T/N}]^{T/M} \quad (104)$$

If M/N is an integer, Equation 104 becomes

$$E = R - G_2 G_1^{T/M} E^{T/N}$$

which indicates

$$E^{T/N} = R^{T/N} - [G_2 G_1^{T/M}]^{T/N} E^{T/N} \quad (105)$$

Solve for the unknown

$$E^{T/M} = [I + (G_2 G_1^{T/M})^{T/N}]^{-1} R^{T/N}$$

using, for example, the algorithm given in the next section. If M/N is not an integer, one would be forced to cast Figure 22 in a vector switch (or some other equivalent state transition) format.

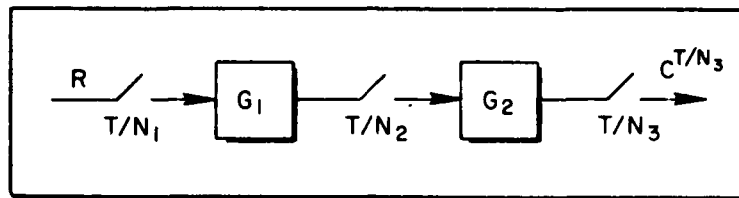


Figure 21. An Open-Loop Configuration

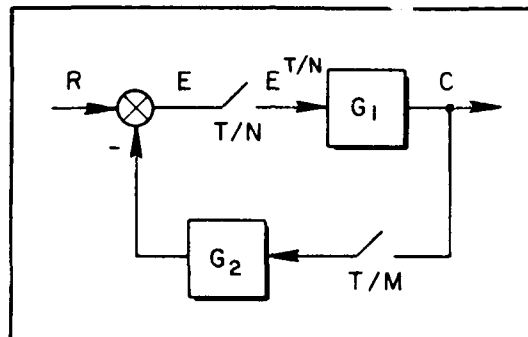


Figure 22. A Closed-Loop Configuration

In a like manner, if N/M is an integer, write

$$\begin{aligned} C &= G_1 [R - G_2 C^{T/M}]^{T/N} \\ &= G_1 R^{T/N} - G_1 G_2^{T/N} C^{T/M} \end{aligned}$$

giving

$$\begin{aligned} C^{T/M} &= [G_1 R^{T/N}]^{T/M} - [G_1 G_2^{T/N}]^{T/M} C^{T/M} \\ C^{T/M} &= [I + (G_1 G_2^{T/N})^{T/M}]^{-1} [G_1 R^{T/N}]^{T/M}, \quad N/M \text{ is an integer} \quad (106) \end{aligned}$$

To summarize, open-loop systems such as Figure 21 can in theory be analyzed without recourse to switch decomposition. Closed-loop systems,

on the other hand, require a fortuitous set of relationships among the frame times.

F. A PARTICULAR THREE-RATE CLOSED-LOOP SYSTEM

There is a natural tendency in the design of digital systems to select sampling ratios in powers of 2. This is probably due to the ease with which clock rates can be doubled (or halved). Such is the case of the three-rate digital controllers for the Shuttle (25, 50, 100 Hz) and the F-18 (20, 40, 80 Hz). It has been our experience that such systems can always be analyzed with operations such as those described in the previous section. For example, consider the closed-loop configuration of Figure 23. One may verify the following operations:

$$E = R - G_2[G_1 E^{T/2}]^T - G_3[G_1 E^{T/2}]^{T/4} \quad (107)$$

$$E = R - G_2[G_1 E^{T/2}]^T - G_3 G_1^{T/4} E^{T/2}$$

$$E^{T/2} = R^{T/2} - G_2^{T/2}[G_1 E^{T/2}]^T - [G_3 G_1^{T/4}]^{T/2} E^{T/2} \quad (108)$$

Therefore,

$$\begin{aligned} E^{T/2} &= [I + (G_3 G_1^{T/4})^{T/2}]^{-1} [R^{T/2} - G_2^{T/2}(G_1 E^{T/2})^T] \\ &= [\cdot]^{-1} R^{T/2} - [\cdot]^{-1} G_2^{T/2}[G_1 E^{T/2}]^T \end{aligned} \quad (109)$$

where

$$[\cdot] = [I + (G_3 G_1^{T/4})^{T/2}]$$

Equation 109 defines $E^{T/2}$ in terms of $R^{T/2}$ and $[G_1 E^{T/2}]^T$. Next, multiply Equation 109 by G_1 and solve for $[G_1 E^{T/2}]^T$:

$$[G_1 E^{T/2}]^T = [G_1 [\cdot]^{-1} R^{T/2}]^T - [G_1 [\cdot]^{-1} G_2^{T/2}]^T [G_1 E^{T/2}]^T$$

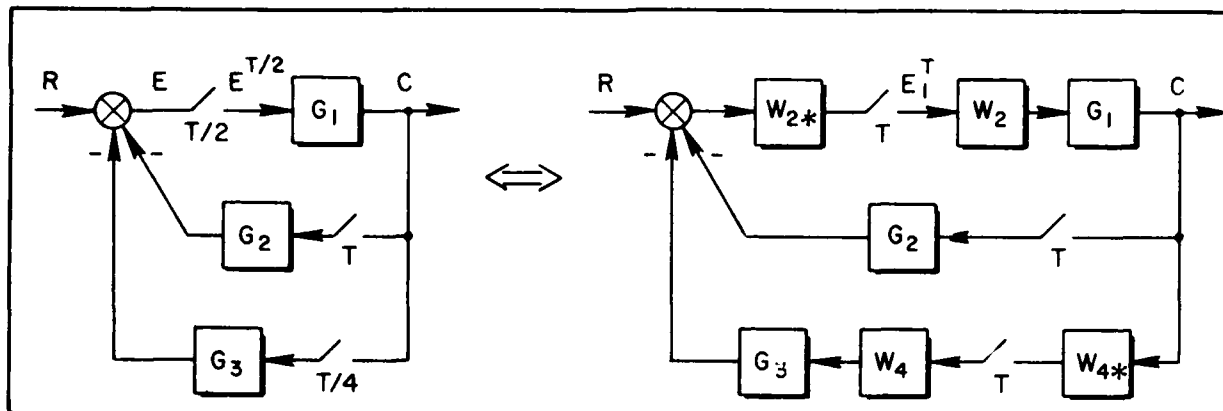


Figure 23. A Three-Rate Configuration; T, T/2, T/4

or

$$[G_1 E^{T/2}]^T = \{1 + [G_1(\cdot) - 1 G_2^{T/2}]^T\}^{-1} [G_1(\cdot) - 1 R^{T/2}]^T \quad (110)$$

Substituting Equation 110 into Equation 109, and using

$$C = G_1 E^{T/2}$$

gives the continuous output in terms of R. One may contrast the complexity of this algebra against the simplicity of switch decomposition. Since

$$C = G_1 W_2 E_1^T = G_1 E^{T/2} - E^{T/2} \quad (111)$$

one need solve only for E_1^T :

$$[I + (W_2^* G_2)^T (G_1 W_2)^T + (W_2^* G_3 W_4)^T (W_4^* G_1 W_2)^T] E_1^T = (W_2^* R)^T \quad (112)$$

Thus, a simple, straightforward block diagram manipulation gives the needed vector, E_1^T , essentially "by inspection":

$$E_1^T = [I + (W_2^* G_2)^T (G_1 W_2)^T + (W_2^* G_3 W_4)^T (W_4^* G_1 W_2)^T]^{-1} (W_2^* R)^T \quad (113)$$

The switch decomposition result, Equation 113, can be used directly to arrive at Equation 108. Premultiply Equation 112 by W_2 and "nest" the four terms. Two terms are obvious:

$$W_2 E_1^T \triangleq E^T/2$$

$$W_2(W_{2*}R)^T \triangleq R^T/2$$

The other two are slightly more laborious. For example:

$$\begin{aligned} (W_{2*}G_3W_4)^T(W_{4*}G_1W_2)^TE_1^T &= \left\{ \left[(W_{2*}G_3W_4)(W_{4*}G_1W_2)E_1^T \right]^T \right\}^T \\ &= \left\{ \left[(W_{2*}G_3W_4)(W_{4*}G_1E^T/2) \right]^T \right\}^T \\ &= \left\{ W_{2*}G_3[G_1E^T/2]^{T/4} \right\}^T \\ &= [W_{2*}G_3G_1^{T/4}E^T/2]^T \end{aligned}$$

but

$$W_2[W_{2*}G_3G_1^{T/4}E^T/2]^T \triangleq [G_3G_1^{T/4}E^T/2]^{T/2} = [G_3G_1^{T/4}]^{T/2} E^T/2 \quad (114)$$

A similar operation on $W_2(W_{2*}G_2)^T(G_1W_2)^TE_1^T$ gives the remaining terms of Equation 108. Specifically,

$$W_2(W_{2*}G_2)^T(G_1W_2)^TE_1^T \triangleq G_2^{T/2}[G_1E^T/2]^T \quad (115)$$

It can be appreciated that switch decomposition, coupled with the nesting operation, can be used (where appropriate) to generate a "scalar" alternative to the switch decomposition model. The use of the word scalar is in the sense that E_1^T is a 2×1 vector in Equation 113 whereas $E^{T/2}$ in Equation 108 and $[G_3G_1^{T/4}]^{T/2}$ in Equation 110 are scalars. The use of the "scalar" results implies the existence of an algorithm for evaluating terms like $[G_3G_1^{T/4}]^{T/2}$. Just such an algorithm is given in Section IV.

G. SECTION SUMMARY

Vector switch decomposition was reviewed from the viewpoint of multi-rate sampling. For particular configurations, it was demonstrated that an operational algebra could be used in lieu of switch decomposition and thus a scalar problem can retain a scalar format. It was conjectured that all open-loop configurations and those closed-loop systems wherein the frame times are ratioed as powers of 2 constitute a class of problems on which the operational algebra can be effectively applied. The algebra requires the evaluation of nested multi-rate operations such as $[G_3 G_1^{T/4}]^{1/2}$.

SECTION IV

A USEFUL ALGORITHM FOR THE ANALYSIS OF MULTI-RATE CONTROLLERS

A. INTRODUCTION

A prevalent trend in digital control systems design is the use of several computational frametimes. For example, both the F-18 and Space Shuttle have three-rate digital controllers (80, 40 and 20 Hz; 100, 50, 25 Hz). Moreover, it is not uncommon to find sophisticated simulations that use more than one computer, each one working in a different frame time (e.g., see the case study of Section IX). The purpose of this section is to present an algorithm which is useful for the analysis of such systems. Starting with a significant generalization of the "skip-sampling theorem," we first comment on the properties of the solution and from these deduce an algorithm for computing two-rate transfer functions. The algorithm requires only the use of synthetic division as the primary analytical tool. Therefore a host of problems associated with alternative methods are circumvented. The two-rate algorithm, when coupled with the generalized skip sampling theorem, expedites the analysis of multi-rate systems.

Examples are used to demonstrate the various properties of the method — perhaps the most important being that the algorithm treats both the so-called high-to-low and low-to-high rate cases, as limiting forms, within a single framework.

B. AN IMPORTANT IDENTITY

Of fundamental concern is the output for the system of Figure 24. As indicated, it is permissible to insert a phantom sampler between G and the T/M sampler if T/NK and T/M are presumed to be integer related. A slightly less general version of Figure 24 wherein $K = M$, is treated in References 1 and 2. Thus

$$C^{T/M} = [G^{T/N}]^{T/M} = [G^{T/NK} R^{T/N}]^{T/M} \quad (116)$$

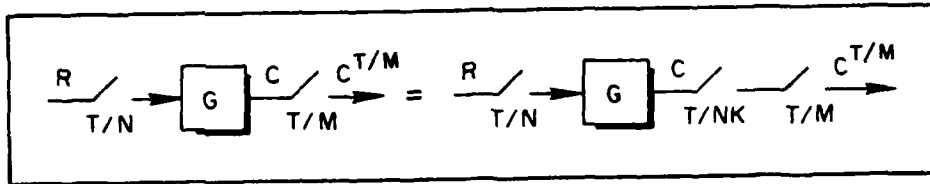


Figure 24. A Phantom Sampler Formulation of a T/N, T/M Sampling Format

where M and N are rational numbers. In Equation 116, the notation of Reference 3 is utilized. Specifically, $G^{[*]}$ designates the z transfer function in a $[*]$ timeframe. For example,

$$\left[\frac{1}{s+1} \right]^{T/2} = \frac{z}{z - e^{-T/2}}, \quad z = e^{sT/2} \quad (117)$$

Also, knowledge of routine operations such as

$$\begin{aligned} \left[\left[\frac{1}{s+1} \right]^{T/2} \right]^{T/6} &= \left[\frac{z}{z - e^{-T/2}} \right]_{z=e^{sT/2}}^{T/6} \\ &= \frac{z^3}{z^3 - e^{-T/2}}, \quad z = e^{sT/6} \end{aligned} \quad (118)$$

is presumed.

For the special case $M = 1$, $K = 1$, Figure 24 reduces to the well-known high-to-low rate transform (for example, see Reference 4).

To compute the entries of Equation 116 one may:

- 1) Determine R by table lookup.
- 2) Replace T by T/N.
- 3) Replace z (in R) with z^K .
- 4) Determine G by table lookup.

- 5) Replace T with T/NK .
- 6) z remains the same (in G).
- 7) Compute $C^{T/M}$ using Equation 119.

$$C^{T/M} = \frac{1}{2\pi j} \int_{\Gamma} G(p) R(p^K) \frac{z}{z - p^{NK/M}} \frac{dp}{p} \frac{dp}{p}, \quad \text{res} \frac{G(p)R(p^K)}{p} \quad (119)$$

In Equation 119, keep in mind the primary requirements; $z = e^{sT/NK}$, NK/M and K must be integers. This in turn requires M and N to be rational numbers. An example, using Figure 24, will clarify the details.

Example 1

Let

$$z = e^{sT/6}, \quad M = 3, \quad N = 2, \quad K = 3$$

$$G = \frac{1}{s+2}, \quad G^{T/6} = \frac{z}{z - e^{-T/3}}$$

$$R = \frac{1}{s+1}, \quad R^{T/2} = \frac{z^3}{z^3 - e^{-T/2}}$$

so that

$$\begin{aligned} C^{T/3} &= \left[\frac{z^4}{(z - e^{-T/3})(z^3 - e^{-T/2})} \right]^{T/3} \\ &= \frac{1}{2\pi j} \int_{\Gamma} \frac{p^4 z}{(p - e^{-T/3})(p^3 - e^{-T/2})(z - p^2)} \frac{dp}{p} \\ &= \frac{1}{2\pi j} \int_{\Gamma} \frac{p^3 z}{(p - e^{-T/3})(p^3 - e^{-T/6})(p^2 + e^{-T/6}p + e^{-2T/6})(z - p^2)} dp \\ &= \text{res} \Big|_{p=e^{-T/3}} + \text{res} \Big|_{p=e^{-T/6}} + \text{res} \Big|_{p=-e^{-T/6}(1/2)+je^{-T/6}(\sqrt{3}/2)} \\ &\quad + \text{res} \Big|_{p=-e^{-T/6}(1/2)-je^{-T/6}(\sqrt{3}/2)} \end{aligned} \quad (120)$$

The task is to evaluate four residues in the z -plane, even though both functions, in the s -plane, were only first order. Evaluating the four residues and placing the sum of the four terms over a common denominator gives

$$\begin{aligned} C^{T/3} &= \frac{z^2(z^2 + e^{-5T/6})}{(z - e^{-2T/3})(z - e^{-T/3})(z^2 + e^{-T/3}z + e^{-2T/3})} \\ &= \frac{z^4 + e^{-5T/6}z^3}{(z - e^{-2T/3})(z^3 - e^{-T})} \end{aligned} \quad (121)$$

Thus one starts with

$$G^{T/6} R^{T/2} = \frac{z^4}{(z - e^{-T/3})(z^3 - e^{-T/2})}, \quad z = e^{sT/6} \quad (122)$$

and finishes with

$$C^{T/3} = \frac{z^4 + e^{-5T/6}z^3}{(z - e^{-2T/3})(z^3 - e^{-T})}, \quad z = e^{sT/3} \quad (123)$$

leading to the following observations:

- 1) The poles of Equation 123 can be directly determined from an inspection of Equation 122 -- the root locations are squared since the ratio between the $T/6$ and $T/3$ frame times is 2.
- 2) The numerator of Equation 123 is fourth order -- one may adopt the viewpoint that the entire analytical effort expended on the evaluation of Equation 119 has the net effect of determining the five numerator coefficients of Equation 123 ($NUM = z^4 + e^{-5T/6}z^3 + 0z^2 + 0z + 0$).

C. OUTLINE OF A NEW PROCEDURE

The illustrative example suggests an alternative to evaluating the residues:

- 1) Determine the denominator polynomial in the new time frame (T/M) from a knowledge of the pole locations in the "old" timeframe (T/NK) utilizing NK/M as the ratio between the two.

- 2) Utilize the knowledge of the poles and zeros in the T/NK timeframe, together with awareness of the pole locations in the T/M timeframe, to generate the zeros in the T/M timeframe.

At this juncture Step 1 is clear enough but a definitive method for implementing Step 2 is needed. We shall demonstrate that matching the time responses of Equations 122 and 123 furnishes a computationally efficient method for implementing Step 2. Before proceeding to this step, the reader may find it advantageous to survey the examples of Appendix A, designed to provide insight into the setup of Equation 119 using Figure 24. In particular, note that both the classical "High-to-Low" and "Low-to-High" rate transforms are treated as limiting cases.

D. IMPULSE RESPONSE MATCHING

The implementation of Step 2 above by matching the impulse response is described next. Given an nth order "transfer function" in a T/N time frame, the transfer function in a T time frame can (computationally) be found by matching the impulse response. Let

$$G^{T/N} = \frac{NUM}{DEN} = a_n + \dots + a_{n-1}z^{-N} + \dots + a_{n-2}z^{-2N} + \dots + a_0z^{-nN} + \dots, \quad z = e^{sT/N} \quad (124)$$

where n is the order of the system and N defines the ratio between the time frames.

From Equation 124, form a vector composed of n + 1 terms from the successive Nth points in the T/N time frame transient response:

$$a = [a_n, a_{n-1}, \dots, a_0]' \quad (125)$$

Postulate a transfer function, in the T timeframe, in which the coefficients of the denominator are known but the numerator coefficients are

not. Nothing essential is lost by setting the denominator lead coefficient to unity.

$$G^T = \frac{c_n z^n + c_{n-1} z^{n-1} + \dots + c_0}{z^n + b_{n-1} z^{n-1} + \dots + b_0} \quad (126)$$

A vector "b" can be formed from the known coefficients of the denominator,

$$b = [1, b_{n-1}, b_{n-2}, \dots, b_0]' \quad (127)$$

Let the vector "c" represent the unknown coefficients of the numerator:

$$c = [c_n, c_{n-1}, c_{n-2}, \dots, c_0]' \quad (128)$$

The solution for "c", deduced from equating the partial fraction expansion of Equation 126 to the correct temporal terms of Equation 124, is

$$\begin{bmatrix} c_n \\ c_{n-1} \\ c_{n-2} \\ c_{n-3} \\ \vdots \\ \vdots \\ \vdots \\ c_0 \end{bmatrix} = \begin{bmatrix} a_n & 0 & 0 & & \\ a_{n-1} & a_n & 0 & 0 & \\ a_{n-2} & a_{n-1} & a_n & & \\ a_{n-3} & a_{n-2} & a_{n-1} & & \\ \vdots & \vdots & \vdots & \ddots & \\ \vdots & \vdots & \vdots & & \\ \vdots & \vdots & \vdots & & \\ a_0 & a_1 & a_2 & \dots & a_n \end{bmatrix} \begin{bmatrix} 1 \\ b_{n-1} \\ b_{n-2} \\ b_{n-3} \\ \vdots \\ \vdots \\ \vdots \\ b_0 \end{bmatrix} \quad (129)$$

To show this, observe that z^{-N} from the old time frame is z^{-1} in the new time frame, and form

$$z^n + b_{n-1}z^{n-1} + b_{n-2}z^{n-2} + \dots + b_0 \sqrt{\begin{matrix} a_n + a_{n-1}z^{-1} + a_{n-2}z^{-2} + \dots + a_0z^{-n} + \dots \\ c_n z^n + c_{n-1}z^{n-1} + c_{n-2}z^{n-2} + \dots + c_0 \end{matrix}}$$

a_n	$a_n b_{n-1}$	$a_n b_{n-2}$	$a_n b_0$
$c_{n-1} - a_n b_{n-1}$	$\cdot \cdot \cdot$	$\cdot \cdot \cdot$	$\cdot \cdot \cdot$
a_{n-1}	$\cdot \cdot \cdot$	$\cdot \cdot \cdot$	$\cdot \cdot \cdot$

(130)

Equating terms gives

$$\begin{aligned} c_n - a_n &= 0 \\ c_n &= a_n \end{aligned} \tag{131}$$

The first division gives

$$c_{n-1} - a_n b_{n-1} = a_{n-1} \tag{132}$$

or

$$c_{n-1} = a_{n-1} + a_n b_{n-1}$$

A second division yields

$$\begin{aligned} c_{n-2} - a_n b_{n-2} - a_{n-1} b_{n-1} &= a_{n-2} \\ c_{n-2} &= a_{n-2} + a_{n-1} b_{n-1} + a_n b_{n-2} \end{aligned} \tag{133}$$

Continuing for n divisions yields the final result, which can be placed in the matrix form of Equation 129. Several examples are given to clarify the details.

Example 2 (a simple check case)

Let

$$c^{T/3} = \frac{z}{z - .9} = 1 + .9z^{-1} + .81z^{-2} + .729z^{-3} + \dots, \quad z = e^{sT/3} \tag{134}$$

Therefore

$$a = [1 \quad .729]$$

The denominator, in the T timeframe, is

$$z - .729 \Rightarrow b = [1 \quad -.729]$$

Evaluating Equation 129:

$$\begin{bmatrix} c_1 \\ c_0 \end{bmatrix} = \begin{bmatrix} 1 & 0 \\ .729 & 1 \end{bmatrix} \begin{bmatrix} 1 \\ -.729 \end{bmatrix} = \begin{bmatrix} 1 \\ 0 \end{bmatrix} \Rightarrow C^T = \frac{z}{z - .729} \quad (135)$$

Example 3

If

$$\begin{aligned} C^{T/2} &= \frac{z^2}{(z-1)(z-2)} \\ &= 1 + 3z^{-1} + 7z^{-2} + 15z^{-3} + 31z^{-4} + \dots \end{aligned} \quad (136)$$

let

$$C^T = \frac{c_2 z^2 + c_1 z + c_0}{(z-1)(z-4)} = \frac{c_2 z^2 + c_1 z + c_0}{z^2 - 5z + 4}$$

Therefore

$$\begin{bmatrix} c_2 \\ c_1 \\ c_0 \end{bmatrix} = \begin{bmatrix} 1 & 0 & 0 \\ 7 & 1 & 0 \\ 31 & 7 & 1 \end{bmatrix} \begin{bmatrix} 1 \\ -5 \\ 4 \end{bmatrix} = \begin{bmatrix} 1 \\ 2 \\ 0 \end{bmatrix} \Rightarrow C^T = \frac{z(z+2)}{(z-1)(z-4)} \quad (137)$$

Example 4

Let

$$\begin{aligned} G^{T/4} &= \frac{z^2 - 4z + 6}{(z - 2)(z^2 - 2z + 2)} = \frac{z^2 - 4z + 6}{z^3 - 4z^2 + 6z - 4} \\ &= 0 + z^{-1} + 0z^{-2} + 0z^{-3} + 4z^{-4} + 16z^{-5} + 40z^{-6} + 80z^{-7} \\ &\quad + 144z^{-8} + 256z^{-9} + 480z^{-10} + 960z^{-11} + 1984z^{-12} + \dots \end{aligned} \quad (138)$$

Since $z^2 - 2z + 2 = [(z - 1)^2 + (1)^2]$, the T timeframe roots are

$$p = 1 + j = \sqrt{2} \angle 45^\circ \Rightarrow p^4 = 4 \angle 180 = -4 + j0$$

$$p = 1 - j = \sqrt{2} \angle -45^\circ \Rightarrow p^4 = 4 \angle -180 = -4 + j0$$

Therefore the denominator, in the T timeframe, is

$$(z - 2^4)(z + 4)(z + 4) = z^3 - 8z^2 - 112z - 256$$

Setting

$$C^T = \frac{c_3 z^3 + c_2 z^2 + c_1 z + c_0}{z^3 - 8z^2 - 112z - 256}$$

one may write

$$\begin{bmatrix} c_3 \\ c_2 \\ c_1 \\ c_0 \end{bmatrix} = \begin{bmatrix} 0 & 0 & 0 & 0 \\ 4 & 0 & 0 & 0 \\ 144 & 4 & 0 & 0 \\ 1984 & 144 & 4 & 0 \end{bmatrix} \begin{bmatrix} 1 \\ -8 \\ -112 \\ -256 \end{bmatrix} = \begin{bmatrix} 0 \\ 4 \\ 112 \\ 384 \end{bmatrix}$$

Summarizing the example, it is seen

$$c^{T/4} = \frac{z^2 - 4z + 6}{(z - 2)(z^2 - 2z + 2)} \Big|_{z=e^{sT/4}} \Rightarrow c^T = \frac{4z^2 + 112z + 384}{(z - 16)(z + 4)^2}$$

or

$$c^T = \frac{4z + 96}{(z - 16)(z + 4)} \Big|_{z=e^{-sT}}$$

(139)

We conclude the examples by revisiting Example 1.

Example 5

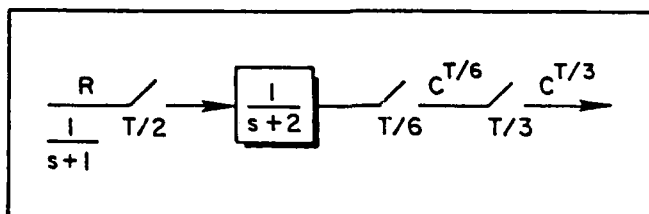


Figure 25. Example 5 (and 1) Block Diagram

From Figure 25,

$$c^{T/3} = \left[\left(\frac{1}{s+2} \right)^{T/6} \left(\frac{1}{s+1} \right)^{T/2} \right]^{T/3} = \left[\frac{z}{(z - e^{-2T/6})} \frac{z^3}{(z^3 - e^{-T/2})} \right]^{T/3}$$

or

$$\begin{aligned}
 c_{T/6} &= \frac{z^4}{z^4 - e^{-T/3}z^3 - e^{-T/2}z + e^{-5/6T}} \\
 &= 1 + e^{-T/3}z^{-1} + e^{-2T/3}z^{-2} + \dots \\
 c_{T/3} &= \frac{c_4z^4 + c_3z^3 + c_2z^2 + c_1z + c_0}{(z - e^{-2T/3})(z^3 - e^{-T})}
 \end{aligned} \tag{140}$$

A tedious but straight forward exercise gives

$$\begin{bmatrix} c_4 \\ c_3 \\ c_2 \\ c_1 \\ c_0 \end{bmatrix} = \begin{bmatrix} a_4 & 0 & 0 & 0 & 0 \\ a_3 & a_4 & 0 & 0 & 0 \\ a_2 & a_3 & a_4 & 0 & 0 \\ a_1 & a_2 & a_3 & a_4 & 0 \\ a_0 & a_1 & a_2 & a_3 & a_4 \end{bmatrix} \begin{bmatrix} 1 \\ -e^{-2T/3} \\ 0 \\ -e^{-T} \\ e^{-5T/3} \end{bmatrix} = \begin{bmatrix} 1 \\ 0 \\ e^{-5T/6} \\ 0 \\ 0 \end{bmatrix} \tag{141}$$

where

$$\begin{aligned}
 a &= [a_4, a_3, a_2, a_1, a_0]' \\
 &= [1, e^{-2T/3}, e^{-4T/3} + e^{-5T/6}, e^{-T} + e^{-2T} + e^{-3T/2}, \\
 &\quad e^{-5T/3} + e^{-8T/3} + e^{-13T/6}]'
 \end{aligned} \tag{142}$$

E. SECTION SUMMARY

The system of Figure 24 can be evaluated using Equation 119, which is, in itself, a significant generalization of the "skip-sampling theorem." In particular, M and N need only be rational numbers. This relaxed requirement on M and N permits the treatment, as limiting cases, of the so called High-to-Low and Low-to-High rate transforms within the same framework. These points are called out in Appendix A.

Once set up via Equation 119, the problem reduces to the evaluation of

$$C^{T/M} = [C^{T/NK}]^{T/M}$$

One may avoid using residue theory by doing a powers series expansion of $C^{T/NK}$ and equating the NK/M spaced points in the T/NK timeframe to the appropriate temporal points in the T/M time frame. This leads to a closed-form solution for the $C^{T/M}$ numerator coefficients. In this regard, it is important to appreciate that the poles of $C^{T/M}$ can be obtained from the known poles of $C^{T/NK}$ "by inspection."

The combination of the generalized skip-sampling algorithm and impulse response matching eases significantly the computational burden encountered in the analysis of multi-rate systems.

SECTION V

MULTI-RATE FREQUENCY RESPONSE: SWITCH DECOMPOSITION CONTRASTED WITH SCALAR ANALYSIS

A. INTRODUCTION

Vector switch decomposition, discussed in Section III, provides a general framework for the frequency response of multi-rate systems (References 1, 2). However, the dimensionality problems associated with switch decomposition encourage the development of a separate theory for the class of systems discussed in Section III. We first review the generally applicable multi-rate frequency response (as presented in Reference 2) in order to make the additional dimensionality problems clear. Following this, a less general method is developed. This "scalar" method is applicable to the class of problems discussed in Subsection E of Section III and will be applied to the simulation case studies of Sections VIII and IX.

B. REVIEW OF MULTI-RATE FREQUENCY RESPONSE, SWITCH DECOMPOSITION MODEL

Let the general multi-rate/multiple-order open-loop system of Figure 26 have a sine wave input. In Figure 26,

$$C_1^\beta = (G_1 R^\alpha)^\beta \quad (143)$$

$$C^{T/N} = [G(G_1 R^\alpha)^\beta]^{T/N} \quad (144)$$

where α , β represent sampling schemes with a basic period of T seconds. For example, α might represent a multiple-order sampling format; β might represent a multi-rate and/or pseudo measurement format (see Reference 2).

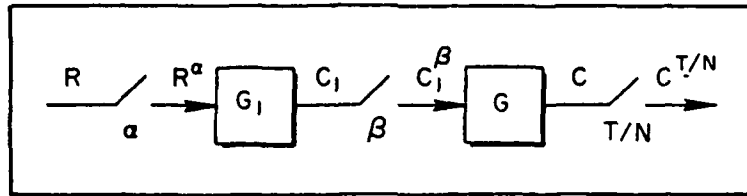


Figure 26. Multi-Rate/Multiple-Order Open-Loop System

Using switch decomposition, Figure 26 takes on the representation of Figure 27. Clearly,

$$C_1^\beta = W_2(W_{2*}G_1W_1)^T(W_{1*}R)^T \quad (145)$$

and

$$C^{T/N} = (GW_2)^{T/N} (W_{2*}G_1W_1)^T (W_{1*}R)^T \quad (146)$$

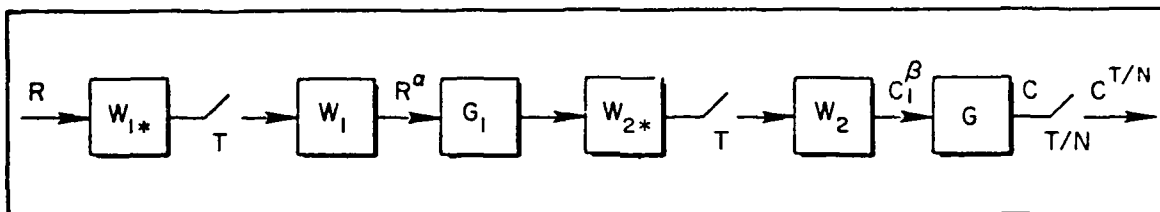


Figure 27. Open-Loop System with Switch Decomposition

If α represents multiple-order sampling and β a pseudo measurement format using multi-rate sampling, the switch decomposition modeling components might appear as:

$$W_1 = [1, e^{-T_0 s}, e^{-T_1 s}, e^{-T_2 s}] \quad (147)$$

$$W_{1*} = \begin{bmatrix} 1 \\ e^{T_0 s} \\ e^{T_1 s} \\ e^{T_2 s} \end{bmatrix} \quad (148)$$

and

$$W_2 = \hat{W}_2 = \begin{bmatrix} 1 & 0 & 0 \\ 0 & e^{-sT/3} & 0 \\ 0 & 0 & e^{-2sT/3} \end{bmatrix} \quad (149)$$

$$W_{2*} = \begin{bmatrix} 1 \\ e^{sT/3} \\ e^{2sT/3} \end{bmatrix} \quad (150)$$

Comparing Equation 146 with Equation 13, we see that only one new facet has entered the problem, namely $(W_{1*} R)^T$ replaces R^T . Consider, therefore, a generic component of $(W_{1*} R)^T$ — for instance the scalar $(e^{\Delta T s} R)^T$, where $0 < \Delta < 1.0$.

For $R = \sin bt$ and Δ zero ($e^{\Delta T s} = 1$), the output equation (Equation 146) becomes

$$C^T/N = (GW_2)^{T/N} (W_{2*} G_1 W_1)^T \frac{z^N \sin bT}{z^{2N} - (2 \cos bT)z^N + 1}, \quad z = e^{sT/N} \quad (151)$$

where R^T is described in terms of a N/T samples per second model. For the sake of brevity write Equation 151 as

$$C^{T/N} = G_A^{T/N} G_B^T \frac{z^N \sin bT}{z^{2N} - (2 \cos bT)z^N + 1} \quad (152)$$

Expand the right-hand side of Equation 152 in partial fractions:

$$C^{T/N} = \sum_{n=0}^{N-1} \frac{A_n z \sin \omega_n(T/N) + B_n z [z - \cos \omega_n(T/N)]}{z^2 - [2 \cos \omega_n(T/N)]z + 1} + [\text{Terms due to modes of } G_A^{T/N} G_B^T] \quad (153)$$

For non-zero Δ , we use the advanced z-transform on $(e^{\Delta Ts} R)^T$ and Equation 153 becomes

$$C^{T/N} = G_A^{T/N} G_B^T \frac{z^N \{(\sin b\Delta T)z^N + \sin [b(1 - \Delta)T]\}}{z^{2N} - (2 \cos bT)z^N + 1} \quad (154)$$

Assume that responses in the modes of $G_A^{T/N} G_B^T$ approach zero as $t \rightarrow \infty$, i.e., that all modes are stable. In Equations 153 and 154

$$\omega_n = b + \frac{2\pi n}{T}, \quad n = 0, 1, 2, \dots, N-1$$

(or one may prefer the $n = 0, \pm 1$, etc., definitions of Section II). The steady-state waveform, at the sampling instants, can be written as

$$C(t)^{T/N} = \left[\sum_{n=0}^{N-1} (A_n \sin \omega_n t + B_n \cos \omega_n t) \right]^{T/N} \quad (155)$$

At this point, pursue the analysis of Section II keeping in mind that the only difference resides in the use of an advanced z-transform for the sine wave input. The analysis proceeds down to the equivalent point of Equation 152 where a division by $z \sin \omega_k(T/N)$ and replacement of k

with n occurs. At this point we pick up the development and find the limiting form:

$$A_n + jB_n = G_A^{T/N} G_B^T \Big|_{z=1 \pm j\omega_n(T/N)} \frac{z^{N-1} \{(\sin b\Delta T)z^N + \sin b(1-\Delta)T\}}{\sin \omega_n(T/N)} \frac{z^2 - [2 \cos \omega_n(T/N)]z + 1}{z^{2N} - (2 \cos bT)z^{N+1}} \Big|_{z=1 \pm j\omega_n(T/N)} \quad (156)$$

Evaluating Equation 156 at $z = 1 \pm j\omega_n(T/N)$ produces

$$A_n + jB_n = G_A^{T/N} G_B^T \Big|_{z=1 \pm j\omega_n(T/N)} \times \left\{ \frac{\{ \sin b\Delta T (\cos \omega_n T + j \sin \omega_n T) + \sin b(1-\Delta)T \} \times [\cos \omega_n(T/N) + j \sin \omega_n(T/N) - \cos \omega_n(T/N)]}{[\sin \omega_n(T/N)]N[\cos \omega_n T + j \sin \omega_n T - \cos bT]} \right\} \quad (157)$$

Simplifying Equation 157 gives

$$\begin{aligned} A_n + jB_n &= G_A^{T/N} G_B^T \Big|_{z=1 \pm j\omega_n(T/N)} \cdot \frac{(\sin b\Delta T)(\cos \omega_n T) + \sin b(1-\Delta)T + j(\sin \omega_n T)(\sin b\Delta T)}{N \sin b} \\ &= G_A^{T/N} G_B^T \Big|_{z=1 \pm j\omega_n(T/N)} \cdot \frac{\sin bT \cos b\Delta T + j \sin \omega_n T \sin b\Delta T}{N \sin bT} \\ &= G_A^{T/N} G_B^T \Big|_{z=1 \pm j\omega_n(T/N)} \cdot \frac{\cos b\Delta T + j \sin b\Delta T}{N} \\ &= G_A^{T/N} G_B^T \Big|_{z=1 \pm j\omega_n(T/N)} \cdot \frac{e^{jb\Delta T}}{N} = \frac{G_A^{T/N} G_B^T}{N} \Big|_{z=1 \pm j\omega_n(T/N)} \cdot e^{\Delta sT} \Big|_{s=jb} \end{aligned} \quad (158)$$

Thus, the only new element added is the factor $e^{\Delta s T}$ evaluated at the input frequency. Since Δ is generic, we draw the same conclusion for every other element of $(W_{1*} R)^T$ and hence arrive at the final steady state result:

$$C^T/N = (GW_2)^{T/N} (W_{2*} G_1 W_1)^T (W_{1*} R)^T = \left[\sum_{n=0}^{N-1} (A_n \sin \omega_n t + B_n \cos \omega_n t) \right]^T$$

where

$$A_n + jB_n = \frac{(GW_2)^{T/N}}{N} \left|_{z=l\omega_n(T/N)}^{z=e^{sT/N}} (W_{2*} G_1 W_1)^T \right|_{\substack{z=l\omega_n T \\ \text{or} \\ z=l\omega_n bT}}^{z=e^{sT}} W_{1*} \Big|_{s=jb} \quad (159)$$

$$\omega_n = b + \frac{2\pi n}{T}, \quad n = 0, 1, \dots, N-1 \quad (160)$$

Letting $N \rightarrow \infty$ gives the "continuous" result

$$A_n + jB_n = \frac{GW_2}{T} \Big|_{s=j\omega_n} (W_{2*} G_1 W_1)^T \Big|_{\substack{z=l\omega_n T \\ \text{or} \\ z=l\omega_n bT}}^{z=e^{sT}} W_{1*} \Big|_{s=jb} \quad n=0, \pm 1, \pm 2, \dots \quad (161)$$

In Equations 159 and 161, an option exists with regard to $(W_{2*} G_1 W_1)^T$ as it may be evaluated at either $l\omega_n T$ or $l\omega_n bT$. However, there is no option with regard to W_{1*} since it must be evaluated at $s = jb$. Clearly, the most efficient procedure is to evaluate $(W_{2*} G_1 W_1)^T$ at $z = l\omega_n bT$ and W_{1*} at $s = jb$, save the result in a polar format, and then evaluate $(GW_2/N)^{T/N}$ -- or GW_2/T -- over the appropriate range of n .

It can be appreciated that the results of Section II are contained in Equations 159 and 161, since Section II considers only the special case of $W_{1*} = 1.0$ (a scalar). Also, note that W_1 and W_2 are symbolic representations that can represent either multi-rate or multiple-order sampling formats (see for example, Reference 2). However, in arriving

at the spectrum of the continuous variable, uniformly spaced time samples in a T/N time frame were used.

C. A CLOSED-LOOP APPLICATION

The ability to cast any multi-rate or multiple-order sampling sequence into a switch decomposition format makes the analysis of closed-loop systems a straightforward task. Consider the system of Figure 28. Proceed as in the single-rate case. Since $C = G_1 W_1 E^T$, one must first solve for E^T :

$$E^T = (W_{1*}R)^T - (W_{1*}G_2W_2)^T(W_{2*}G_1W_1)^T E^T \quad (162)$$

or

$$E^T = [I + (W_{1*}G_2W_2)^T(W_{2*}G_1W_1)^T]^{-1}(W_{1*}R)^T \quad (163)$$

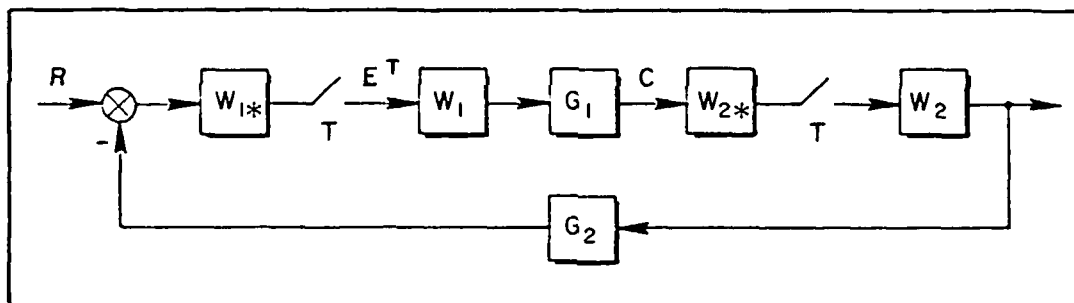


Figure 28. Closed-Loop System with Switch Decomposition

Therefore

$$CT/N = (G_1W_1)^T/N [I + (W_{1*}G_2W_2)^T(W_{2*}G_1W_1)^T]^{-1} (W_{1*}R)^T \quad (164)$$

The coefficients for the steady-state waveform are then

$$A_n + jB_n = \frac{G_1 W_1}{T} \bigg|_{s=j\omega_n} [I + (W_1^* G_2 W_2)^T (W_2^* G_1 W_1)^T]^{-1} \bigg|_{\substack{z=e^{sT} \\ z=1 \pm j\omega_n T \\ \text{or } z=1 \pm j\omega_n T}} W_1^* \bigg|_{s=j\omega_n} \quad (165)$$

$n = 0, \pm 1, \pm 2, \dots$

Section IV of Reference 2 gives a detailed example on the interpretation of Equation 165 and we will not repeat it here. However, an important point made in Reference 2 will be re-emphasized here — namely the presence of $W_1^* \big|_{s=j\omega_n}$ forces the use of "multiple Bode plots", one for each component of W_1^* . This is yet another facet of the dimensionality problems associated with switch decomposition.

For a particular class of problem (discussed in Section III), the dimensionality problems can be avoided by using a more direct approach which follows.

D. A DIRECT APPROACH

As pointed out in Section III, open-loop systems and a class of closed-loop multi-rate systems can be analyzed without recourse to switch decomposition. Such is the case with the generic system of Figure 29.

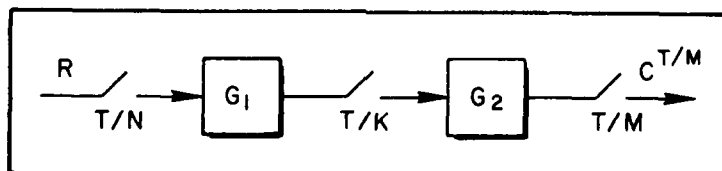


Figure 29. A Three-Rate Scalar Configuration

Clearly,

$$C^{T/M} = \{G_2 [G_1 R^{T/N}]^{T/K}\}^{T/M} \quad (166)$$

It would be fortuitous indeed for the ratios of N, K, M to be such that all the operators in Equation 166 "operated" through. However, knowing that N, K, and M are rational, one may use the algorithm of the previous section to evaluate

$$G_A^{T/K} = [G_1 R^{T/N}]^{T/K} \quad (167)$$

The poles of $R^{T/N}$, in a T/N time frame, will survive intact in the T/K time frame, indicating that the input R can be "tracked" through the T/N and T/K operations. In a like manner

$$C^{T/M} = \{G_2 G_A^{T/K}\}^{T/M} \quad (168)$$

can be evaluated and the poles of R, in a T/M time frame, can be clearly identified. This suggests a possible method for avoiding the switch decomposition frequency response by factoring out a sine wave in the T/M time frame, thus placing the investigator in a position to apply single-rate frequency response results directly. This viewpoint is flawed, as can be appreciated by studying a particular case. Suppose K/N is an integer and M/K is an integer. Equation 166 becomes

$$C^{T/M} = G_2^{T/M} G_1^{T/K} R^{T/N} \quad (169)$$

and clearly the poles of R appear, in the T/M time frame ($z = e^{sT/M}$) in terms of $z^{M/N}$, i.e.,

$$z^2 - 2 \cos(bT/N)z + 1 \Rightarrow z^{2M/N} - 2 \cos(bT/N)z^{M/N} + 1 \quad (170)$$

Thus, the frequency response of $C^{T/M}$ requires M/N sinusoids in order to match the output samples in a T/M time frame. That is, one sine wave, in a T/M time frame, is not a sufficient descriptor of the sampled T/M steady state waveform.

One may obtain a consistent evaluation for the spectral content of the output, in the context of generating the minimum set of sinusoids which will exactly match the output samples, by careful use of the generalized skip-sampling theorem developed in Section IV. We will use

examples to demonstrate the methodology and proceed to discuss a definitive set.

Example #1:

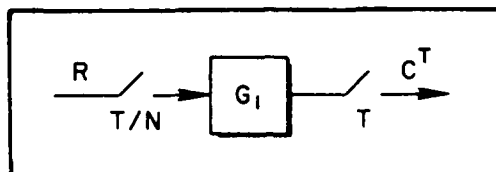


Figure 30. Illustrative Example #1

$$C^T = [G_1 R T/N]^T = [G_1^T / N^T / N]^T \quad (171)$$

For ease of identification, let $G_1 = (1/s + 1)$, $R = \sin bt$.

Therefore,

$$C^T = \left[\frac{z}{z - e^{-T/N}} \cdot \frac{z \sin(bT/N)}{z^2 - 2 \cos(bT/N)z + 1} \right]^T \quad (172)$$

Since the ratio between the frame times is N , the root at $z = e^{-T/N}$ in a T/N time frame goes to $z = e^{-T}$ in a T time frame. The roots corresponding to the sine wave in T/N , where

$$z = \cos(bT/N) \pm j \sin(bT/N) = 1 \pm j bT/N \quad (173)$$

jump to $z^N = (1 \pm j bT/N)^N$ or $z = 1 \pm j bT$. Thus C^T will have the form

$$C^T = \frac{N(z)}{(z - e^{-T})[z^2 - (2 \cos bT)z + 1]}, \quad z = e^{sT} \quad (174)$$

and it can be appreciated that only one sine wave is needed to match the steady state response (only because of fast input-slow output sampling format).

Example #2:

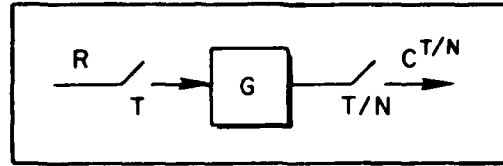


Figure 31. Fast Output, Slow Input Example

$$\begin{aligned}
 C^{T/N} &= [G R^T]^{T/N} = G^{T/N} R^T \\
 &= \frac{z}{(z - e^{-T/N})} \frac{z^N \sin bT}{[z^{2N} - (2 \cos bT)z^N + 1]} \bigg|_{z=e^{sT/N}} \quad (175)
 \end{aligned}$$

It is apparent that the sum of N sinusoids is required to exactly match the T/N output samples.

Example #3:

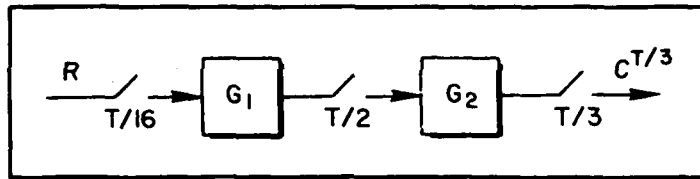


Figure 32. Three Rate Example

Again, for ease of identification, let $G_1 = 1/(s + 1)$ and $G_2 = 1/(s + 2)$.

$$C^{T/3} = \{G_2 [G_1 R^{T/16}]^{T/2}\}^{T/3} \quad (176)$$

The inner operation will yield, using the method of Section IV,

$$\begin{aligned}
 &\left[\frac{z}{z - e^{-T/16}} \frac{z^2 \sin(bT/16)}{z^2 - [2 \cos(bT/16)]z + 1} \right]^{T/2} \\
 &= \frac{N(z)}{(z - e^{-T/2})(z^2 - [2 \cos(bT/2)]z + 1)} \bigg|_{z=e^{sT/2}} \quad (177)
 \end{aligned}$$

since the ratio between the frame times is eight. The next operation must be initiated in a $T/6$ time frame, which gives a form like

$$\left[G_2^{T/6} [G_1 R^{T/16}]^{T/2} \right]^{T/3} = \left[\frac{z}{(z - e^{-2T/6})} \cdot \frac{N(z^3)}{(z^3 - e^{-T/2})(z^6 - [2 \cos(bT/2)]z + 1)} \right]^{T/3} \quad (178)$$

The ratio between $T/6$ and $T/3$ is two, and looking at the $T/6$ roots:

$$\begin{aligned} z &= e^{-2T/6}, \quad z^2 = e^{-2T/3} \Rightarrow (z - e^{-2T/3}) \text{ in } T/3 \\ z^3 &= e^{-T/2}; \quad z^6 = e^{-T} \Rightarrow (z^3 - e^{-T}) \text{ in } T/3 \\ z^3 &= 1 \pm bT/2, \quad z^6 = 1 \pm bT \Rightarrow [z^6 - (2 \cos bT)z^3 + 1] \text{ in } T/3 \end{aligned} \quad (179)$$

$C^{T/3}$ has a form

$$C^{T/3} = \frac{N_1(z)}{(z - e^{-2T/3})(z^3 - e^{-T})(z^6 - (2 \cos bT)z^3 + 1)} \Big|_{z=e^{sT/3}} \quad (180)$$

Thus the "fragmentation" of the sine wave through $T/16$, $T/2$, and $T/3$ time frames requires the use of three sinusoids to match the output steady state waveform (at the sampling instant).

In this example, one can therefore use single rate results (avoid switch decomposition) by setting up a new transfer function via

$$C^{T/3} = \frac{N_1(z)}{(z^3 \sin bT)(z - e^{-2T/3})(z^3 - e^{-T})} \times \frac{z^3 \sin bT}{z^6 - (2 \cos bT)z^3 - 1} \quad (181)$$

$$= G_1(z) \frac{z^3 \sin bT}{z^6 - (2 \cos bT)z^3 + 1} ; z = e^{sT/3} \quad (182)$$

$$= G_1^{T/3} \left|_{z=e^{sT/3}} \times \frac{z \sin bT}{z^2 - (2 \cos bT)z + 1} \right|_{z=e^{sT}} \quad (183)$$

Thus

$$A_n + jB_n = \frac{1}{3} G_1(z) \Big|_{z = e^{j\omega_n T/3}} , \quad \omega_n = b + (2\pi n/T) \\ n = 1, \pm 1, \text{ or } 0, 1, 2$$

Clearly, the same problem which surfaced in the switch decomposition frequency response also surfaces here. Namely, in switch decomposition W_* was evaluated at the input frequency b ; it was not permissible to let its value range with ω_n . In $G_1^{T/3}$, it is necessary to keep the scale factor, $\sin bT$ in the denominator of G_1 , fixed at the value b .

These examples make it clear that the use of this scalar theory, as an alternative to switch decomposition, requires insight into the manner in which the poles are manipulated between successive time frames.

E. SECTION SUMMARY

The frequency response of multi-rate systems, using a switch decomposition format was reviewed with a sinusoidal input. Decomposition of the input $(W_*R)^T$ requires a number of "Bode plots" equal to the dimension of W_* . An alternative "scalar approach," using the tool developed in Section IV, was presented. This approach, where applicable, is dimensionally more attractive than vector switch decomposition. It does require a keen awareness (on the user's part) of the number of sinusoids required to match the sampled output steady-state waveform.

SECTION VI

SIMULATION MODELS

A. INTRODUCTION

There is a natural extension of the previous results which make switch decomposition (or its equivalent) and frequency response techniques ideal for the error analysis of simulations. Before discussing that topic in explicit detail, we will first develop models for treating a given computer code under the assumption that it introduces an inherent throughput delay. The limited ability of "time advanced" digital filters to compensate for throughput delay is briefly treated. A key idea, the use of a zero-order hold to model a buffer storage register between two computers (working in different frame times) and/or different elements of a computer program, is introduced first.

B. MODELING A BUFFER REGISTER

The use of a ZOH to model a storage register is depicted in Figure 33. There the output of the filter $G(z)$ is stored in an intermediate buffer register, M_O . The output C is given as

$$C = M_O G^T R^T \quad (184)$$

and clearly

$$C^T = M_O^T G^T R^T = G^T R^T \quad (185)$$

since $M_O^T \equiv 1$, i.e.,

$$\left(\frac{1 - e^{-sT}}{s} \right)^T \equiv \frac{z - 1}{z} \left[\frac{1}{s} \right]^T = \frac{z - 1}{z} \frac{z}{z - 1} \quad (186)$$

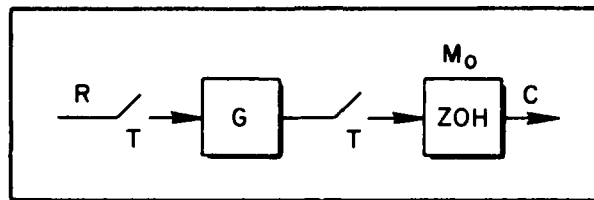


Figure 33. Model of a Buffer Register

The utility of this model, therefore, lies not in the situation where C is sampled at $(1/T)$ Hz, but rather when some other type of output operation is performed. For example, one may visualize C as being the input for the next (serial) recursion operation to be performed in a different frame time, say $T/3$ (refer to Figure 34). Express C as

$$C = M_3 G_2^{T/3} [M_1 G_1^T R^T]^{T/3} = M_3 G_2^{T/3} M_1^{T/3} G_1^T R^T \quad (187)$$

where the subscripts on the data holds are used to indicate the integer values of their frame time, i.e.,

$$M_1 = \frac{1 - e^{-sT}}{s}, \quad M_3 = \frac{1 - e^{-sT/3}}{s} \quad (188)$$

To illustrate the use of Figure 32, suppose a recursion equation like

$$X_k = -.2X_{k-1} + .4R_k + .3R_{k-1} \quad (189)$$

in a T frame time is followed by another recursion equation in a $T/3$ time frame:

$$Y_k = +.6Y_{k-1} + .3X_k \quad (190)$$

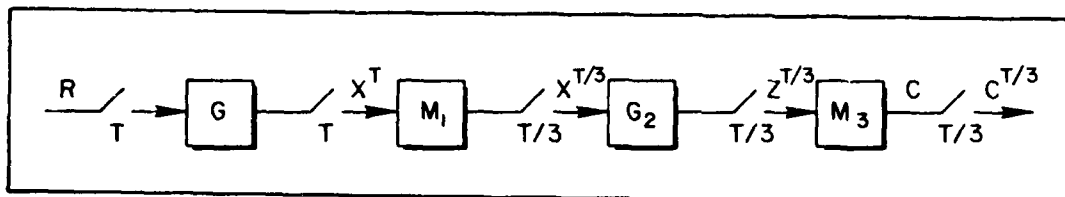


Figure 34. A Particular Serial Operation

The transfer functions, with z commensurate with the indicated time frames, are:

$$G_1^T = \frac{.4z + .3}{z + .2}, \quad G_2^{T/3} = \frac{.5z}{z - .6} \quad (191)$$

Equation 187 in terms of a $T/3$ time frame is:

$$C = \frac{1 - e^{-sT/3}}{s} \cdot \frac{5}{z - .6} \left[\frac{1 - e^{-sT}}{s} \right]^{T/3} \left(\frac{.4z^3 + .3}{z^3 + .2} \right) R(z^3) \quad (192)$$

or

$$C = \frac{1 - e^{-sT/3}}{s} \cdot \frac{5}{z - .6} \left[\frac{z^2 + z + 1}{z^2} \right] \left(\frac{.4z^3 + .3}{z^3 + .2} \right) R(z^3) \quad (193)$$

The term $(z^2 + z + 1)/z^2$ models the fact that recursion Equation 190 asks recursion Equation 189 for an input every $T/3$ seconds, but picks up the same number two out of every three times.

C. MODELING THROUGHPUT DELAY

Multiplication and addition of a recursion equation require a finite amount of machine time for their execution. Thus, it is necessary to understand the timing of a simulation. For example, the recursion equation of Equation 194 can be machine executed in several different ways:

$$y_k = a_1 y_{k-1} + a_2 y_{k-2} + a_3 y_{k-3} + b_0 x_k + b_1 x_{k-1} \quad (194)$$

- a) Bring in the new x_k , do five multiplies and four adds, and (as quickly as possible) output the new value of y_k . There will be a throughput delay, say T_0 seconds.

- b) Same as a) except y_k is not updated until the start of the next machine cycle. There will be a throughput delay equal to the frame time, T seconds.

Yet another alternative is to perform all the multiplies and adds associated with the past values as a "background" computation. Then, at the start of the new frame time, one need only bring in the new value of x_k , perform one multiply, add using the "background" number, and output y_k as quickly as possible. This would minimize throughput delay. Explicitly,

$$y_k = b_0 x_k + b_k \quad (195)$$

$$b_k = a_1 y_{k-1} + a_2 y_{k-2} + a_3 y_{k-3} + b_1 x_{k-1} \quad (196)$$

Thus, while the delay in updating x_k and outputting y_k as quickly as possible must be minimized, say in T_1 seconds, the background can be done in a more leisurely manner provided it can be "fitted in" in the remaining $T - T_1$ seconds.

A model which fits all three cases is shown in Figure 35. There the nonsynchronous sampler model of Section III is used to model the throughput delay. This model envisages that the delay inherent in either the time required to multiply and add (or perhaps a deliberate delay of one frame time) can be lumped as a skewed data operation after the data hold. Thus the recursion modeled by $G_1(z)$ is done instantaneously and passed to a storage register, and its output is out of step with the master clock by T_0 seconds. This is depicted in Figure 36.

A final comment is in order. When an element of a simulation is modeled as a recursion equation (computer code), a single, distinct frame time is implied. This means that the pulse transfer function used to model it must have the same frame time operation on both input and output.

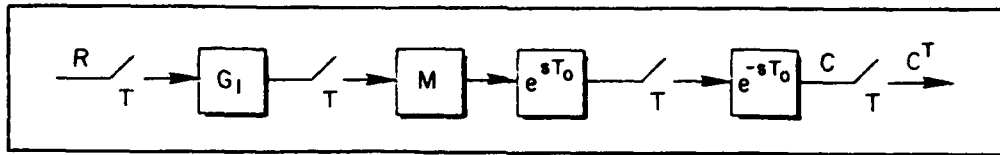


Figure 35. Buffer Register Model with Throughput Delay

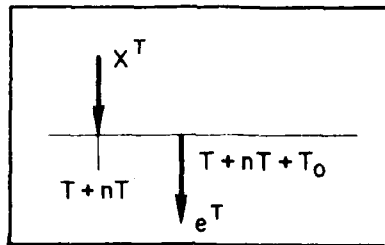


Figure 36. Timing Diagram

D. SWITCH DECOMPOSITION MODEL

In Equation 187, it was possible to operate through the T time frame with the $T/3$ operator. This will not always be possible and we may, once again, have to resort to switch decomposition.

With switch decomposition, one is in a position to evaluate configurations such as the one shown in Figure 37 (the vector switch decomposition is shown in Figure 38).

From Figure 38,

$$C = M_2 W_2 (W_{2*} G_2 W_2)^T (W_{2*} M_3 W_3)^T (W_{3*} G_1 W_3)^T (W_{3*} R)^T \quad (197)$$

The evaluation of terms such as $(W_{2*} M_3 W_3)^T$ is routine; our concern is with terms like $(W_{3*} G_1 W_3)^T$ when $G_1^{T/3}$ is given as a software specification (e.g., computer algorithm). Focusing on $(W_{3*} G_1 W_3)^T$, we find

AD-A128 497

ELEMENTS OF SIMULATION ERROR ANALYSIS(U) SYSTEMS
TECHNOLOGY INC HAWTHORNE CA R F WHITBECK JUN 82
TR-1173-1 AFWAL-TR-82-3022 F33615-81-C-3606

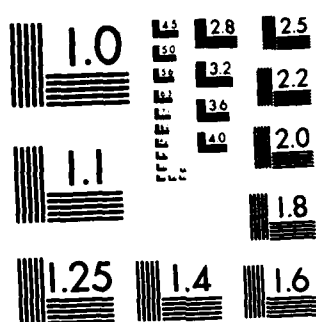
22

UNCLASSIFIED

F/G 12/1

NL

END
DATE
FILMED
6 83
DTIC



MICROCOPY RESOLUTION TEST CHART
NATIONAL BUREAU OF STANDARDS-1963-A

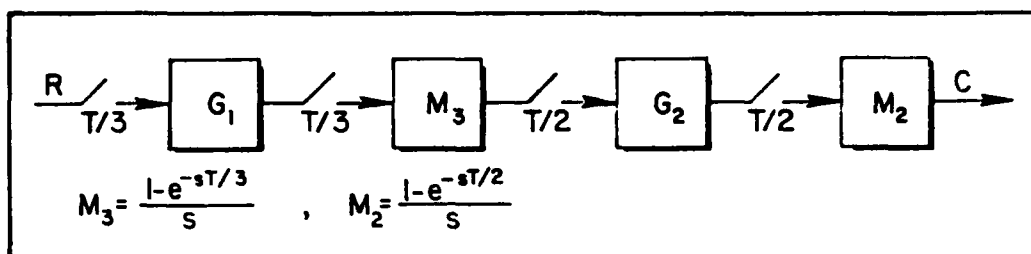


Figure 37. Example Two-Rate Open-Loop System

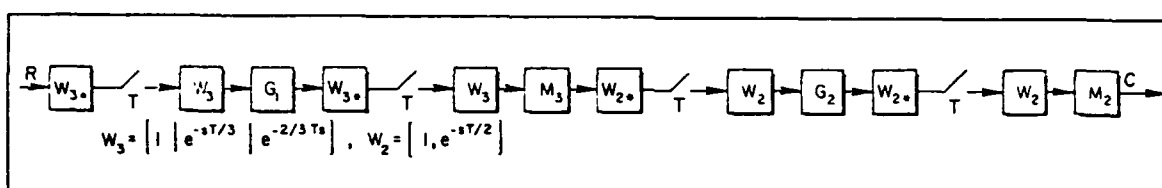


Figure 38. Switch Decomposition Formulation for Figure 35

$$\begin{aligned}
 (W_{3*} G_1 W_3)^T &= \left\{ \begin{bmatrix} 1 \\ \hline e^{sT/3} \\ \hline e^{2sT/3} \end{bmatrix} G_1 \begin{bmatrix} 1 & e^{-sT/3} & e^{-2sT/3} \end{bmatrix} \right\}^T \\
 &= \left\{ G_1 \begin{bmatrix} 1 & e^{-sT/3} & e^{-2sT/3} \\ e^{sT/3} & 1 & e^{-sT/3} \\ e^{2sT/3} & e^{sT/3} & 1 \end{bmatrix} \right\}^T \quad (198)
 \end{aligned}$$

$$(W_{3*}G_1W_3)^T = \begin{bmatrix} 1 & e^{-sT}(e^{2sT/3}) & e^{-sT}(e^{sT/3}) \\ G_1(e^{sT/3}) & 1 & e^{-sT}(e^{2sT/3}) \\ (e^{2sT/3}) & (e^{sT/3}) & 1 \end{bmatrix}^T \quad (199)$$

Observe the super-diagonal terms. They are simply appropriate sub-diagonal terms multiplied by e^{-sT} . It is only necessary to compute the first column entries in order to completely determine $(W_{3*}G_1W_3)^T$.

Next, observe that the problem statement stipulates $G_1^{T/3}$, perhaps defined through a substitution rule. If $e^{sT/3}$ is defined as z we have:

$$(W_{3*}G_1W_3)^T = \begin{Bmatrix} G_1^{T/3} & z^{-3}(z^2G_1^{T/3}) & z^{-3}(zG_1^{T/3}) \\ zG_1^{T/3} & G_1^{T/3} & z^{-3}(z^2G_1^{T/3}) \\ z^2G_1^{T/3} & zG_1^{T/3} & G_1^{T/3} \end{Bmatrix}^T, \quad z = e^{sT/3} \quad (200)$$

Thus one may, for all the super diagonal terms, factor out $1/z$ (in a T time frame). Although each term in Equation 200 can be evaluated, using the algorithm of Section IV, only the first column entries need be computed (i.e., the three entries of column one are sufficient to define all nine entries).

E. TIME-ADVANCED DIGITAL FILTERS

In synthesizing a recursion equation for a particular element of a simulation, the designer can often compensate for part of the throughput

delay introduced by the digital computer. To see this, consider the task of implementing a low-pass filter via a recursion equation (refer to Figure 39). One way to do it is to visualize the input to the (sampled) filter as being smoothed with a data hold (of the designer's choosing) and then advanced in time by the operator $e^{\Delta s T}$. If $G = a/(s + a)$ and M is a ZOH, compute the pulse transfer function as

$$G(z) = \left[\frac{1 - e^{-sT}}{s} e^{\Delta s T} \left(\frac{a}{s + a} \right) \right]^T \quad (201)$$

or

$$\begin{aligned} GT &= \frac{z-1}{z} \left\{ e^{\Delta s T} \left[\frac{1}{s} - \frac{1}{s+a} \right] \right\}^T \\ &= \frac{(1 - e^{-\Delta a T})z + (e^{-\Delta a T} - e^{-aT})}{z - e^{-aT}} \end{aligned} \quad (202)$$

It can be appreciated that a full time period advance, which is not physically realizable in the analog world, can be realized on the discrete domain, since

$$C_n = e^{-aT} C_{n-1} + (1 - e^{-aT}) R_n \quad (203)$$

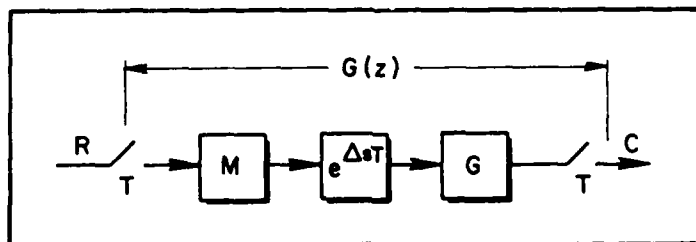


Figure 39. A "Time Advanced" Filter Section

can be realistically approximated by a very fast computer. This method works well for low-pass sections but there is little to be gained by trying it on washout networks or high passes. To see this, consider a limiting form, such as a differentiator:

$$G(z) = \left[\frac{1 - e^{-sT}}{s} \cdot e^{\Delta sT} \cdot s \right]^T \quad (204)$$

Here any $\Delta \neq 0$ results in a physically unrealizable component. Of course, one may utilize a higher-order data hold, for instance, the "slewer."

$$G(z) = \left[\frac{(1 - e^{-sT})^2}{Ts^2} \cdot e^{\Delta sT} \cdot s \right]^T \quad (205)$$

When $\Delta = 0$, the smoother is called a slewer; when $\Delta = 1$ the smoother is recognized as the triangular data hold. Clearly,

$$G(z) = \frac{1}{T} \frac{(z-1)^2}{z^2} \frac{e^{\Delta sT}}{s} \Big|_s^z \equiv \frac{z-1}{Tz} \quad (206)$$

regardless of the value of Δ .

We close this facet of the discussion with a look at an integrator when the smoother is a time-advanced slewer or a time-advanced ZOH and compare the results with the Tustin transforms of $1/s$.

Slewer:

$$G(z) = \frac{(z-1)^2}{Tz^2} \frac{e^{\Delta sT}}{s^3}$$

$$= \frac{(z-1)^2}{Tz^2} \cdot \frac{z \left[(\Delta^2/2) + (1/2 - \Delta^2 + \Delta)z + (1/2 - \Delta + \Delta^2) \right]}{(z-1)^3} \quad (207)$$

For a full period advance

$$G(z) = \frac{T}{2} \left(\frac{z+1}{z-1} \right) \quad (208)$$

ZOH:

$$G(z) = \left[\frac{z-1}{z} \right] \left[\frac{e^{sT}}{s^2} \right]^T = \frac{z-1}{z} \cdot \frac{zT[\Delta z + (1-\Delta)]}{(z-1)^2} \quad (209)$$

For a half period advance (unrealizable if $\Delta = 1$)

$$G(z) = \frac{T}{2} \left(\frac{z+1}{(z-1)} \right) \quad (210)$$

Tustin Transform:

$$G(z) = \left[\frac{1}{s} \right]_{\text{Tustin}} = \frac{T}{2} \frac{(z+1)}{z-1} \quad (211)$$

Thus Tustin transform of $1/s$ is the same as smoothing with a ZOH, advanced in time by half a period, or a slewer with an advance of T .

F. DIFFERENCE EQUATIONS FOR MODELING AN INTEGRATOR

A frequently used technique for deriving recursion equations from a given transfer function is to rearrange the transfer function in terms of "nested" values of $1/s$. For example, the network

$$G(s) = \frac{a_2 s^2 + a_1 s + a_0}{s^3 + b_2 s^2 + b_1 s + b_0} \quad (212)$$

can be written as

$$\begin{aligned} G(s) &= \frac{a_2/s + a_1/s^2 + a_0/s^3}{1 + b_2/s + b_1/s^2 + b_0/s^3} \\ &= \frac{[a_0/s + a_1]1/s + a_2}{[(b_0/s + b_1)1/s + b_2]1/s + 1} \end{aligned} \quad (213)$$

This approach emphasizes the importance of having a viable discrete representation of the integrator. Indeed, this has been the prime focus of the classical integrator approach. That is, given an input \dot{x} , the integrator produces x and one may tabulate a set of classical integration algorithms, all of which can be derived using the approach of the previous section (see Table 2). In the remainder of this report, it will be assumed that the recursion equations are given and the focus is on evaluating of the fidelity of the overall simulation.

G. SECTION SUMMARY

Analytical models for incorporating recursion equations into a framework which accounts for throughput delay were developed. The switch decomposition model of a simulation element was shown to have a recursive pattern which required the evaluation of only the first column of the describing matrix. From this column vector all other entries of the matrix can be generated. A fundamental step was the use of a ZOH to model a buffer storage register. The use of time advanced digital filters to compensate for throughput delay was briefly discussed and the classical equations for integrators were summarized in tabular form.

TABLE 2. CLASSICAL INTEGRATORS

INTEGRATION EQUATION	NAME
$x_n = x_{n-1} + T(2\dot{x}_{n-1} - \dot{x}_n)$	--
$x_n = x_{n-1} + \frac{T}{2} (3\dot{x}_{n-1} - \dot{x}_n)$	--
$x_n = x_{n-1} + T(\dot{x}_{n-1})$	Euler
$x_n = x_{n-1} + \frac{T}{2} (\dot{x}_n + \dot{x}_{n-1})$	Trapezoidal
$x_n = x_{n-1} + T(\dot{x}_n)$	Rectangular
$x_n = x_{n-1} + \frac{T}{2} (3\dot{x}_n - \dot{x}_{n-1})$	Implicit Adams Second-Order
$x_n = x_{n-1} + T(2\dot{x}_n - \dot{x}_{n-1})$	--

SECTION VII

A T/2, T/3 CLOSED-LOOP SIMULATION CASE STUDY

A. INTRODUCTION

The topic of this section is a case study using the tools developed in Sections III through VI. The rates involved in this closed-loop analysis force the use of switch decomposition. Later sections will treat case studies where switch decomposition can be avoided.

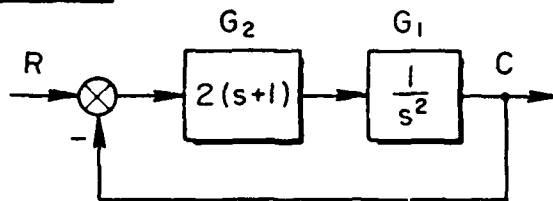
Specifically, we investigate a case where an idealized control element ($1/s^2$) is under the influence of a continuous feedback controller with an (idealized) compensation network in the forward path. The objective is to generate Bode plots given (1) a digital implementation of the continuous controller and (2) a digital simulation of the overall system; treating both the continuous and discrete controller cases. Of special interest is the case where the compensation is modeled on one computer and the controlled element is modeled on a different computer, with each computer working in a different frame time. In all, four cases will be discussed.

B. PROBLEM DESCRIPTION

The situation described by Case I in Figure 40 assumes a controlled element ($1/s^2$) under the influence of a continuous feedback controller with an (idealized) compensation network $2(s + 1)$ in the forward path. Case II depicts the same controlled element under the influence of a discrete feedback controller which smooths the output of the digital computer with a ZOH (passing on a "staircased" signal to the control point). The discretized version of $2(s + 1)$ was computed, using the first back difference algorithm resulting in the model $(42z - 40)/z$ (at a sampling rate of 20 Hz).

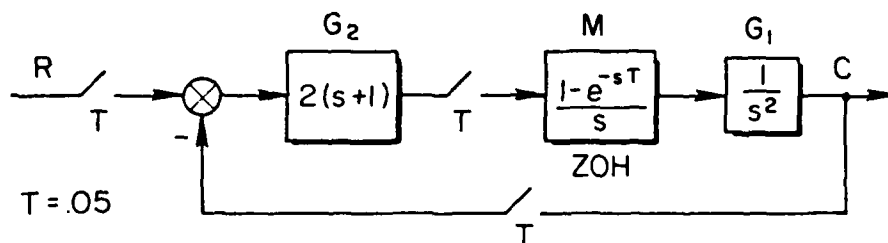
Case III is a simulation of Case II (or I) wherein the plant, $1/s^2$, is modeled using a "substitution-for-s" rule (Tustin transform). The output variable C is modeled as the output of a storage register (ZOH).

CASE I

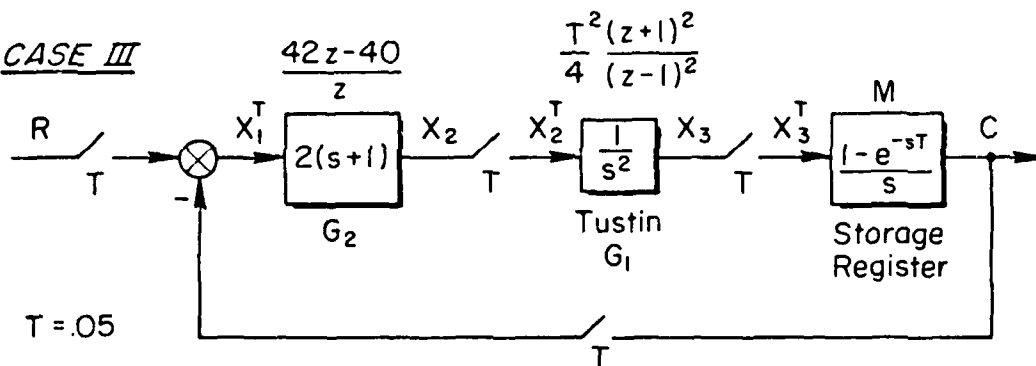


CASE II

$$G_2(z) = \frac{42z-40}{z}$$



CASE III



CASE IV

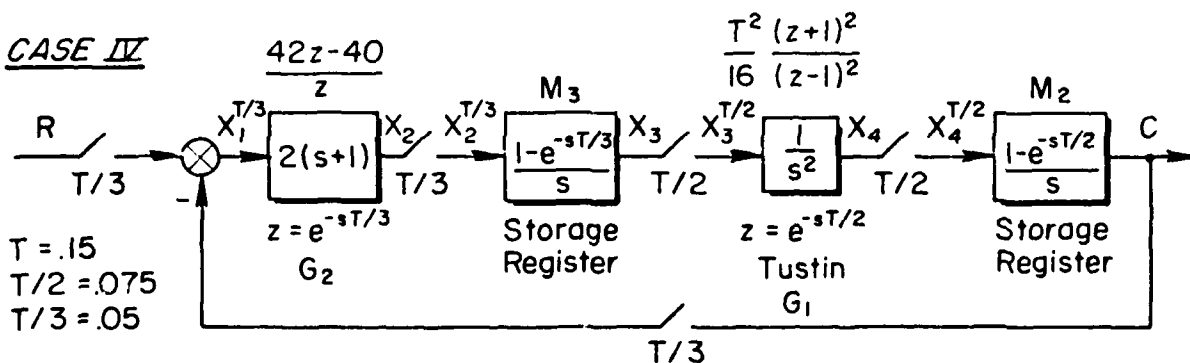


Figure 40. A Vector Switch Decomposition Simulation Case Study

Finally, Case IV depicts a situation wherein one part of a simulation is coded for one computer while another part is coded on a second computer. Typically, the computers are working in different frame times and therefore will, on occasion, pass "old data" back and forth. It is assumed that the compensation is modeled in a 0.05 sec time frame, while the plant is modeled in a 0.075 sec time frame. Data transfer between the two computers is via appropriate buffer registers, modeled as a ZOH in a $T/3$ time frame (M_3) and a ZOH in a $T/2$ time frame (M_2).

This completes the problem description; we may now write the appropriate equations for each case and discuss the analytical difficulties.

Case I is straightforward since

$$C(s) = [I + G_1 G_2]^{-1} G_1 G_2 R \quad (214)$$

Case II appears straightforward but does present a contradiction in the output equation

$$C^T = [I + (G_1 M)^T G_2^T]^{-1} (G_1 M)^T G_2^T R^T \quad (215)$$

That is,

$$(G_1 M)^T = \left[\frac{1 - e^{-sT}}{s} \frac{1}{s^2} \right]^T = \frac{T^2}{2} \frac{(z + 1)}{(z - 1)^2} \quad (216)$$

is readily computed using a transform table. However, it was not the intent of the designer, who used a substitution technique to model $2(s + 1)$ as $(42z - 40)/z$, to compute

$$G_2^T = [2(s + 1)]^T \quad (217)$$

using the z -transform. Indeed, what does $[s]^T$ mean? Clearly, the intent of the simulation designer was to assign $G_2^T = (42z - 40)/z$.

This difficulty surfaces again in Case III since

$$C^T = [I + G_1^T G_2^T]^{-1} G_1^T G_2^T R^T \quad (218)$$

after taking due note that $M^T \equiv 1$.

Now it is necessary to interpret both G_1^T and G_2^T as given functions of z rather than z -transform operations. For example, assign (via the Tustin transform)

$$G_1^T = \frac{T^2}{4} \frac{(z+1)^2}{(z-1)^2} \quad (219)$$

rather than (via the z -transform)

$$G_1^T = \left[\frac{1}{s^2} \right]^T = \frac{Tz}{(z-1)^2} \quad (220)$$

Difficulties in the "assignment" procedure also surface when we write the output equation for Case IV (see Figure 41).

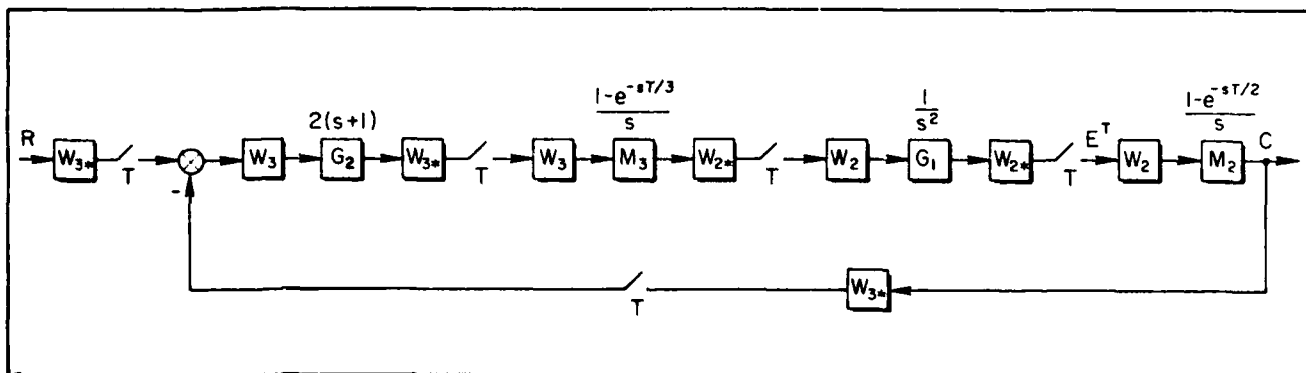


Figure 41. Case IV, Switch Decomposition Model

$$G = (M_2 W_2) [I + (W_2^* G_1 W_2)^T (W_2^* M_3 W_3)^T (W_3^* G_2 W_3)^T (W_3^* M_2 W_2)^T]^{-1} \\ \times (W_2^* G_1 W_2)^T (W_2^* M_3 W_3)^T (W_3^* G_2 W_3)^T (W_3^* R)^T \quad (221)$$

where

$$W_2 = [1, e^{-sT/2}] \quad , \quad W_3 = [1, e^{-sT/3}, e^{-sT/6}] \quad (222)$$

The meaning of some terms in Equation 221 are clear; others are not. For example, a straightforward computation yields

$$(W_3^* M_2 W_2)^T = \left\{ \begin{bmatrix} 1 \\ e^{sT/3} \\ e^{s2T/3} \end{bmatrix} \frac{1-e^{-sT/2}}{s} [1 \quad e^{-sT/2}] \right\}^T = \left\{ \frac{1-e^{-sT/2}}{s} \begin{bmatrix} 1 & e^{-sT/2} \\ e^{sT/3} & e^{-sT/6} \\ e^{s2T/3} & e^{sT/6} \end{bmatrix} \right\}^T \quad (223)$$

$$\left[\begin{array}{c|c} \frac{1}{s} - \frac{e^{-sT} e^{sT/2}}{s} & \frac{e^{-sT}(e^{sT/2} - 1)}{s} \\ \hline \frac{e^{sT/3}}{s} - \frac{e^{-sT} e^{s5T/6}}{s} & e^{-sT} \left[\frac{e^{s5T/6}}{s} - \frac{e^{sT/3}}{s} \right] \\ \hline \frac{e^{s2T/3}}{s} - \frac{e^{sT/6}}{s} & \frac{e^{sT/6}}{s} - \frac{e^{-sT} e^{s2T/3}}{s} \end{array} \right]^T = \begin{bmatrix} 1 & 0 \\ 1 & 0 \\ 0 & 1 \end{bmatrix} \quad (224)$$

In a similar manner,

$$(W_2 \star M_3 W_3)^T = \left\{ \left[\begin{array}{c} 1 \\ \frac{1 - e^{-sT/3}}{s} \\ e^{sT/2} \end{array} \right] \left[\begin{array}{ccc} 1 & e^{-sT/3} & e^{-s2T/3} \end{array} \right] \right\}^T \quad (225)$$

$$= \left(\frac{1 - e^{-sT/3}}{s} \left[\begin{array}{ccc} 1 & e^{-sT/3} & e^{-s2T/3} \\ e^{sT/2} & e^{sT/6} & e^{-sT/6} \end{array} \right] \right)^T$$

Clearing through and writing Equation 225 in terms of the advanced z-transform for 1/s:

$$(W_2 \star M_3 W_3)^T = \left[\begin{array}{c|c|c} \frac{1}{s} - \frac{e^{-sT} e^{s2T/3}}{s} & \frac{e^{-sT} e^{s2T/3}}{s} - \frac{e^{-sT} e^{sT/3}}{s} & \frac{e^{-sT} e^{sT/3}}{s} - \frac{e^{-sT}}{s} \\ \hline \frac{e^{sT/2}}{s} - \frac{e^{sT/6}}{s} & \frac{e^{sT/6}}{s} - \frac{e^{-sT} e^{s5T/6}}{s} & \frac{e^{sT} e^{s5T/6}}{s} - \frac{e^{-sT} e^{sT/2}}{s} \end{array} \right]^T$$

$$= \left[\begin{array}{ccc} 1 & 0 & 0 \\ 0 & 1 & 0 \end{array} \right] \quad (226)$$

However, the meaning of $(W_3 \star G_2 W_3)^T$ or $(W_2 \star G_1 W_2)^T$ is not clear. When the designer specified $G_2 = (42z - 40)/z$, he intended (for a T time frame) the recursion relationship

$$n) = 42(R_n - C_n) - 40(R_{n-1} - C_{n-1}) \quad (227)$$

In a like manner, the Tustin substitution for $1/s^2$ was meant to yield

$$X_4(n) = 2X_4(n-1) - X_4(n-2) + \frac{T^2}{16} [X_3(n) + 2X_3(n-1) + X_3(n-2)] \quad (228)$$

Clearly, the information available in Case IV is

$$G_2^{T/3} = \frac{42z - 40}{z}, \quad T/3 = 0.05, \quad z = e^{sT/3} \quad (229)$$

and

$$G_1^{T/2} = \frac{T^2}{16} \frac{(z+1)^2}{(z-1)^2}, \quad T/2 = 0.075, \quad z = e^{sT/2} \quad (230)$$

Using only the given computer code, how does one compute $(W_3^* G_2 W_3)^T$ and $(W_2^* G_1 W_2)^T$? This problem is treated next.

C. DECOMPOSITION OF $G_1^{T/2}$ AND $G_2^{T/3}$

Using the results of Section VI, write

$$(W_3^* G_2 W_3)^T = (W_3^* G_2^{T/3} W_3)^T \quad (231)$$

This is a simple but crucial step because we do not know (or care) what the underlying $G(s)$ was. However, we are given $G_1^{T/3}$ as computer code or, equivalently, a pulse transfer function in a $T/3$ time frame. The $G_2^{T/3}$ transfer function from the Case IV simulation example has the form:

$$G_2^{T/3} = \frac{a_0 z + a_1}{z}, \quad z = e^{sT/3} \quad (232)$$

Equation 231 has the terms

$$(W_{3*}G_2^{T/3}W_3)^T = \begin{Bmatrix} G_2^{T/3} & z^{-3}[z^2G_2^{T/3}] & z^{-3}[zG_2^{T/3}] \\ zG_2^{T/3} & G_2^{T/3} & z^{-3}[z^2G_2^{T/3}] \\ z^2G_2^{T/3} & zG_2^{T/3} & G_2^{T/3} \end{Bmatrix}^T \quad (233)$$

where $z = e^{sT/3}$. The final result will be in a T time frame and therefore the z^{-3} in the superdiagonal terms can be factored out and treated as a z^{-1} , where $z = e^{sT}$.

Only the entries for the first column need be computed:

$$\left[\frac{a_0z + a_1}{z} \right]^T, \quad \left[\frac{z(a_0z + a_1)}{z} \right]^T, \quad \left[\frac{z^2(a_0z + a_1)}{z} \right]^T \quad (234)$$

Consider the first term:

$$\left[\frac{a_0z + a_1}{z} \right]^T = \frac{1}{2\pi j} \int \frac{a_0p + a_1}{p} \frac{z}{z - p^3} \frac{dp}{p} \quad (235)$$

$$= \frac{d}{dp} \left[\frac{(a_0p + a_1)z}{z - p^3} \right]_{p=0} = a_0 \quad (236)$$

This result is easily verified using the algorithm of Section IV. In the $T/3$ time frame, algebraic long division gives

$$\frac{a_0 z + a_1}{z} = a_0 + a_1 z^{-1} + 0z^{-2} + 0z^{-3} + \dots \quad (237)$$

The root at $z = 0$ in the $T/3$ time frame remains at $z = 0$ in the T time frame. Therefore,

$$\left[\frac{a_0 z + a_1}{z} \right]^T = \frac{c_1 z + c_0}{z} \quad (238)$$

where

$$\begin{bmatrix} c_1 \\ c_0 \end{bmatrix} = \begin{bmatrix} a_0 & 0 \\ 0 & 0 \end{bmatrix} \begin{bmatrix} 1 \\ 0 \end{bmatrix} = \begin{bmatrix} a_0 \\ 0 \end{bmatrix} \quad (239)$$

and we see

$$\left[\frac{a_0 z + a_1}{z} \right]^T = a_0 \quad (240)$$

The second term in Equation 234 can, of course, be evaluated using residue theory:

$$([a_0 z + a_1])^T = \frac{1}{2\pi j} \int_{\Gamma} \frac{(a_0 p + a_1)z}{p(p - p^3)} dp = \left. \frac{(a_0 p + a_1)z}{z - p^3} \right|_{p=0} = a_1 \quad (241)$$

and

$$[z^2(a_0 z + a_1)]^T = \frac{1}{2\pi j} \int \frac{(a_0 p + a_1)z}{z - p^3} dp \equiv 0 \text{ (no poles enclosed)} \quad (242)$$

In this regard, note that the algorithm of Section IV was set up to treat only rational functions since polynomials in z can be easily treated by inspection. That is:

$$[a_0 z + 1 \ a_1]^T = [a_0 e^{sT/3} + a_1]^T = [a_0 e^{sT/3}]^T + [a_1]^T \quad (243)$$

But $a_0 e^{sT/3}$ is just a $T/3$ time advanced impulse and therefore a sampler, working in a T time frame, sees zero. $[a_1]^T$ is an impulse of strength a_1 at $t = 0$ and the T sampler "sees it" at $t = 0$, giving $a_1^T = a_1$.

In a like manner,

$$[a_0 z^2 + a_1 z]^T = [a_0 e^{2sT/3}] + [a_1 e^{-sT/3}]^T \equiv 0 \quad (244)$$

Next, use the "push down" column principle and generate

$$(W_{3*} G_2^{T/2} W_3)^T = \begin{bmatrix} a_0 & 0 & a_1/z \\ a_1 & a_0 & 0 \\ 0 & a_1 & a_0 \end{bmatrix}, \quad z = e^{sT} \quad (245)$$

The next task is to generate

$$(W_{2*} G_1 W_2)^T = (W_{2*} G_1^{T/2} W_2)^T \quad (246)$$

given

$$G_1^{T/2} = \frac{T^2}{16} \frac{(z+1)^2}{(z-1)^2}, \quad z = e^{sT/2} \quad (247)$$

Write

$$(W_{2*} G_1^{T/2} W)^T = \left\{ \begin{bmatrix} 1 \\ z \end{bmatrix} [1 \quad z^{-1}] G_2^{T/2} \right\}^T = \left\{ \frac{T^2}{16} \frac{(z+1)^2}{(z-1)^2} \begin{bmatrix} 1 & z^{-1} \\ z & 1 \end{bmatrix} \right\}^T \quad (248)$$

The first term of column one is

$$\begin{aligned}
 \left[\frac{T^2(z+1)^2}{16(z-1)^2} \right]^T &= \frac{1}{2\pi j} \int_{\Gamma} \frac{T^2}{16} \frac{(p+1)^2}{(p-1)^2} \frac{z}{z-p^2} \frac{dp}{p} = \text{res} \Big|_{p=0} + \text{res} \Big|_{p=1} \\
 &= \frac{T^2}{16} + \frac{T^2}{16} \frac{d}{dp} \frac{(p+1)^2 z}{p(z-p^2)} \Big|_{p=1} = \frac{T^2}{16} \left[1 + \frac{8z}{(z-1)^2} \right] \\
 &= \frac{T^2}{16} \frac{(z^2 + 6z + 1)}{(z-1)^2}, \quad z = e^{sT} \quad (249)
 \end{aligned}$$

The second term of the first column is easier to compute:

$$\begin{aligned}
 \frac{1}{2\pi j} \int_{\Gamma} \frac{T^2}{16} \frac{p(p+1)^2}{(p-1)^2} \frac{z}{(z-p^2)} \frac{dp}{p} &= \text{res} \Big|_{p=1} \\
 &= \frac{T^2}{16} \frac{d}{dp} \frac{z(p+1)^2}{(z-p^2)} \Big|_{p=1} \\
 &= \frac{T^2}{4} \frac{z(z+1)}{(z-1)^2} \quad (250)
 \end{aligned}$$

Again use the push down column principle and write

$$(W_2 \star G_1 W_2)^T = \frac{\begin{bmatrix} \frac{T^2}{16} (z^2 + 6z + 1) & \frac{T^2}{4} (z + 1) \\ \frac{T^2}{4} z(z + 1) & \frac{T^2}{16} (z^2 + 6z + 1) \end{bmatrix}}{(z-1)^2} \quad (251)$$

The algorithm of Section V can also be used. To demonstrate, derive the first entry by observing

$$\frac{T^2}{16} \frac{(z+1)^2}{(z-1)^2} = \frac{T^2}{16} [1 + 4z^{-1} + 8z^{-2} + 12z^{-3} + 16z^{-4} + \dots] \quad (252)$$

Since a root at $z = 1$ in $T/2$ remains at $z = 1$ in a T time frame, write

$$\left[\frac{T^2}{16} \frac{(z+1)^2}{(z-1)^2} \right]^T = \frac{c_2 z^2 + c_1 z + c_0}{z^2 - 2z + 1}, \quad z = e^{sT} \quad (253)$$

the numerator coefficients are easily found

$$\begin{bmatrix} c_2 \\ c_1 \\ c_0 \end{bmatrix} = \frac{T^2}{16} \begin{bmatrix} 1 & 0 & 0 \\ 8 & 1 & 0 \\ 16 & 8 & 1 \end{bmatrix} \begin{bmatrix} 1 \\ -2 \\ 1 \end{bmatrix} = \frac{T^2}{16} \begin{bmatrix} 1 \\ 6 \\ 1 \end{bmatrix} \quad (254)$$

checking the residue results.

D. RESULTS

With the assignments of the previous subsection all terms in Equation 221 are defined and the Bode plots descriptive of Cases I-IV can be computed. The results (magnitude plots only) are shown in Figures 42 through 47.

Inspection of Figure 42 discloses no surprises. The digitally controlled system is a reasonably faithful reproduction of the analog system until the folding frequency (approximately equal to 62.8 rad/sec) is passed. Notice that in the discretely controlled system, minimum response points in the Bode plot (notches) occur at multiples of sampling frequency (approximately equal to 125.66 rad/sec).

The comparison of the single-rate simulation against the baseline design exhibits fidelity over a shorter low-frequency range (Figure 43).

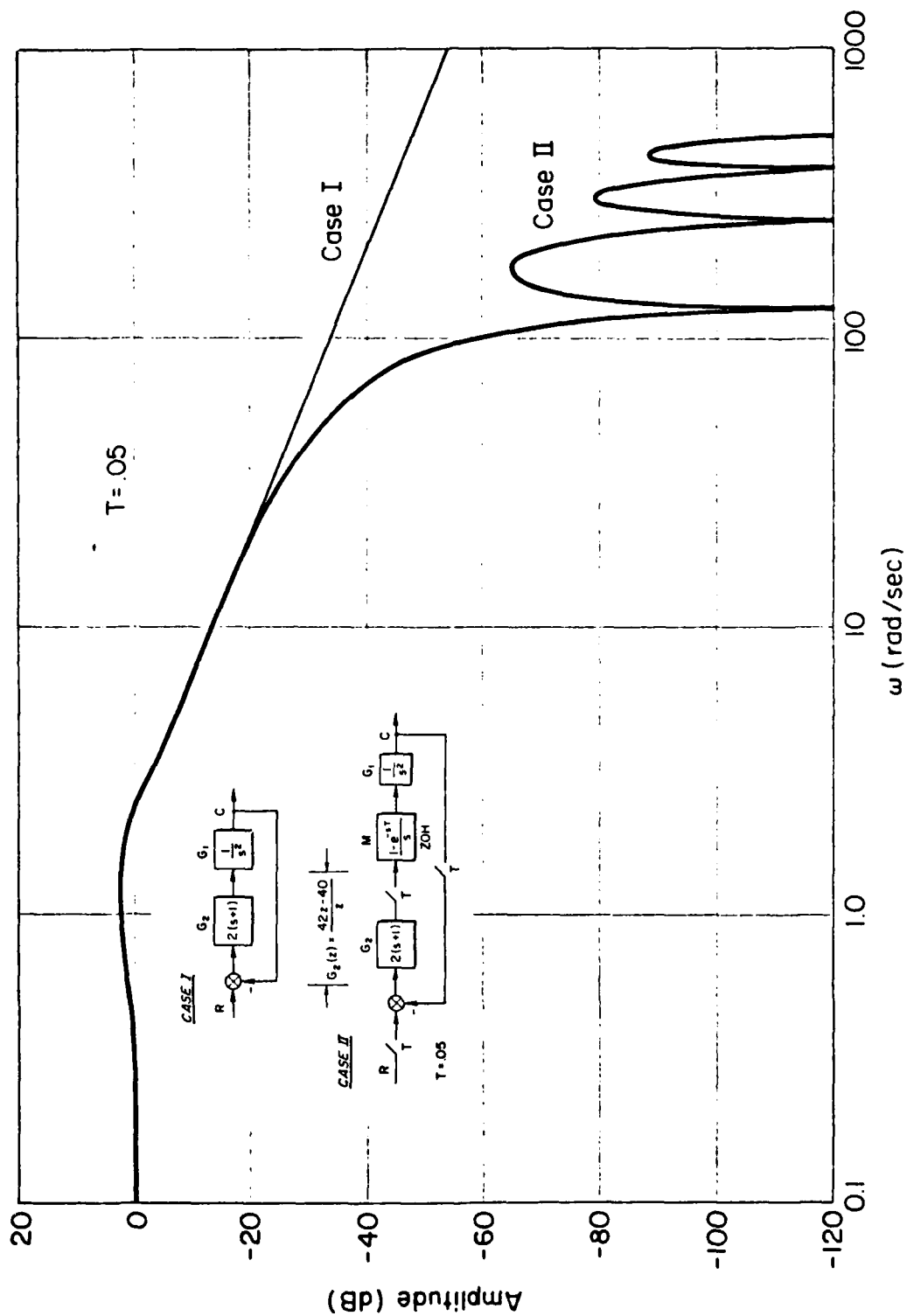


Figure 42. Magnitude Plot; Case I, Case II



105

Of particular importance is that the aliased bands exhibit a much higher amplitude response than did the aliased bands of the digitally controlled system (Case II). Moreover, the "notches" now occur at multiples of the folding frequency rather than the sampling frequency. In addition, there are very sharp notches which occur close to odd multiples of the folding frequency; these are a consequence of the zeros of the Tustin transform introduced by $(z + 1)^2$. A direct comparison between Cases II and III is given in Figure 44.

Figure 45 compares the two independent processor case (Case IV) against the continuous baseline design. Large, sharp resonant peaks have been introduced in the aliased bands and, in addition, there is a significant overshoot in the first fold. A comparison between the two rate simulation (Case IV) and the digitally controlled continuous system (Case II) is given in Figure 46. Figure 47 compares all the cases.

There are significant differences in the spectral content of the four cases which would be hidden if one only looked at the sampled spectrum (that is, looked only at the frequency content from zero to the first folding frequency). Even in the first fold, there is a significant difference in the Bode plot of the continuous case and the two-rate simulation; the reason for the added overshoot in the two-rate simulation will be discussed in the next subsection.

E. INTRODUCTION OF LIGHTLY DAMPED MODES

We may use the illustrative example of Section V to discuss the additional modes introduced by a multi-rate process. Specifically, for Figure 48, let

$$z = e^{sT/6}, \quad M = 3, \quad N = 2 \quad (255)$$

$$G = \frac{1}{s + 2}, \quad GT/6 = \frac{z}{z - e^{-T/3}} \quad (256)$$

$$R = \frac{1}{s + 1}, \quad RT/2 = \frac{z^3}{z^3 - e^{-T/2}} \quad (257)$$

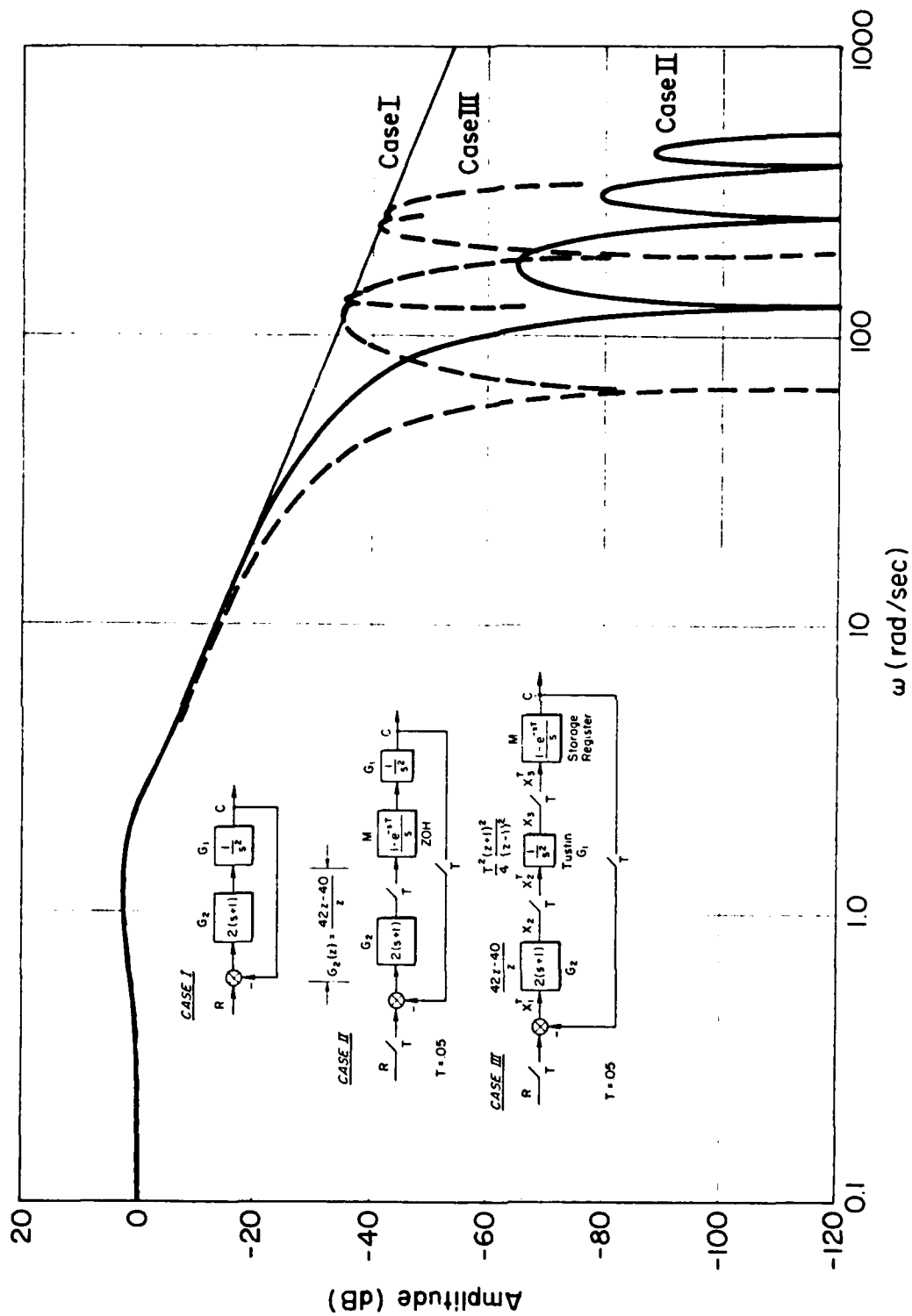


Figure 44. Comparison; Case II and Case III

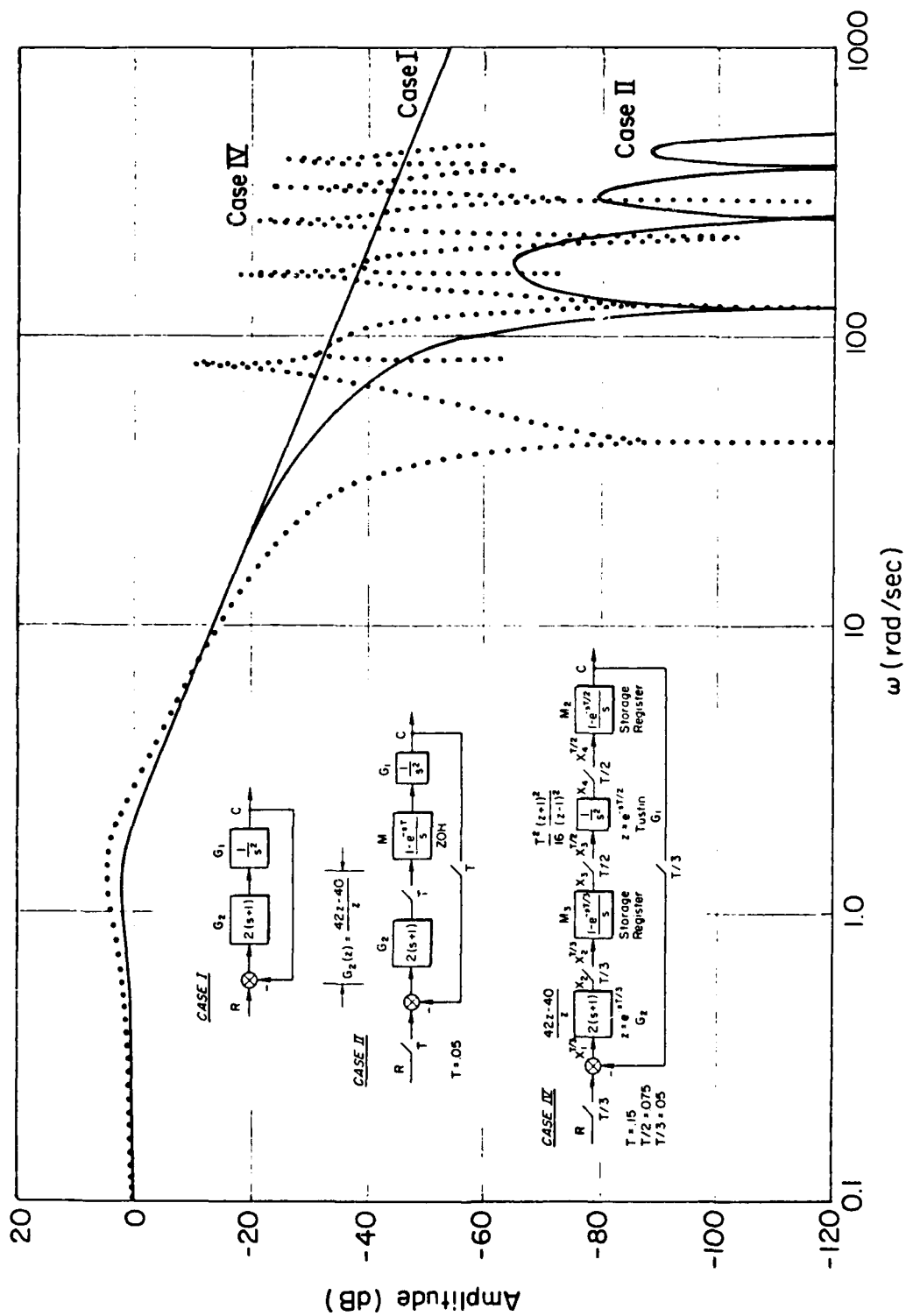


Figure 46. Comparison, Case II and Case IV

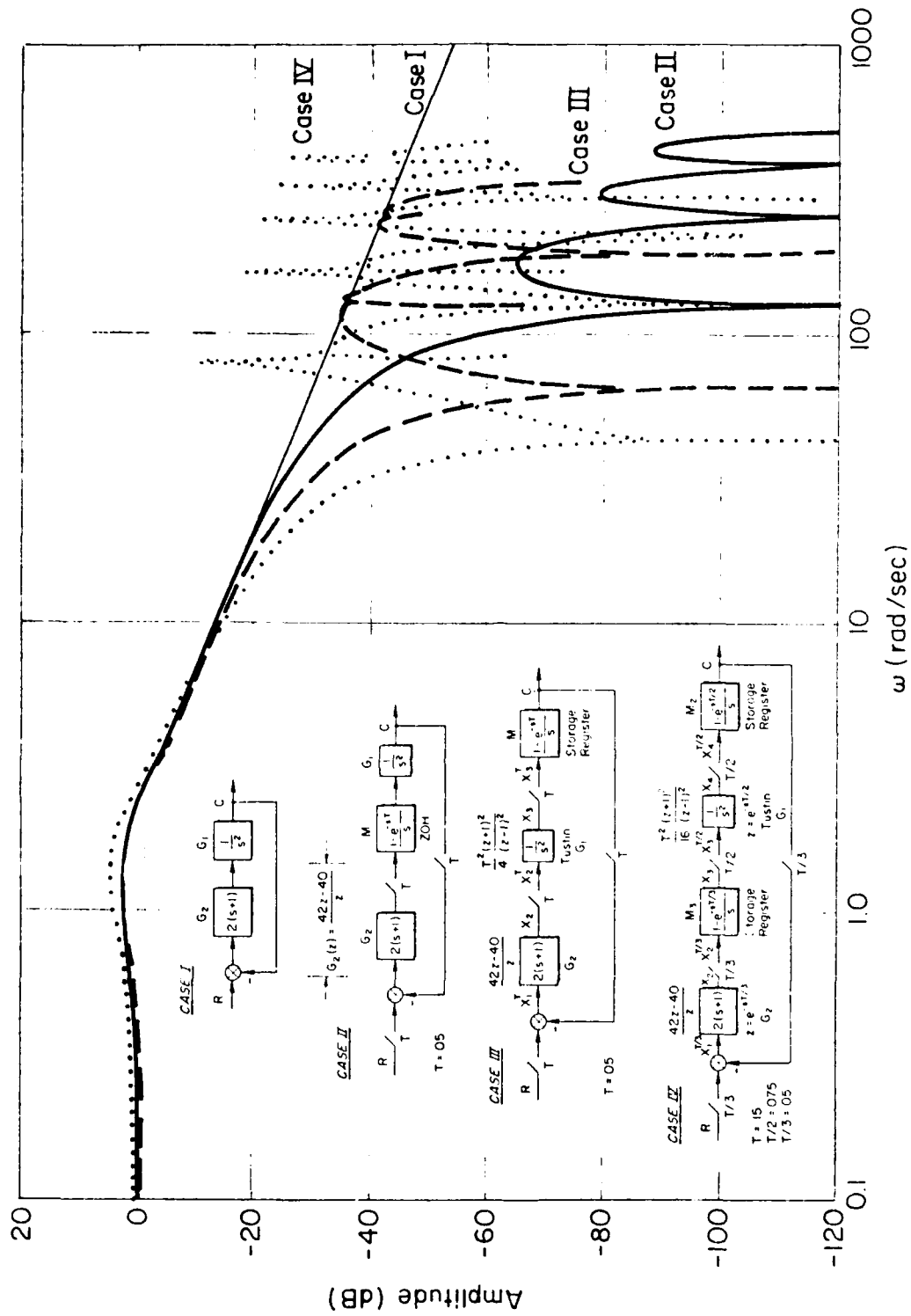


Figure 47. Comparison, All Cases

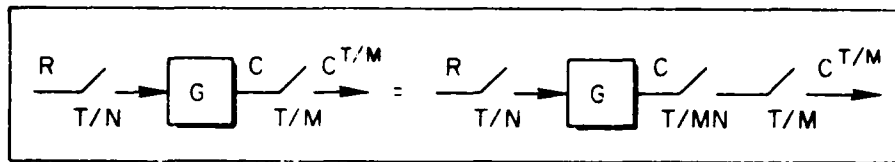


Figure 48. A Phantom Sampler Formulation of a T/N, T/M Sampling Format

so, as found in Section V,

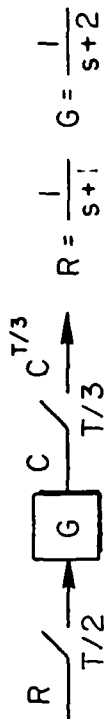
$$C^{T/3} = \frac{z^2(z^2 + e^{-5T/6})}{(z - e^{-2T/3})(z - e^{-T/3})[z^2 + (e^{-T/3})z + e^{-2T/3}]}, \quad z = e^{sT/3} \quad (258)$$

Observe that the T/2, T/3 sampling format has produced additional lightly damped modes in the output response. The reality of the additional modes can be better appreciated by first plotting the continuous variable $C(t)$ and then picking off the T/3 sample points. This is done in Figure 49. Joining the sample points with a smooth curve emphasizes the lightly damped nature of the response. This effect was also present in the two-rate simulation analysis of the previous subsection (recall the additional "overshoot" in the first fold of Figure 45).

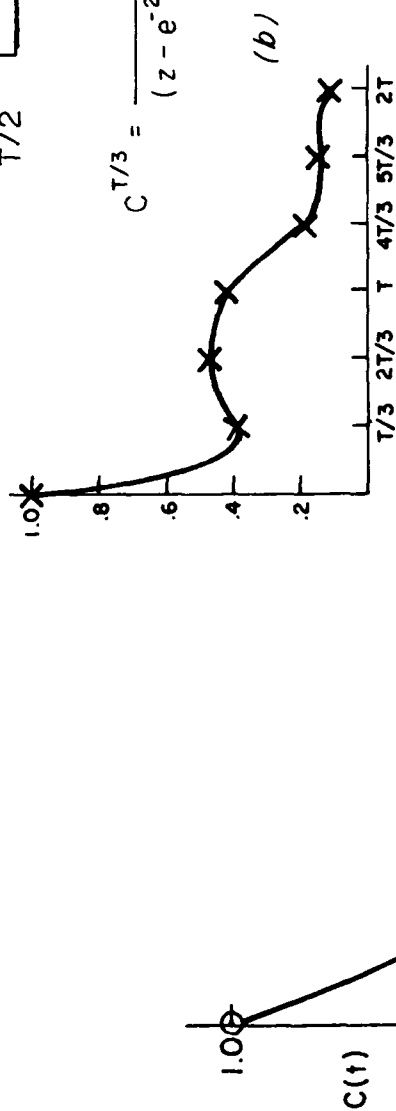
F. SECTION SUMMARY

A case study, which required the use of switch decomposition, was used to demonstrate the significant spectral differences that occur when a closed-loop system (either an analog or digital controller) is compared with an all-digital simulation of the closed-loop system. The example also treated the problems encountered when a simulation software is put up on two different (independent) computers, each working in a slightly different frame time.

In following sections, simulation case studies amenable to more direct analysis (e.g., no need for switch decomposition) will be studied.



$$R = \frac{1}{s+1} \quad G = \frac{1}{s+2}$$



$$C^{T/3} = \frac{z^2(z^2 + e^{-5/6T})}{(z - e^{-2T/3})(z - e^{-T/3})(z^2 + e^{-T/3}z + e^{-2T/3})}$$

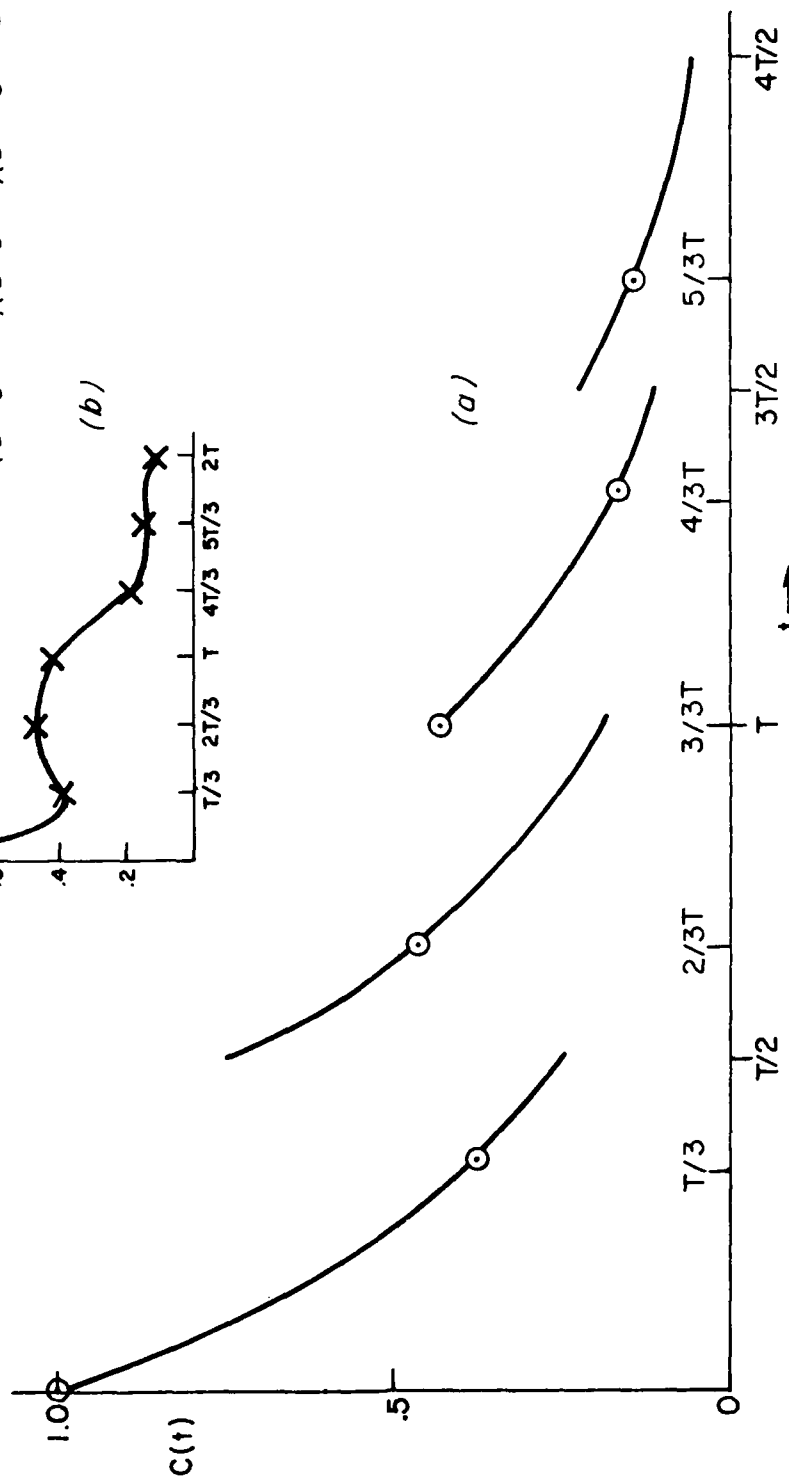


Figure 49. Response of a $T/2$ Input Sampled, $T/3$ Output Sampled System

SECTION VIII

INTERPRETATION OF MULTI-RATE FREQUENCY RESPONSE

A. INTRODUCTION

A simulation case study of the previous section required the use of switch decomposition. This section treats an open-loop case which can be analyzed by the more direct "scalar" approach discussed in Section V, affording the opportunity to gain insight in interpreting the frequency response of a multi-rate system.

It is shown, for a $T/2$ input, $T/3$ output, that three components are required to produce an exact steady-state match to the output sample sequence.

This simple case study also affords the opportunity to contrast the mathematics of the scalar approach against that of vector switch decomposition. This is done by working the scalar example through using switch decomposition notation.

B. A $T/2$ INPUT, $T/3$ OUTPUT SIMULATION EXAMPLE

The study is defined in Figure 50. Our objective is to verify that three sinusoidal components are needed to exactly match the steady state sampled points, $C^{T/3}$. From Figure 50, with $r = \sin bt$, write

$$C^{T/3} = \left\{ M_2 \left[\frac{1 - e^{-T/2}}{z - e^{-T/2}} \cdot \frac{z \sin bT/2}{z^2 - 2(\cos bT/2)z + 1} \right] \right\}^{T/3}, \quad z = e^{sT/2} \quad (259)$$

A term of

$$C^{T/3} = \left[M_2 \left(\frac{M_2}{s + 1} \right)^{T/2} R^{T/2} \right]^{T/3} \quad (260)$$

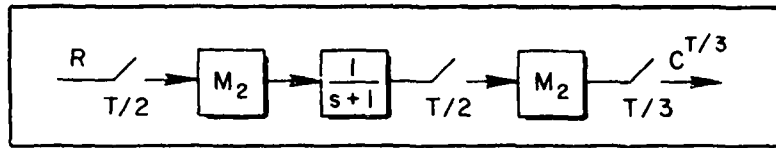


Figure 50. A Two Rate Experiment

is in a $T/2$ time frame. Since the commensurate time frame is $T/6$, z^3 must be substituted for z . Moreover, $M_2^{T/6}$ becomes, in a $T/6$ time frame

$$M_2^{T/6} = \left| \frac{1 - e^{-sT/2}}{s} \right|^{T/6} = \frac{z^3 - 1}{z^3} \cdot \frac{z}{z - 1} \equiv \frac{z^2 + z + 1}{z^2} \quad (261)$$

Therefore

$$\begin{aligned} C^{T/3} &= \left[\frac{z^2 + z + 1}{z^2} \frac{(1 - e^{-T/2}) z^3 \sin \frac{bT}{2}}{(z^3 - e^{-T/2})(z^6 - 2 \cos \frac{bT}{2} z^3 + 1)} \right]^{T/3} \\ &= \left[\frac{(1 - e^{-T/2}) \sin \frac{bT}{2} (z^3 + z^2 + z)}{z^9 - (e^{-T/2} + 2 \cos \frac{bT}{2}) z^6 + (1 + 2e^{-T/2} \cos \frac{bT}{2}) z^3 - e^{-T/2}} \right]^{T/3} \end{aligned} \quad (262)$$

As an alternative to the use of Section IV for the evaluation of Equation 262, we will use Sklansky's Identity (Appendix B) and a frame time of $T = 0.1$ seconds:

$$[G^{T/2}(z)]^T = \frac{1}{2} [G(z) + G(-z)] \quad (263)$$

Since the ratio of $T/6$ to $T/3$ is 2, the rational form of $C^{T/3}$ will be given by

$$C^{T/3} = \frac{R_{16}z^6 + R_{15}z^5 + \dots + R_{11}z + R_{10}}{R_{29}z^9 + R_{26}z^6 + R_{23}z^3 + R_{20}} \quad (264)$$

where the R_{ij} coefficients are as listed in Table 3.

Dividing the denominator of Equation 264 into the numerator gives the transient response in a $T/3$ time frame. This response is sketched in Figure 51 as a solid line but the actual discrete response follows a 2-1-2-1-2-1-2... repetition pattern (note the insert in Figure 51).

Returning to Equation 264, observe $z^2 - (2 \cos bT)z + 1$, in a T time frame, is a factor of the denominator. After factoring out this term, the denominator has the form:

$$\begin{aligned} & (R_{29}z^9 + R_{26}z^6 + R_{23}z^3 + R_{20}) \Big|_{z=e^{sT/3}} \\ &= R_{29}z^3 + R_{26}z^2 + R_{23}z + R_{20} \Big|_{z=e^{sT}} \\ &= [z^2 - (2 \cos bT)z + 1](z - .904837421) \quad (265) \end{aligned}$$

Write Equation 264, recognizing $R_{10} \equiv 0$, as

$$\begin{aligned} C^{T/3} &= \frac{(R_{16}z^6 + R_{15}z^5 + \dots + R_{11})}{[\sin(bT)]z^2} \Big|_{z=e^{sT/2}} \cdot \frac{1}{z - .904837421} \Big|_{z=e^{sT}} \\ &\cdot \frac{z \sin bT}{z^2 - (2 \cos bT)z + 1} \quad (266) \end{aligned}$$

TABLE 3. COEFFICIENTS FOR $C^{T/3}$

R10	=	0.000000000
R11	=	0.002318634
R12	=	0.007868985
R13	=	0.007068985
R14	=	0.007187567
R15	=	0.002437513
R16	=	0.002437513
R20	=	-0.904837418
R21	=	0.000000000
R22	=	0.000000000
R23	=	2.800633998
R24	=	0.000000000
R25	=	0.000000000
R26	=	-2.894845752
R27	=	0.000000000
R28	=	0.000000000
R29	=	1.000000000

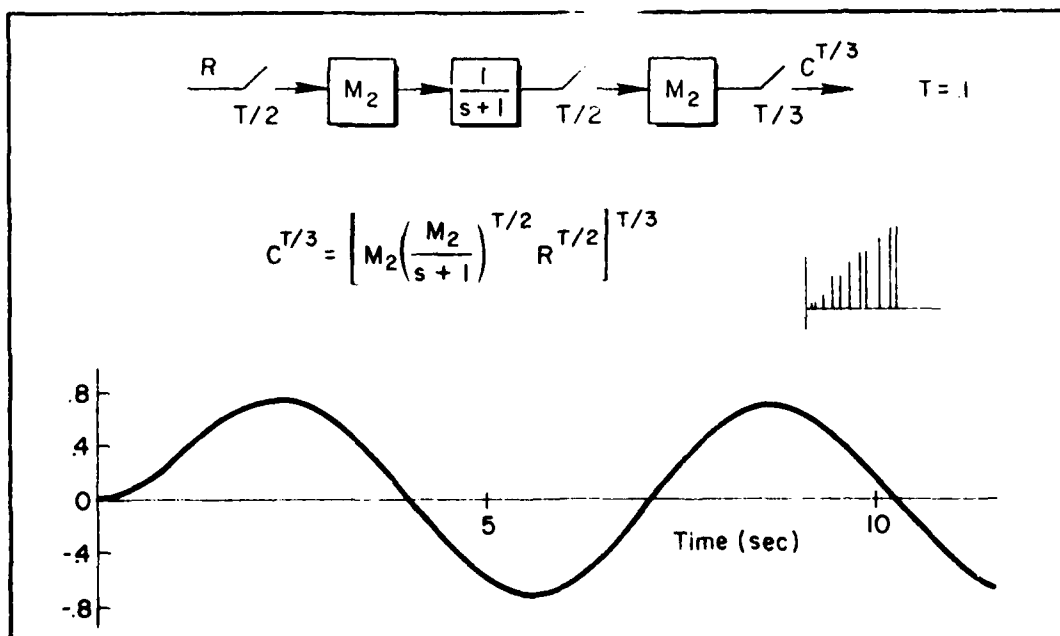


Figure 51. $C^{T/3}$ Versus Time

Equation 266 has the input factored out, in a T time frame, and therefore is equivalent to the switch decomposition approach.

The spectral coefficients are determined from the equation

$$A_n + jB_n = \frac{1}{3 \sin bT} \frac{R_{16}z^6 + R_{15}z^5 + \dots + R_{11}}{z^2} \bigg|_{z=1 \pm j\omega_b T/2} \times \frac{1}{z - .904837421} \bigg|_{1 \pm j\omega_n T/2} \quad (267)$$

where

$$\omega_n = b + \frac{2\pi n}{T}, \quad n = 0, 1, 2 \quad (268)$$

and

$$[C^{T/3}]_{ss} = \left[\sum_{n=0}^2 (A_n \sin \omega_n t + B_n \cos \omega_n t) \right]^{T/3} \quad (269)$$

Notice an important point — the scale factor $\sin bT$ and the coefficients R_{11} through R_{16} are held fixed at the input frequency but the various z 's, in their respective frame times, are evaluated at ω_n ! A consequence of ignoring this point, and running the program from scratch each time (generating $R_{11} \rightarrow R_{16}$, etc.) in terms of ω_n instead of b , will result in an erroneous set of coefficients. To verify this, we implement both procedures and compare the results.

In Table 4, the coefficients (and $\sin bT$) are first evaluated using the input frequency b . They are then "frozen" and the next two spectral components are generated. In Table 4b, the evaluation is repeated, $n = 0, 1, 2$, treating ω_n as a new input frequency. As can be seen, the first and third coefficients are unchanged but the second components disagree.

We next generate the sum of the three sine waves for each case and see how they compare against the actual sinusoidal transient response,

TABLE 4. SPECTRAL COEFFICIENTS FOR EQUATION 277

n=0	MAG	-3.010199322	-3.010199412	MAG
	ζ	-47.39926233	-47.39926170	ζ
	ω	1.000000000	1.000000000	ω
n=1		-43.30234384	-35.68901104	
		-287.3992625	-242.4231347	
		63.83185308	63.83185308	
n=2		-43.38592638	-43.38592638	
		-707.3992644	-707.3992644	
		126.6637062	126.6637062	
(a)		(b)		

as tabulated in Table 5. It can be seen that the Table 4a coefficients generate the sums of three sine waves which agree extremely well with the transient response at the T/3 sampling instant. The Table 4b set produces a sum of three sine waves, which is far less precise (sometimes disagreeing in the first significant figure).

The important result is that the T/3 output signal required three sinusoidal components for the correct steady-state fit. Contrasting this result with the switch decomposition/Bode approach of Section V affords an interesting comparison. First of all, the approach of Section V is "dimensioned" by $(W_*R)^T$, which in this case is two since R is sampled in a T/2 time frame. How is this reconciled with the present result, which insists on three output components?

In reality, there is no disagreement, since the Section V approach would use two Bode plots to pick off the same three components. We can verify this by reworking the subject example using switch decomposition.

TABLE 5. COMPARISON OF STEADY-STATE TRANSIENT RESPONSES

-.69393	-0.69394	-0.68198	
-.69393	-0.69394	-0.70351	
-.68625	-0.68626	-0.68810	
-.67686	-0.67687	-0.66536	
-.67686	-0.67687	-0.68721	a) Transient response of
-.66578	-0.66579	-0.56638	Equation 264, from z^{-360}
-.65304	-0.65305	-0.64209	to z^{-397} , where $z=e^{sT/3}$,
-.65304	-0.65305	-0.66404	$T = 0.1$.
-.63866	-0.63867	-0.63800	
-.62268	-0.62269	-0.61240	b) Sum of three sine waves
-.62268	-0.62269	-0.63424	using amplitudes and
-.60515	-0.60516	-0.60325	phase angles of Table 4a.
-.58611	-0.58612	-0.57660	
-.58611	-0.58612	-0.59810	c) Sum of three sine waves
-.56560	-0.56561	-0.56247	using amplitudes and
-.54368	-0.54369	-0.53503	phase angles of Table 4b.
-.54368	-0.54369	-0.55598	
-.52040	-0.52041	-0.51606	
-.49582	-0.49582	-0.48812	
-.49582	-0.49582	-0.50831	
-.47000	-0.47000	-0.46451	
-.44300	-0.44301	-0.43633	
-.44300	-0.44301	-0.45556	
-.41490	-0.41490	-0.40831	
-.38576	-0.38576	-0.38018	
-.38576	-0.38576	-0.39826	
-.35566	-0.35566	-0.34803	
-.32466	-0.32466	-0.32023	
-.32466	-0.32466	-0.33698	
-.29286	-0.29286	-0.28427	
-.26032	-0.26032	-0.25708	
-.26032	-0.26032	-0.27233	
-.22714	-0.22713	-0.21767	
-.19338	-0.19338	-0.19137	
-.19338	-0.19338	-0.20496	
-.15914	-0.15914	-0.14890	
-.12451	-0.12450	-0.12374	
-.12451	-0.12450	-0.13555	
(a)	(b)	(c)	

C. SWITCH DECOMPOSITION DEVELOPMENT

For comparison purposes, we next use switch decomposition on the subject example and redraw Figure 50 as Figure 52. From Figure 52,

$$C^T/3 = W_3(W_3^* M_2 W_2)^T (W_2^* \frac{1}{s+1} M_2 W_2)^T (W_2^* R)^T \quad (270)$$

$$= \begin{bmatrix} 1, e^{-sT/3}, e^{-(2/3)sT} \end{bmatrix} \begin{bmatrix} 1 & 0 \\ 1 & 0 \\ 0 & 1 \end{bmatrix} \begin{bmatrix} e^{-T/2} - e^{-T} & 1 - e^{-T/2} \\ \frac{z(1 - e^{-T/2})}{z - e^{-T}} & \frac{e^{-T/2} - e^{-T}}{z - e^{-T}} \end{bmatrix} \begin{bmatrix} R^T \\ (e^{sT/2} R)^T \end{bmatrix} \quad (271)$$

The theory of Section V gives the coefficients as

$$A_n + jB_n = \frac{[1 + e^{-sT/3} \quad e^{-(2/3)sT}]}{3} \times \frac{\begin{bmatrix} e^{-T/2} - e^{-T} & 1 - e^{-T/2} \\ (1 - e^{-T/2})z & e^{-T/2} - e^{-T} \end{bmatrix}}{z - e^{-T}} \begin{bmatrix} 1 \\ 1 \\ 1 \end{bmatrix} \quad (272)$$

$$n = 0, 1, 2$$

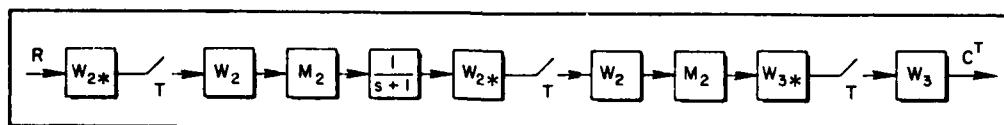


Figure 52. Switch Decomposition Model for Figure 48

Therefore,

$$\omega_n = b + \frac{2\pi n}{T}$$

$$A_n + jB_n = \frac{[1 + 1 \angle -\omega_n T/3 \quad 1 \angle -(2/3)\omega_n T]}{3}$$

(273)

$$\times \frac{\begin{bmatrix} e^{-T/2} - e^{-T} & 1 - e^{-T/2} \\ (1 - e^{-T/2}) \angle \omega_n T & e^{-T/2} - e^{-T} \end{bmatrix}}{1 \angle \omega_n T - e^{-T}} \begin{bmatrix} 1 \\ 1 \angle bT/2 \end{bmatrix}$$

$$n = 0, 1, 2 \text{ (or } n = 0, \pm 1)$$

From Equation 273, it is evident that there is no conflict between switch decomposition and the scalar approach since, for $n = 0, 1, 2$, we obtain the spectral coefficients listed in Table 4a. The switch decomposition approach confirms that three components are required ($n = 0, \pm 0.1$); in addition, $(W \star R)^T$ requires that the input remain fixed at b rad/sec. The tradeoff between the scalar approach and switch decomposition is now clear. Switch decomposition has a greater dimensionality problem, but it also has a format which protects the user from making an error since the correct uses of ω_n and b are explicitly called out. In this regard, the user must have a clear understanding of the scalar approach in order to use ω_n and b in the correct sequence.

D. SECTION SUMMARY

A scalar example was used to compare the "scalar" approach with switch decomposition. It was shown that both yield identical results.

SECTION IX

A THREE-RATE SIMULATOR CASE STUDY

A. INTRODUCTION

The simulation error analysis case studies, up to this point, have been restricted to low-order examples. Here we depart from this motif by investigating a simulation involving three computers, each working within a different frame time.

As we shall see, no new theoretical tools, other than those already introduced, will be needed to carry out the analysis. However, the reader is alerted to the fact that many computational difficulties were encountered during the course of this case study. These difficulties forced, for example, the "invention" of the multi-rate algorithm given in Section IV. The nature of the difficulties encountered will be indicated by first describing a lower dimensional example which retains the basic structure of the large-scale system study. After this, we proceed with the analysis of the title study.

B. A SIMPLIFIED THREE-RATE STUDY AND ASSOCIATED DIMENSIONAL DIFFICULTIES

For clarity, utilize a precise set of s-plane parameters in order to produce numerically convenient numbers in the z-plane. Consider the continuous system of Figure 53a which is to be simulated with the three rate configuration of Figure 53b). In Figure 53, let $T = 0.1$ sec (10 Hz),

$$\left. \begin{aligned} G_1 &= \frac{4.52569504}{s + 4.52569504} \\ G_2 &= \frac{2.2222222}{s + 2.2222222} \end{aligned} \right\} \quad (274)$$

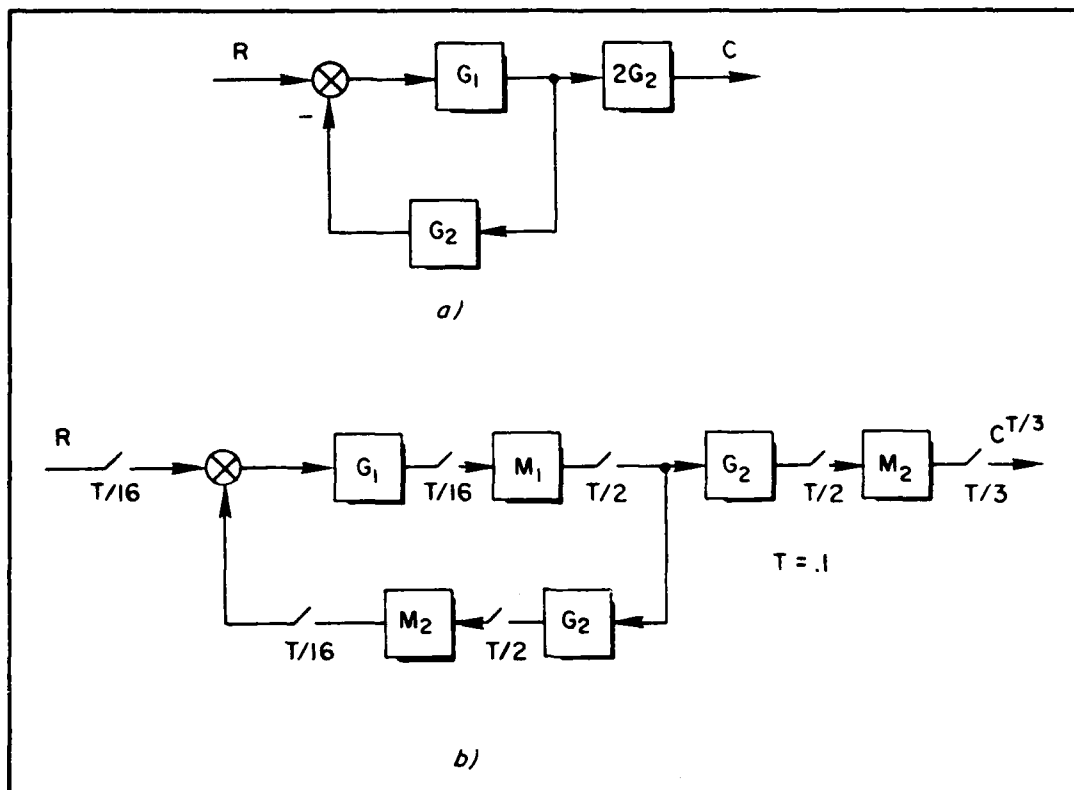


Figure 53. A Three Rate Example

and

$$M_1 = \frac{1 - e^{-sT/16}}{s}, \quad M_2 = \frac{1 - e^{-sT/2}}{s} \quad (275)$$

Assume the "digitization" required in Figure 53b is carried out using rectangular integration $[s \rightarrow (z-1)/Tz]$. For comparison purposes, the transfer function of the continuous, baseline system is

$$\frac{C}{R} = \frac{2G_1G_2}{1 + G_1G_2} = \frac{20.11420018}{s^2 + 6.747917262s + 20.11420018} \quad (276)$$

Utilizing the analysis technique of Section III gives $C^{T/3}$:

$$\begin{aligned} C^{T/3} &= \{ 2M_2 G_2^{T/2} [1 + (M_1 G_1^{T/16} M_2^{T/16})^{T/2} G_2^{T/2}]^{-1} (M_1 G_1^{T/16} R^{T/16})^{T/2} \}^{T/3} \\ &= [M_2 G_A^{T/2} (M_1 G_1^{T/16} R^{T/16})^{T/2}]^{T/3} \end{aligned} \quad (277)$$

Step I: Begin the evaluation of Equation 277 with the term

$$(M_1 G_1^{T/16} M_2^{T/16})^{T/2} = (M_1^{T/16} G_1^{T/16} M_2^{T/16})^{T/2} \quad (278)$$

Therefore

$$(G_1^{T/16} M_2^{T/16})^{T/2} = \left[\frac{.02750752/z}{z - .972492473} \cdot \frac{(z^8 - 1)}{z^8} \cdot \frac{z}{z - 1} \right]^{T/2} \quad (279)$$

since rectangular integration gives

$$\frac{a}{s + a} \Rightarrow \frac{\left(\frac{aT}{1 + aT}\right)z}{z - \left(\frac{1}{1 + aT}\right)} \quad (280)$$

and

$$\left(\frac{1 - e^{-sT/2}}{s}\right)^{T/16} = \frac{z}{z - 1} \cdot \frac{z^8 - 1}{z^8}, \quad z = e^{sT/16} \quad (281)$$

Rearrange Equation 279 as

$$[G_1^{T/16} M_2^{T/16}]^{T/2} = \left[\frac{k_0(z^7 + z^6 + z^5 + \dots + 1)}{z^7 - k_1 z^6} \right]^{T/2} \quad (282)$$

Using the techniques of Section IV, divide the denominator into the numerator and save every eighth number, since the ratio between the two frame times is eight (see Table 6, and also note $0^8 = 0$; $k_1^8 = 0.8$).

TABLE 6. THE "a" VECTOR, STEP I

a_7	0.027507527
a_6	0.194498493
a_5	0.155598794
a_4	0.124479035
a_3	0.099583228
a_2	0.079666583
a_1	0.063733266
a_0	0.050986613

Setting

$$[G_1^{T/16} M_2^{T/16}]^{T/2} = \frac{c_7 z^7 + c_6 z^6 + \dots + c_0}{(z - .8)z^6}, \quad z = e^{sT/2} \quad (283)$$

gives

$$\begin{bmatrix} c_7 \\ c_6 \\ c_5 \\ c_4 \\ c_3 \\ c_2 \\ c_1 \\ c_0 \end{bmatrix} = \begin{bmatrix} a_7 & 0 & & \\ a_6 & a_7 & & \\ a_5 & a_6 & & \\ a_4 & a_5 & \dots & \\ a_3 & a_4 & & \\ a_2 & a_3 & & \\ a_1 & a_2 & & \\ a_0 & a_1 & & \end{bmatrix} \begin{bmatrix} 1 \\ -.8 \\ 0 \\ 0 \\ 0 \\ 0 \\ 0 \\ 0 \end{bmatrix} \quad (284)$$

Solving the set of Equation 284 gives the T/2 frame time transfer function

$$\begin{aligned} [G_1^{T/16} M_2^{T/16}]^{T/2} &= \frac{.027507527z + .172492471}{(z - .8)} \\ &= \frac{R_0 z + R_1}{z - .8}, \quad z = e^{sT/2} \end{aligned} \quad (285)$$

In Equation 284, only the first two columns of the A matrix are needed since the "C" vector has only two components. Further, note

$$\begin{aligned} c_5 &= a_5 - .8a_6 = 0 \\ c_4 &= a_4 - .8a_5 = 0 \\ &\vdots \\ c_0 &= a_0 - .8a_1 = 0 \end{aligned} \quad (286)$$

verifying that z^6 is a common factor of both the numerator and denominator of Equation 283.

At this point it is clear that modeling the "buffer registers" between computers as ZOHs introduces dimensionality problems which get larger as the ratio between the frame times increases. The evaluation of Equation 283, using residue theory, would be tedious since it involves a root at the origin of multiplicity six! This multiplicity would increase significantly if the rates had been, for example, 20 Hz and 156 Hz since the ratios between frame times, in the last step, jumps to 39 (see examples A-3 through A-5 of Appendix A). While the computational burden would become simply enormous using residue theory, the algorithm of Section IV is affected in a far less sensitive way; since the only change required is the storage of every 39th value (instead of every eighth value) of the power series expansion.

Step II:

Since

$$G_2^{T/2} = \left[\frac{2.2222}{s + 2.2222} \right]_{s=(z-1)/(T/2)z}^{T/2} = \frac{.1z}{z - .9}, \quad T = .1 \quad (287)$$

the evaluation of

$$[\cdot]^{-1} = \left[I + (M_1 G_1^{T/16} M_2^{T/16})^{T/2} G_2^{T/2} \right]^{-1} = \left[1 + \frac{.1z(R_0 z + R_1)}{(z - .8)(z - .9)} \right]^{-1} \quad (288)$$

$$= \frac{(z - .8)(z - .9)}{(1 + .1R_0)z^2 + (.1R_1 - 1.7)z + .72} \quad (289)$$

is routine.

Dividing out the lead coefficient of the denominator:

$$[\cdot]^{-1} = \frac{.997256793(z - .8)(z - .9)}{z^2 - 1.678134619z + .718024891} = \frac{R_3(z - .8)(z - .9)}{z^2 + R_4z + R_5} \quad (290)$$

Computing $2G_A^{T/2}$ is also straightforward:

$$2G_A^{T/2} = 2G_2^{T/2} [\cdot]^{-1} = \frac{.2R_3(z - .8)z}{z^2 + R_4z + R_5} \quad (291)$$

Step III:

Next, treat the input term, assuming a unit amplitude sine wave at b rad/sec:

$$[M_1 G_1^{T/16} R^{T/16}]^{T/2} = [G_1^{T/16} R^{T/16}]^{T/2} \quad \text{since } M_1^{T/16} \text{ is unity} \quad (292)$$

$$= \left[\frac{.027507527z}{z - .972492473} \cdot \frac{z \sin bT/16}{z^2 - 2 \cos(bT/16)z + e^{-bT/16}} \right]^{T/2}$$

In the computer program, b is left as a free input parameter. Here the interest is in scoping dimensionality problems associated with the evaluation of Equation 277; therefore we pick a numerically convenient value for b in order to obtain an explicit expression for Equation 292.

Let

$$\cos \frac{bT}{2} = .8, \quad \sin \frac{bT}{2} = .6 \quad (293)$$

giving

$$\begin{aligned} [G_1^{T/16} R^{T/16}]^{T/2} &= \left[\frac{(.027507527)(.080350925)z^2}{(z - .972492473)(z^2 - 1.993533274z + 1)} \right]^{T/2} \\ &= \left[\frac{R_6 z^2}{z^3 + R_7 z^2 + R_8 z + R_9} \right]^{T/2} \end{aligned} \quad (294)$$

In the $T/2$ time frame, the poles of Equation 294 map into

$$D = (z - .8)(z^2 - 1.6z + 1) = z^3 - 2.4z^2 + 2.28z - .8 \quad (295)$$

giving the form for $[G_1^{T/16} R^{T/16}]^{T/2}$ as

$$[G_1^{T/16} R^{T/16}]^{T/2} = \frac{c_3 z^3 + c_2 z^2 + c_1 z + c_0}{z^3 - 2.4z^2 + 2.28z - .8} \quad (296)$$

Dividing the denominator into the numerator of Equation 294, gives the "a" vector (save each eighth number). Therefore

$$\begin{bmatrix} c_3 \\ c_2 \\ c_1 \\ c_0 \end{bmatrix} = \begin{bmatrix} a_3 & 0 & 0 & 0 \\ a_2 & a_3 & 0 & 0 \\ a_1 & a_2 & a_3 & 0 \\ a_0 & a_1 & a_2 & a_3 \end{bmatrix} \begin{bmatrix} 1 \\ -2.4 \\ 2.28 \\ -.8 \end{bmatrix} \quad (297)$$

Solving Equation 297 gives the solution; see Table 7 for a listing of the "a" and "c" vectors. Explicitly,

$$\begin{aligned} [G_1^{T/16} R^{T/16}]^{T/2} &= \frac{(.071804007z + .05238627)z}{(z - .8)(z^2 - 1.6z + 1)} \\ &= \frac{(R_{10}z + R_{11})z}{(z - .8)(z^2 - 1.6z + 1)} \end{aligned} \quad (298)$$

TABLE 7. THE "a" AND "c" VECTORS, STEP III

a_3	0.000000000	c_3	0.000000000
a_2	0.071804007	c_2	0.071804007
a_1	0.224715895	c_1	0.052386278
a_0	0.375604980	c_0	0.000000000

Step IV:

The last step introduces another dimensionality problem. The result, to this point, is

$$\begin{aligned} C^{T/3} &= \left[M_2 G_A^{T/2} (M_1 G_1^{T/16} R^{T/16})^{T/2} \right]^{T/3} \\ &= \left[\frac{1 - e^{-sT/2}}{s} \cdot \frac{(.2R_3)(z - .8)z}{z^2 + R_4z + R_5} \cdot \frac{(R_{10}z + R_{11})z}{(z - .8)(z^2 - 1.6z + 1)} \right]^{T/3} \end{aligned} \quad (299)$$

where the local definition of z is $z = e^{sT/2}$.

Follow carefully the next set of manipulations, which produces a ninth/twelfth order transfer function! (Let $(z^2 + R_4z + R_5) \times (z^2 - 1.6z + 1) = z^4 + R_{14}z^3 + \dots + R_{17}$.

$$C^{T/3} = \left[\left(\frac{1 - e^{-sT}}{s} \right)^{T/6} \cdot \frac{(R_{12}z + R_{13})z^2}{z^4 + R_{14}z^3 + R_{15}z^2 + R_{16}z + R_{17}} \right]_{z=e^{sT/2}}^{T/3} \quad (300)$$

$$= \left[\frac{z^3 - 1}{z^3} \cdot \frac{z}{z - 1} \cdot \frac{R_{12}z^3 + R_{13}}{z^{12} + R_{14}z^9 + R_{15}z^6 + R_{16}z^3 + R_{17}} \right]_{z=e^{sT/6}}^{T/3} \quad (301)$$

Cancelling powers of z and dividing $z^3 - 1$ into $z^3 - 1$ gives

$$C^{T/3} = \left[\frac{(z^2 + z + 1)z^4(R_{12}z^3 + R_{13})}{z^{12} + R_{14}z^9 + R_{15}z^6 + R_{16}z^3 + R_{17}} \right]_{z=e^{sT/6}}^{T/3} \quad (302)$$

Considering that one starts with two first-order transfer functions in the s -plane, the ninth/twelfth order transfer function in z is disconcerting. It is a good example of how the order of the system grows in a multi-rate architecture.

The ratio between the time frames is two. Finding the denominator polynomial in the $T/3$ time frame can be considerably simplified by noting the denominator is a polynomial in z^3 . Therefore, letting $x = z^3$ gives the denominator polynomial, in $T/6$, as:

$$D = (x^2 - 1.6x + 1)(x^2 - 1.678134619x + .718024891), T/6$$

$$x_{1,2} = .8 \pm j.6 \text{ in } T/6 \quad x_{3,4} = +.839067310 + j.118283309$$

$$= 1 \angle .643501109 \quad x_{3,4} = .847363494 \angle .140047156$$

$$x_{1,2}^2 \Rightarrow 1 \angle 1.28700218 \quad x_{3,4}^2 = .718024891 \angle .280094313$$

$$\Rightarrow .28 \pm j.96 \quad x_{3,4}^2 = .690043009 \pm j.198495315$$

$$\begin{array}{ccc} \Downarrow & & \Downarrow \\ x^2 - .56x + 1 \text{ in } T/3 & & x^2 - 1.380086018x + .515559744 \text{ in } T/3 \end{array}$$

Thus

$$\begin{aligned}
 D &= (z^6 - .56z^3 + 1)(z^6 - 1.380086018z^3 + .515559744) \\
 &= z^{12} - 1.940086018z^9 + 2.288407914z^6 \\
 &\quad - 1.668799475z^3 + .515559744
 \end{aligned} \tag{303}$$

in the T/3 time frame, and also defines the "c" vector.

Observe that

$$z^6 - .56z^3 + 1 = z^3 - 2(\cos bT)z + 1 \tag{304}$$

represents the poles of the sine wave input in a T time frame since $z^3 = (e^{sT/3})^3 = e^{sT}$.

To this point,

$$c^{T/3} = \left[\frac{.014321407(z^9 + z^8 + z^7) + .010448513(z^6 + z^5 + z^4)}{z^{12} - 3.278134619z^9 + 4.40304021z^6 - 2.82697445z^3 + .718024891} \right]^{T/3} \tag{305}$$

Dividing the numerator into the denominator, and saving every other value (since the ratio of time frames is 2), gives the "a" vector (see Table 8).

The answer will have the form

$$c^{T/3} = \frac{c_{12}z^{12} + c_{11}z^{11} + \dots + c_0}{(z^6 - 1.380086018z^3 + .515559744)(z^6 - .56z^3 + 1)} \tag{306}$$

where

$$\begin{bmatrix} c_{12} \\ c_{11} \\ \vdots \\ c_0 \end{bmatrix} = \begin{bmatrix} a_{12} & 0 \\ a_{11} & a_{12} \\ \vdots & a_{11} \\ \vdots & \vdots \\ \vdots & \vdots \\ a_0 & a_0 & a_{12} \end{bmatrix} \begin{bmatrix} b_{12} \\ b_{11} \\ \vdots \\ b_0 \end{bmatrix} \tag{307}$$

The entries of the "a", "b" and "c" vectors are tabulated in Table 8.

TABLE 8. a, b, and c VECTORS, PART III

a		b		c	
a ₁₂	0.000000000	b ₁₂	1.000000000	c ₁₂	0.000000000
a ₁₁	0.000000000	b ₁₁	0.000000000	c ₁₁	0.000000000
a ₁₀	0.014321407	b ₁₀	0.000000000	c ₁₀	0.014321407
a ₉	0.057396013	b ₉	-1.940086018	c ₉	0.057396013
a ₈	0.057396013	b ₈	0.000000000	c ₈	0.057396013
a ₇	0.125094126	b ₇	0.000000000	c ₇	0.097309364
a ₆	0.197844678	b ₆	2.288407914	c ₆	0.086491475
a ₅	0.197844678	b ₅	0.000000000	c ₅	0.086491475
a ₄	0.24740949	b ₄	0.000000000	c ₄	0.039820806
a ₃	0.259992496	b ₃	-1.668799475	c ₃	0.007502293
a ₂	0.259992496	b ₂	0.000000000	c ₂	0.007502293
a ₁	0.222152094	b ₁	0.000000000	c ₁	0.000000000
a ₀	0.147440916	b ₀	0.515559744	c ₀	0.000000000

Step IV:

The equation for $C^{T/3}$ (Equation 306) has now been expressed in terms of a sine wave input in a T time frame, since it can be written as

$$C^{T/3} = \frac{c_{12}z^{12} + c_{11}z^{11} + \dots + c_0}{\sin bT(z^6 - 1.380086018z^3 + .515559744)z^3} \Big|_{z=e^{sT/3}} \quad (308)$$

$$\times \frac{\sin bTz}{z^2 - 2 \cos bTz + 1} \Big|_{z=e^{sT}}$$

Following Section III and Section VIII, the three components which match the output samples are determined by

$$A_n + jB_n = \frac{1}{3 \sin bT} \times \frac{[c_{12}z^{12} + c_{11}z^{11} + \dots + c_0]}{[z(z^3 - 1.380086018z + .515559744)]} \Big|_{z=1 \pm j \omega_n T} \quad (309)$$

The precautions noted in Section VIII must be observed. The coefficients of Equation 309 are tied to the input frequency b , but the evaluation of z is carried out in terms of ω_n , where

$$\omega_n = b + \frac{2\pi n}{T}, \quad n=0, \pm 1 \quad (310)$$

To obtain a feel for the effect of the three-rate sampling format on the Bode plot, run a comparison with the continuous baseline case (Equation 286) by passing $C^{T/3}$ through a ZOH. Thus, we may suppose the $C^{T/3}$ samples are being reconstructed into a staircase signal in order to drive, perhaps, a motion-base simulator actuator. In this event,

$$A_n + jB_n = \frac{1 - e^{-sT/3}}{Ts} \Big|_{s=j\omega_n} \times \frac{[c_{12}z^{12} + \dots + c_0]_{z=1 \pm j \omega_n T/3}}{\sin bT[z^6(z^3 - \dots)]_{z=1 \pm j \omega_n T/3}} \quad (311)$$

$$\omega_n = b + \frac{2\pi n}{T}, \quad n = 0, \pm 1, \pm 2, \dots \quad (312)$$

The resultant "primary" Bode plot is shown in Figure 54. Recall, from Section V, that this Bode plot is only one of the two needed to completely define the coefficients.

A most interesting phenomenon is evident in Figure 54, namely the digitized system has less phase lag than the continuous baseline system! This is different than the results one would expect from a single-rate simulation and therefore deserves careful analysis.

First of all, the phase lead noted at 10 rad/sec cannot be attributed to a failure of the computer program to add in a correct multiple of 2π , since we do not expect to see a phase difference of approximately 300 deg at this low frequency between the baseline and its discrete version.

Next, a small experiment was performed wherein the transient response was run for a sine wave input. The three sine wave components given by the $N = 3$ discrete theory were found to match the steady-state output samples exactly. Thus, the algorithms appear to be correctly implemented in the computer code.

One might also speculate that Figure 54 represents only one of the two Bode plots needed to completely specify the infinite set of sine waves needed to match the staircased signal that is reconstructed by the ZOH. Hence, one could argue that the lead shown at, for example, 20 rad/sec might be completely negated by the phase contributions of other components.

As we shall see, the same sort of phase lead phenomenon arises in the larger-scale case study, to be discussed next. At this juncture, it is felt that the evidence is not strong enough to draw the blanket conclusion that a multi-rate sampling format is an effective way to introduce phase lead into a simulation.

C. THE A-10, DISPLAYED PITCH TO PILOT STICK FORCE CASE STUDY

This case study represents an important element extracted from an overall simulation of the A-10 aircraft. It was initially coded for use

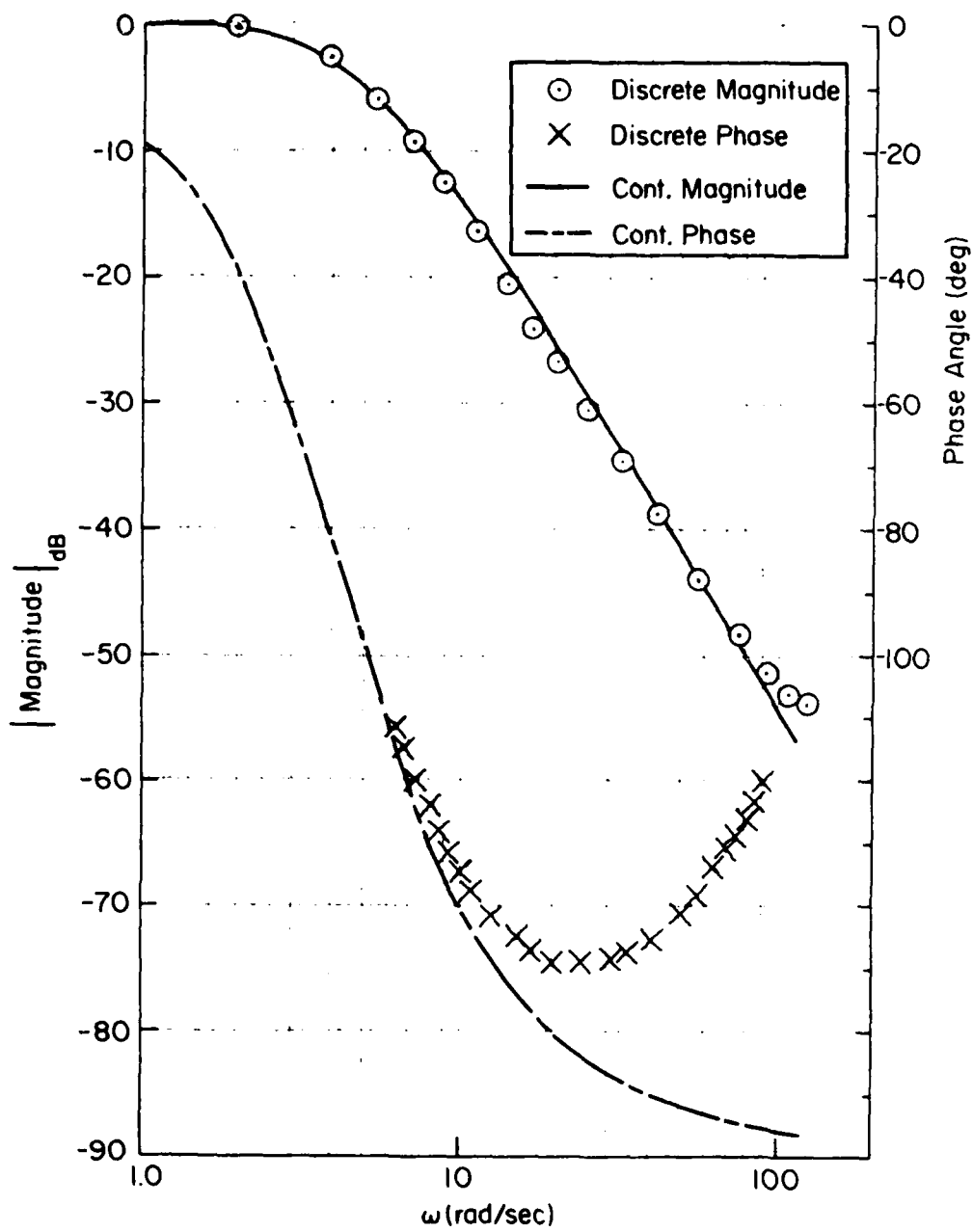


Figure 54. A-10 Like Example

in a training (moving-base) simulator. Engineers of the Simulator System Program Office (ASD/ENETS) proposed it as a case study because of its interesting structure. Specifically, three elements of the displayed pitch angle to pilot stick force input simulation were implemented on three different computers.

The initial rendering of the three-rate A-10 example resulted in the representation shown in Figure 55. Shown also are the s-plane representations for the eleven transfer functions involved. The intent of this figure is to convey the following:

1. Each transfer function is digitized using rectangular integration.
2. The G_1 algorithm feeds G_2 , the G_3 algorithm feeds G_9 and G_7 , etc.

The representation of Figure 55 is a "shorthand" which introduces no difficulties if it is understood that each transfer function is digitized individually. The Figure 55 representation would cause problems if z-transform operations were to be carried out since $[G_1(s)G_2(s)]^T \neq G_1^T(s) \times G_2^T(s)$. To emphasize the individual digitization and the three different rates, we may redraw Figure 55 as shown in Figure 56, where data holds are used to model storage registers. In Figure 55, the T_1 data rate was changed from 156 Hz to 160 Hz so that a basic interval of 0.1 second (as opposed to 1.0 second) could be assigned to T . That is

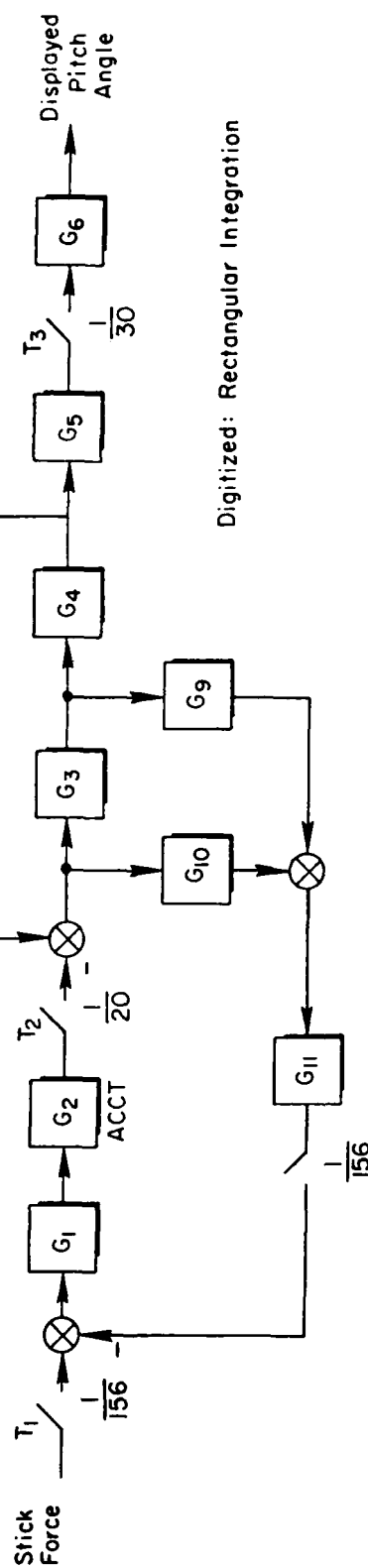
$$\frac{1}{160} = \frac{.1}{16} , \quad \frac{1}{20} = \frac{.1}{2} , \quad \frac{1}{30} = \frac{.1}{3}$$

so that, when $T = 0.1$, the rates can be represented as

$$T_1 = \frac{T}{16} , \quad T_2 = \frac{T}{2} , \quad T_3 = \frac{T}{3}$$

At the time this decision was made, it was felt that these rates were sufficiently separated to expose the basic character of the three-rate problems and to "simplify" the integers involved.

Also indicated in Figure 56 is a suggested change to the initial drawing. It is probably realistic to model the displayed pitch angle as



$$\begin{aligned}
 G_1 &= \frac{50.6}{s^2 + 66s + 3025} & G_2 &= \frac{25}{s + 25} & G_3 &= \frac{-s(4.78s + 4.1)}{s^2 + 2.1s + 3.51} \\
 G_4 = G_5 &= \frac{1}{s} & G_6 &= e^{-.07s} & G_7 &= \frac{.55(s+10)(s+20)}{(s+2)(s+5)(s+40)} \\
 G_8 &= \frac{50}{s^2 + 35s + 2500} & G_9 &= .2792 & G_{10} &= \frac{.01745(.56s^2 + .04s - 55)}{s^2 + 21s + 3.51} \\
 G_{11} &= 3.0
 \end{aligned}$$

Figure 55. A-10 Case Study - Original Representation

a staircased function; therefore, a data hold, in a $T/3$ frame time, should be inserted before the $e^{-.075}$ pure time delay.

Since several of the operations occur at the same rate, we may elect to simplify the blocks by referring to Figure 56. From the figure, write

$$D^{T/2} = G_{11}^{T/2} [G_{10}^{T/2} + G_9^{T/2} G_3^{T/2}] C^{T/2} \quad (313)$$

$$= G_c^{T/2} C^{T/2} \quad (314)$$

$$B^{T/2} = G_4^{T/2} G_3^{T/2} C^{T/2} = G_B^{T/2} C^{T/2} \quad (315)$$

$$E^{T/2} = G_5^{T/2} G_4^{T/2} G_3^{T/2} C^{T/2} = G_5^{T/2} G_B^{T/2} C^{T/2} \quad (316)$$

$$A^{T/2} = G_8^{T/2} G_7^{T/2} B^{T/2} = G_D^{T/2} B^{T/2} \quad (317)$$

Using the definitions of Equations 314 through 317 we may draw the more compact diagram of Figure 57.

D. A-10 SWITCH DECOMPOSITION MODEL

The switch decomposition model for Figure 57 is shown in Figure 58. We must now inquire as to whether or not the switch decomposition model for Figure 57 would give the same answer as a switch decomposition model of the more detailed Figure 56. That is, the switch decomposition model of Figure 59b will give the same answer as Figure 59a. Will the switch decomposition model of Figure 59c also give the correct answer? The answer to this is in the affirmative.

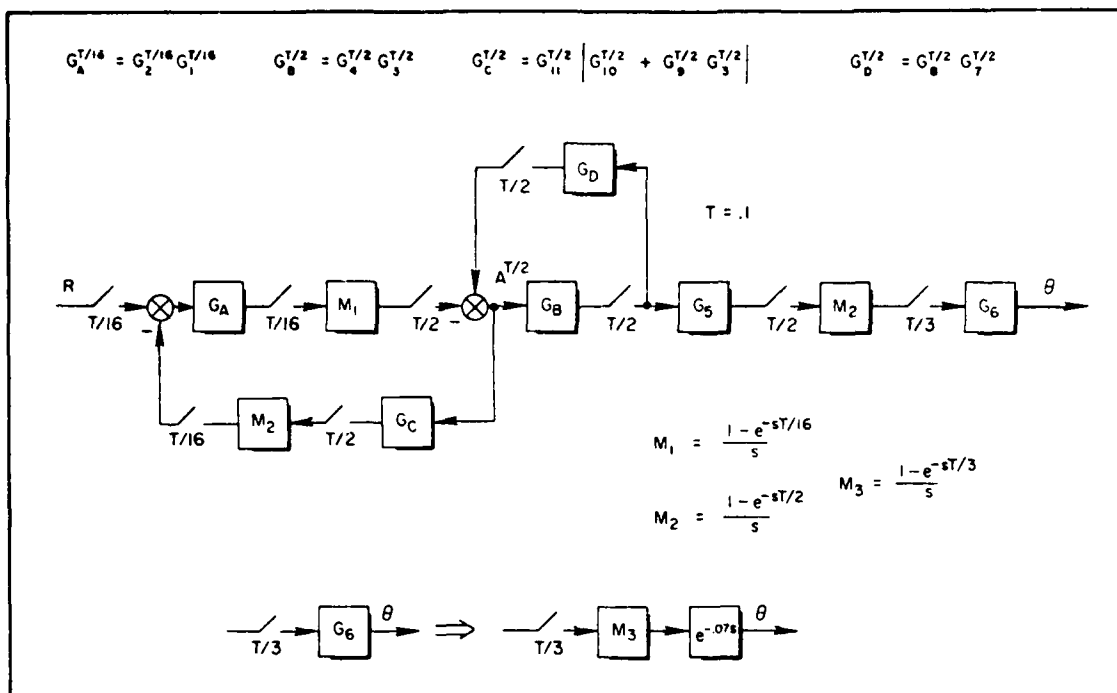


Figure 57. A-10 Case Study-Simplified Block Diagram

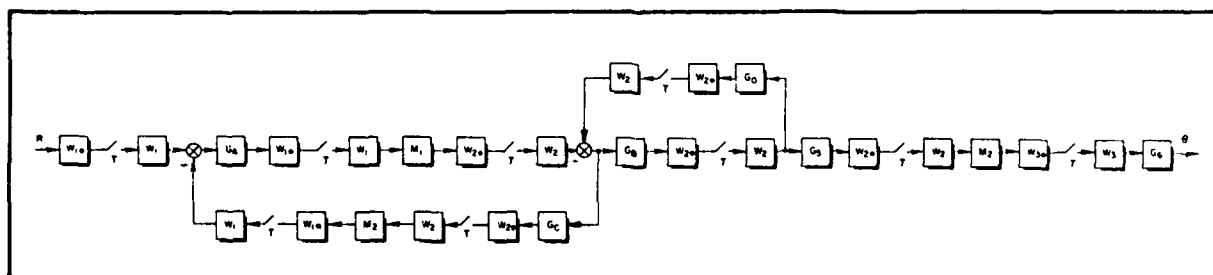


Figure 58. Switch Decomposition Block Diagram

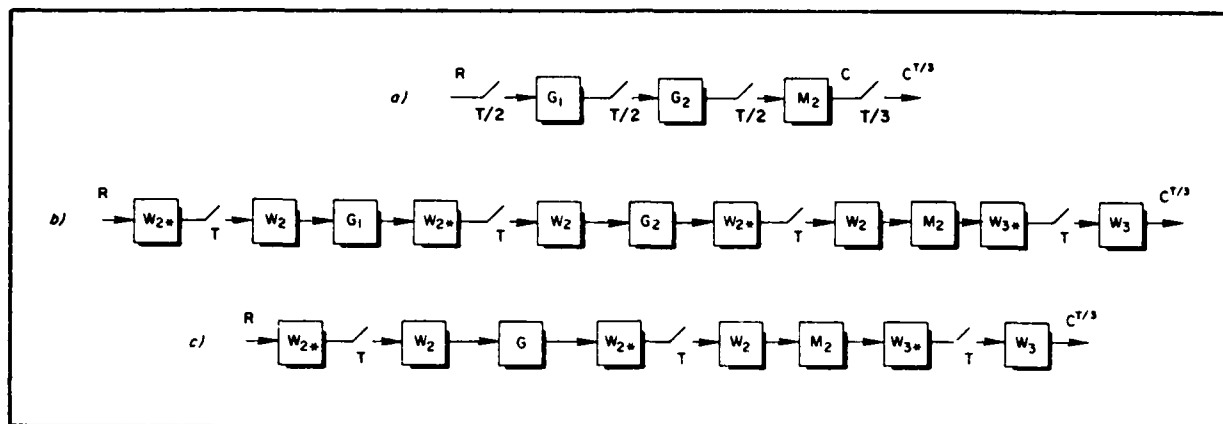


Figure 59. Equivalent Models

From Figure 59a

$$C^{T/3} = [M_2 G_2^{T/2} G_1^{T/2}]^{T/3} \quad (318)$$

and from Figure 59b,

$$C^{T/3} = W_3 (W_3^* M_2 W_2)^T (W_2^* G_2 W_2)^T \times (W_2^* G_1 W_2)^T (W_2^* R)^T \quad (319)$$

From Figure 59c, one finds

$$C^{T/3} = W_3 (W_3^* M_2 W_2)^T (W_2^* G W_2)^T (W_2^* R)^T \quad (320)$$

Now, rearrange Equation 320 (nest the T operators)

$$C^{T/3} = \{ [W_3 (W_3^* M_2 W_2) (W_2^* G W_2) (W_2^* R)^T]^T \}^T \quad (321)$$

Notice $W_2 (W_2^* R)^T \triangleq R^{T/2}$, therefore

$$C^{T/3} = \{ [W_3 (W_3^* M_2 W_2) (W_2^* G R^{T/2})^T]^T \}^T$$

Next, note $W_2(W_2^*GR^{T/2})^T$ is by definition $G^{T/2}R^{T/2}$ which is, in turn, $G_2^{T/2}G_1^{T/2}R^{T/2}$. The last T operator,

$$C^{T/3} = W_3(W_3^*M_2G_2^{T/2}G_1^{T/2}R^{T/2})^T \triangleq [M_2G_2^{T/2}G_1^{T/2}R^{T/2}]^{T/3} \quad (322)$$

Thus the switch decomposition model of Figure 59c is exactly equivalent to the model of Figure 59b.

When this study was initiated, switch decomposition appeared to be the logical solution to the problem. However, the developments of Section III pushed the decomposition approach into the background. Figures 58 and 59 are therefore given only to illustrate an alternate approach.

E. ALGEBRAIC MANIPULATIONS

Referring to Figure 57, write

$$\begin{aligned} A^{T/2} = & - [M_1G_A^{T/16}R^{T/16}]^{T/2} + \{M_1G_A^{T/16}[M_2G_C^{T/2}A^{T/2}]^{T/16}\}^{T/2} \\ & + G_B^{T/2}G_D^{T/2}A^{T/2} \end{aligned} \quad (323)$$

Simplify Equation 323:

$$\begin{aligned} A^{T/2} = & - [M_1G_A^{T/16}R^{T/16}]^{T/2} + [M_1G_A^{T/16}M_2^{T/16}]^{T/2} G_C^{T/2}A^{T/2} \\ & + G_B^{T/2}G_D^{T/2}A^{T/2} \end{aligned} \quad (324)$$

Therefore,

$$\begin{aligned} A^{T/2} = & - \{I - [M_1G_A^{T/16}M_2^{T/16}]^{T/2} G_C^{T/2} - G_B^{T/2}G_D^{T/2}\}^{-1} \\ & \times [M_1G_A^{T/16}R^{T/16}]^{T/2} \end{aligned} \quad (325)$$

The final result is

$$\theta = G_6 [M_2 G_5^{T/2} G_B^{T/2} A^{T/2}]^{T/3} \quad (326)$$

or

$$\begin{aligned} \theta = & -G_6 \{ M_2 G_5^{T/2} G_B^{T/2} [I - (M_1 G_A^{T/16} M_2^{T/16})^{T/2} - G_B^{T/2} G_D^{T/2}]^{-1} \\ & \times [M_1 G_A^{T/16} R^{T/16}]^{T/2} \}^{T/3} \end{aligned} \quad (327)$$

Comparing this with Equation 277, it can be appreciated that the A-10 case study reduces to the same type of computations required for the simpler example. The dimensionality will be, of course, considerably higher. We will, therefore, not repeat the analysis of the previous section, but merely note that a computer program was written for Equation 327 and the results computed on a Tymshare terminal. The s- and z-plane transfer functions are listed in Table 14 in Appendix D. We proceed immediately to a discussion of the results. To compare the difference, the continuous baseline Bode plot is shown with the Bode plot obtained by assuming that the displayed pitch angle sample sequence is reconstructed with a ZOH (in order to drive the display generator).

F. COMPARISON WITH BASELINE

The Bode plot associated with the three-rate simulation, together with that of the continuous baseline system, is shown in Figure 60. Again, one must keep in mind that this is only one of the two plots needed to completely define the spectral components (although it does appear to be the primary one).

As was the case with the lower-order examples used previously, we note the phase lead, at low frequencies, is less for the digitized version than it is for the continuous model. Clearly, this phenomenon requires further study and we caution against adopting the viewpoint that a multi-rate sampling format is a technique which will always introduce phase lead into a simulation.

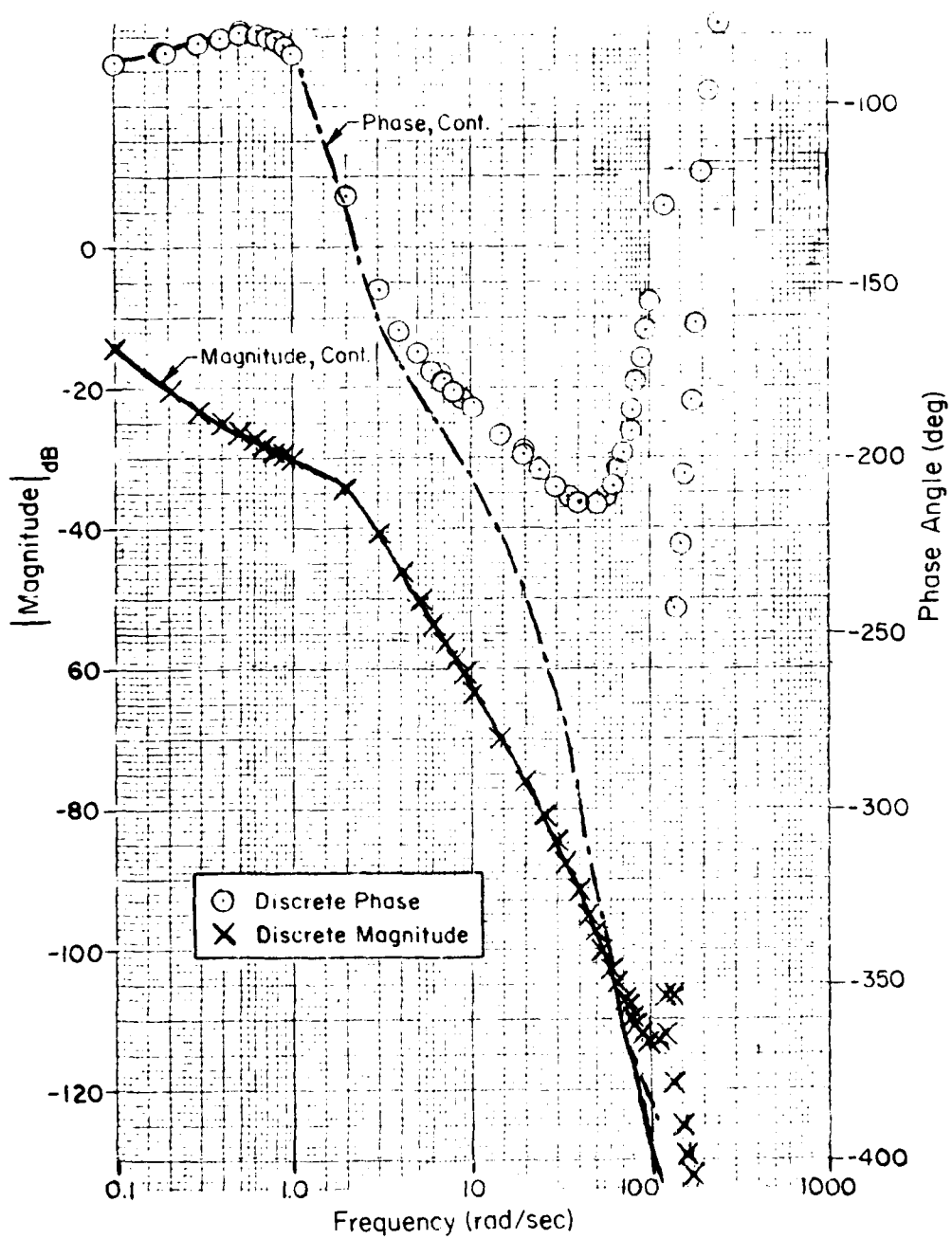


Figure 60. Display Pitch Angle to Stick Force Input

G. SUMMARY AND CONCLUSIONS

Two case studies, which utilized three different sampling rates, were analyzed. Each introduced phase lead into the first fold of the frequency response, a result which contradicts our intuitive expectations. It was shown that the multi-rate analysis tool, developed in Section IV, was an effective tool for treating the dimensional problems introduced by the variations in the three sampling frequencies.

SECTION X
AN ORDER-OF-CALL CASE STUDY

A. INTRODUCTION

This section focuses on a single-rate case study which is concerned with order-of-call effects. These anomalies are introduced when one element of code calls another element containing results predicated on "fresh" input data but which, in reality, used "stale" data (because the new data were not yet available). Specifically, we study a roll/sway washout network simulation wherein a pure delay is introduced in an integration algorithm. This case study was suggested by AFWAL/FIGD personnel who are associated with LAMARS. The problem was first described in Reference 5. The following description of the problem is excerpted from that reference.

B. DESCRIPTION OF WASHOUT COMPUTATION

In the LAMARS motion washout routine, transfer functions are implemented by representing the output variable as a function of the input variable and also representing it implicitly as integrals of the output variable itself. The output equation is evaluated first, then the derivatives of the states are computed based upon the output and lower states, then finally all integrations are performed using the Adams-Bashforth second-order predictor algorithm.

For a third-order washout filter of the form used in the \dot{w} path, the implementation is developed as follows:

$$\frac{\text{Output}}{\text{Input}} = \frac{y}{r} = \frac{b_3 s^3}{s^3 + a_2 s^2 + a_1 s^1 + a_0} \quad (328)$$

[Divide through by s^3]

$$\frac{y}{r} = \frac{b_3}{1 + \frac{a_2}{s} + \frac{a_1}{s^2} + \frac{a_\phi}{s^3}} \quad (329)$$

[Cross multiply]

$$\left(1 + \frac{a_2}{s} + \frac{a_1}{s^2} + \frac{a_\phi}{s^3}\right) y = b_3 r \quad (330)$$

[Move integrations to input side]

$$y = b_3 r - \frac{1}{s} \left[a_2 + \frac{1}{s} \left(a_1 + \frac{1}{s} a_\phi \right) \right] y \quad (331)$$

[Define output in terms of input and highest-order state]

$$y = b_3 r - w_3$$

[Define states from deepest nesting outward]

$$\dot{w}_1 = a_\phi y \quad \Rightarrow \quad w_1 = \frac{1}{s} \dot{w}_1$$

$$\dot{w}_2 = a_1 y + \frac{1}{s} a_\phi y = a_1 y + w_1 \quad \Rightarrow \quad w_2 = \frac{1}{s} \dot{w}_2 \quad (332)$$

$$\dot{w}_3 = a_2 y + \frac{1}{s} a_1 y + \frac{1}{s} 2a_\phi y = a_2 y + w_2 \quad \Rightarrow \quad w_3 = \frac{1}{s} \dot{w}_3$$

Thus, the input is seen immediately in the output and thence in all derivatives of the states, but the states themselves are not updated. The expansion outward from the nesting results in state equations which assume in their form that updated states are continuously available. However, since all loops are then implicitly expanded in full prior to

any integrations, a lag with respect to the system state response is introduced, while immediacy of response with respect to the input is preserved.

C. THIRD-ORDER WASHOUT CASE STUDY

The analog block diagram of the previous equations is given in Figure 61b and then translated into the digital version of Figure 61a. In Figure 61a, there is an explicit model of the order of call. That is, the integrations are performed last in the cycle. This has been interpreted to mean, on any given machine cycle, that w_1 , w_2 , w_3 are the old values (previous frame time values). Thus, the integration of \dot{w}_1 that contributes to \dot{w}_2 is one frame time old, the integration of \dot{w}_2 which contributes to \dot{w}_3 is a frame time old, as is the integration of \dot{w}_3 which produces w_3 .

In evaluating $(1/s)^T$, Reference 5 calls for the use of an Adams-Bashforth second-order predictor algorithm. It was later agreed that nothing essential would be lost by using "Implicit" Adams-Bashforth second-order, which is described by Figure 62 and the equations

$$X_n = X_{n-1} + (T/2)[3\dot{X}_n - \dot{X}_{n-1}] \quad (333)$$

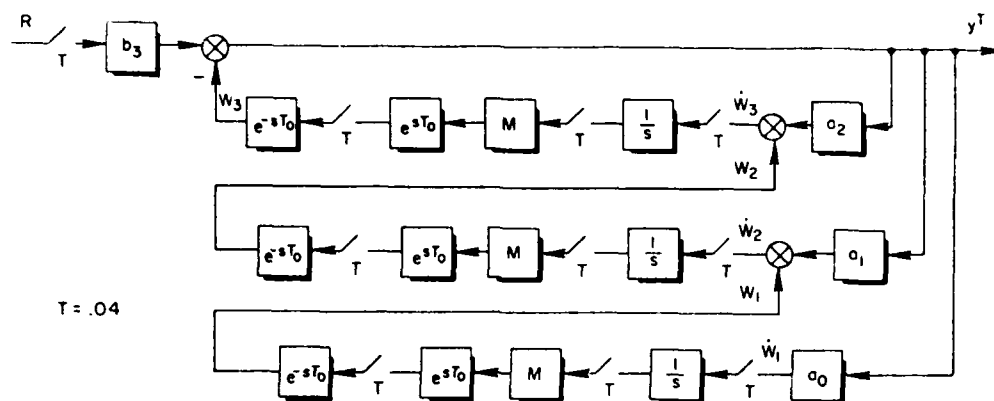
which gives,

$$\frac{\dot{X}}{X} = \frac{(T/2)(3z - 1)}{z - 1} \quad (334)$$

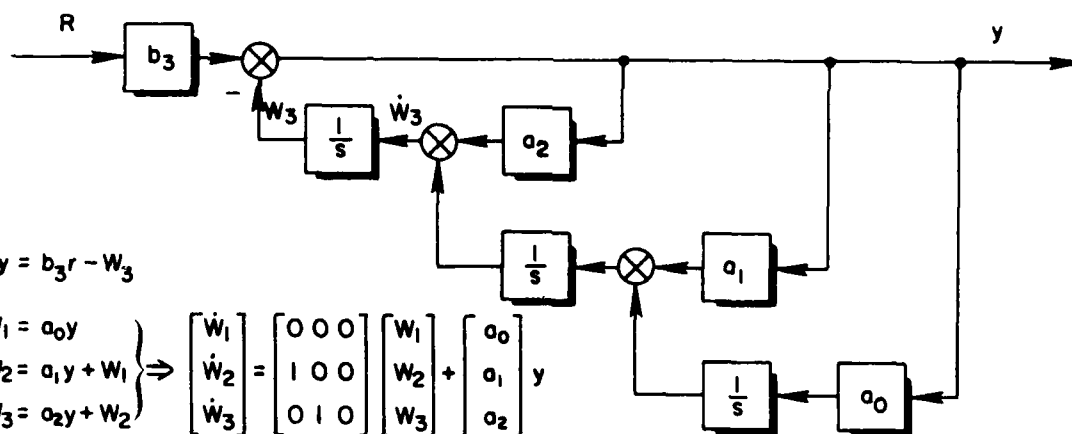
If the integrations could be accomplished with very little throughput delay, $T_0 = 0$, one could write, after setting

$$G(z) = \frac{(T/2)(3z - 1)}{z - 1} \quad (335)$$

$$y^T = b_3 R^T - [a_2 G + a_1 G^2 + a_0 G^3] y^T \quad (336)$$



a)



1) $y = b_3 r - W_3$

2) $\begin{cases} \dot{W}_1 = a_0 y \\ \dot{W}_2 = a_1 y + W_1 \\ \dot{W}_3 = a_2 y + W_2 \end{cases} \Rightarrow \begin{bmatrix} \dot{W}_1 \\ \dot{W}_2 \\ \dot{W}_3 \end{bmatrix} = \begin{bmatrix} 0 & 0 & 0 \\ 1 & 0 & 0 \\ 0 & 1 & 0 \end{bmatrix} \begin{bmatrix} W_1 \\ W_2 \\ W_3 \end{bmatrix} + \begin{bmatrix} a_0 \\ a_1 \\ a_2 \end{bmatrix} y$

3) $W_1 = \frac{1}{s} \dot{W}_1$

$W_2 = \frac{1}{s} \dot{W}_2$

$W_3 = \frac{1}{s} \dot{W}_3$

b)

Figure 61. Washout Analog Block Diagrams

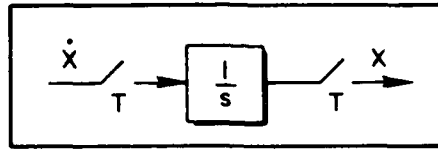


Figure 62. Discrete Integrator

or

$$y^T = [I + a_2G + a_1G^2 + a_0G^3]^{-1} b_3 R^T \quad (337)$$

With time delay, the equation for W_2 in terms of \dot{W}_2 becomes

$$W_2 = e^{-sT_0} \left(e^{sT_0 M} \right)^T \left(\frac{1}{s} \right)^T \dot{W}_2 \quad (338)$$

If $T_0 = T$, this reduces to

$$W_2 = \frac{(T/2)(3z - 1)}{z(z - 1)} \dot{W}_2 \quad (339)$$

G is modified by the factor z^{-1} . This procedure can be repeated on the other two "nestings" giving the same result. Each G of the no-delay case is only modified by z^{-1} and Equation 347 can be used for both cases.

The result obtained requires careful validation since it forces the characteristic equation of Equation 337 to increase by an order of two. To see this, insert the appropriate $G(z)$'s and clear through:

$$\begin{aligned} & \{ [1 + (3/2)Ta_2 + (9/4)T^2a_1 + (27/8)T^3a_0]z^3 \\ & + [-3 - (7/2)Ta_2 - (15/4)T^2a_1 - (27/8)T^3a_0]z^2 \\ & + [3 + (5/2)Ta_2 + (7/4)T^2a_1 + (9/8)T^3a_0]z \\ & + [-1 - (T/2)a_2 - (T/4)^2a_1 - (T/8)^3a_0] \} y^T = b_3(z - 1)^3 R^T \end{aligned} \quad (340)$$

No Delay

$$\begin{aligned}
& \{z^6 + [-3 + (3/2)Ta_2]z^5 \\
& + [3 - (7/2)Ta_2 + (9/4)T^2a_1]z^4 \\
& + [-1 + (5/2)Ta_2 - (15/4)T^2a_1 + (27/8)T^3a_0]z^3 \\
& + [-(7/2)a_2 + (7/4)T^2a_1 - (27/8)T^3a_0]z^2 \\
& + [-(7/4)^2a_1 + (9/8)T^3a_0]z - (7/8)^3a_0\} y^T = b_3z^3(z-1)^3R^T \\
& \text{Delay}
\end{aligned} \tag{341}$$

For $G = (6s^3)/(s^3 + 6s^2 + 11s + 6)$ and $T = 0.04$, Equation 340 yields three real roots, all interior to the unit circle (we are using convenient numbers; more realistic parameter values will be used for a sixth-order case, which follows).

$$\Delta(z) = (z - .898304953)(z - .962264027)(z - .928571684) \tag{342}$$

With the frame time delay in the integration, Equation 351 gives

$$\begin{aligned}
\Delta(z) = & (z - .887598)(z - .960815504)(z - .92332214) \\
& \times (z + .067598089)(z + .043321992)(z + .020815562)
\end{aligned} \tag{343}$$

The results for the sixth- and third-order models are summarized in Equations 344a and 344b, the data for which are given in Table 9.

$$G_1 = \frac{a_0(z^3)(z-1)^3}{z^6 + b_5a^5 + b_4z^4 + b_3z^3 + b_2z^2 + b_1z + b_0} \tag{344}$$

or

$$G_2 = \frac{C_0(z-1)}{z^3 + d_2z^2 + d_1z + d_0} \tag{345}$$

TABLE 9. THIRD, SIXTH MODEL DATA

b_0	-0.000048000	d_0	-0.802663438
b_1	-0.003968000	d_1	2.592078213
b_2	-0.090496000	d_2	-2.789140664
b_3	-0.464704000	c_0	4.282973183
b_4	2.199600000		
b_5	-2.640000000		
a_0	6.000000000		

The results of this analysis are most interesting. They indicate the order of call has introduced an effective filter which essentially doubles the order of the analytical model describing the software. In the illustrative example we see that the "delay" case tracks very well with the continuous baseline and no delay case (See Table 10). Indeed, one could conclude that the delay case is superior to the no delay case.

The correctness of the result can also be checked by running the impulse response using both the analytical model of the simulation and the actual computer code. The results shown in Table 11 indicate an extremely close agreement.

Thus we see that the manner in which an algorithm is implemented can introduce filtering over and above that intended by the designer. We shall explore this in more depth by next considering a sixth-order washout using parameter values supplied by FIGD personnel.

D. SIXTH-ORDER WASHOUT EXAMPLE

Here we treat a sixth-order model where the transfer function represents lateral acceleration (\ddot{Y}_{m2}) to roll rate (P_A):

TABLE 10. SOME REPRESENTATIVE BODE DATA

CONT	DIS	DIS; DELAY	CONT	DIS	DIS; DELAY
-120.0005911	-120.0006642	-120.0005999	14.01735774	12.28653932	13.97503999
-91.05040044	-91.11899830	-91.05044330	54.46232222	50.09119130	55.69590270
0.010000000	0.010000000	0.010000000	6.000000000	6.000000000	6.000000000
-180.0000059	-180.0000182	-180.0000084	14.40216873	12.61310126	14.36740142
-90.10504226	-90.11210010	-90.10512690	47.27408877	43.31053680	48.76104630
0.001000000	0.001000000	0.001000000	7.000000000	7.000000000	7.000000000
-60.05888036	-60.06541674	-60.05905324	14.66097293	12.83135607	14.63628342
-100.4821508	-101.1664380	-100.4821864	41.71730504	38.08537770	43.45181610
0.100000000	0.100000000	0.100000000	8.000000000	8.000000000	8.000000000
-4.436974992	-4.859473342	-4.449544768	14.84282270	12.98402528	14.83040444
-180.0000000	-184.9740046	-179.9521582	37.30394825	33.94152068	39.28017040
1.000000000	1.000000000	1.000000000	9.000000000	9.000000000	9.000000000
6.464791314	5.521755650	6.434095066	14.97521290	13.09480294	14.97704684
-232.1250164	-238.3150849	-231.9073447	33.71976986	30.57707520	35.93191140
2.000000000	2.000000000	2.000000000	10.00000000	10.00000000	10.00000000
10.49814172	9.205298706	10.45565385	15.41233429	13.45817456	15.64614335
-262.8749837	91.13307980	97.57903360	17.10376398	14.83205510	21.33261120
3.000000000	3.000000000	3.000000000	20.00000000	20.00000000	20.00000000
12.39243523	10.88323365	12.34511523	15.49572925	13.52683445	16.09003628
77.47119230	72.03590910	78.18395500	11.43382040	9.186341600	16.88152970
4.000000000	4.000000000	4.000000000	30.00000000	30.00000000	30.00000000
13.41272264	11.76876536	13.36592433	15.52510709	13.55065151	16.55775257
64.07509848	59.20992870	65.04994550	8.583654736	6.108470500	14.18775600
5.000000000	5.000000000	5.000000000	40.00000000	40.00000000	40.00000000

MAG (dB)
 ϕ degrees
 ω rad/sec

TABLE 11. IMPULSE RESPONSES

k	6th ORDER MODEL	COMPUTER CODE
	6.000000000	6.000000000
1	3.840000000	3.840000000
2	2.940000000	2.940000000
3	2.103360000	2.103360000
4	1.413485760	1.413485760
5	0.842594150	0.842594150
6	0.374368440	0.374368444
7	-0.005989020	-0.005989006
8	-0.311312900	-0.311312875
9	-0.552761020	-0.552760985
10	-0.740018250	-0.740018208
11	-0.881479430	-0.881479389
12	-0.984410188	-0.984410140
13	-1.055088400	-1.055088363
14	-1.098928750	-1.098928718
15	-1.120592090	-1.120592066
16	-1.124081650	-1.124081640
17	-1.112827510	-1.112827520
18	-1.089760760	-1.089760787
19	-1.057378550	-1.057378593
20	-1.017801150	-1.017801208
21	-0.972821940	-0.972822016
22	-0.923951200	-0.923951295
23	-0.872454410	-0.872454524
24	-0.819385750	-0.819385882
25	-0.765617360	-0.765617512
26	-0.711864890	-0.711865060
27	-0.658709770	-0.658709954
28	-0.606618610	-0.606618808
29	-0.555960090	-0.555968303

$t = k \Delta t, \Delta t = 0.04 \text{ sec}$

$$G = \frac{1.61s^4(s + 1.56923)}{[s^2 + .07s + .0025](s + 1.57)(s^3 + 1.56923s^2 + s + .266)} \quad (346)$$

or

$$= \frac{\overbrace{1.61s}^{R_{23}} + \overbrace{2.5264603s^4}^{R_{22}}}{R_{30}s^6 + R_{29}s^5 + R_{28}s^4 + R_{27}s^3 + R_{26}s^2 + R_{25}s + R_{24}} \quad (347)$$

where the R_{ij} 's are listed in Figure 63. We may nest Equation 347 as follows:

$$\left[1 + \frac{R_{29}}{s} + \frac{R_{28}}{s^2} + \frac{R_{27}}{s^3} + \frac{R_{26}}{s^4} + \frac{R_{25}}{s^5} + \frac{R_{24}}{s^6} \right] \ddot{Y}_{m2} = \left(\frac{R_{23}}{s} + \frac{R_{22}}{s^2} \right) P_A \quad (348)$$

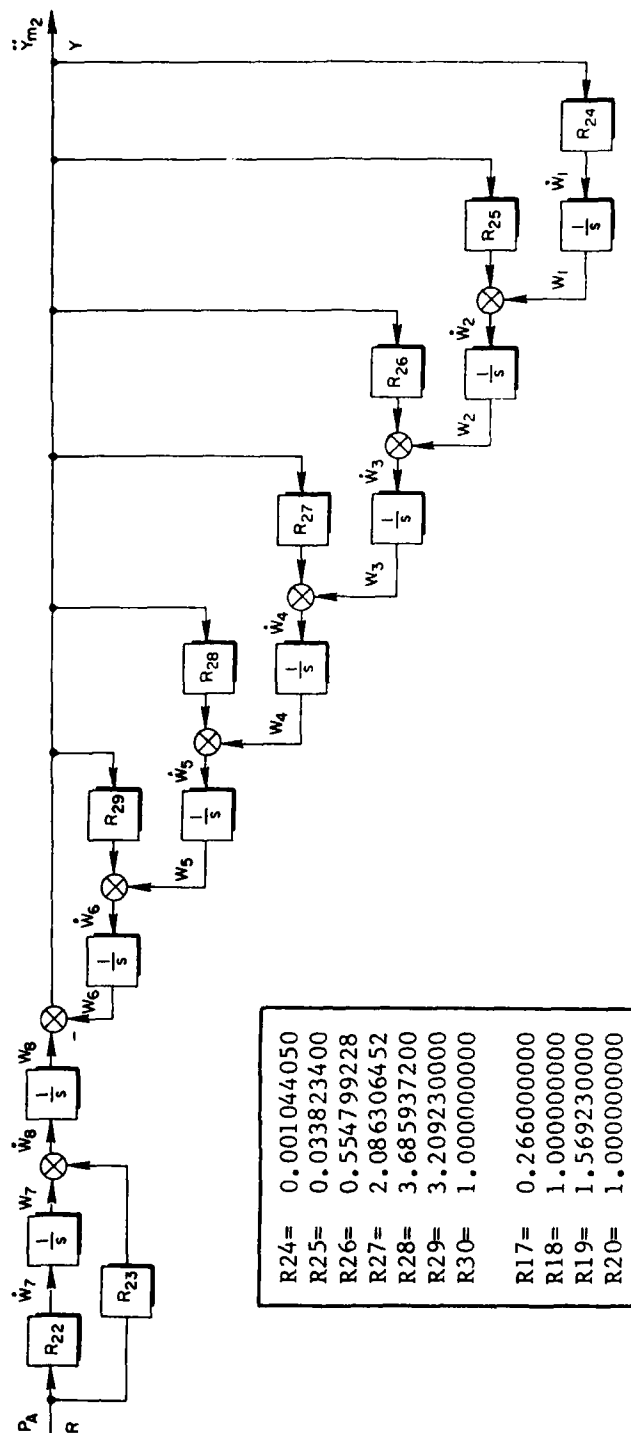
$$\ddot{Y}_{m2} = \left(\frac{R_{23}}{s} + \frac{R_{22}}{s^2} \right) P_A \quad (349)$$

$$- \frac{1}{s} \left[R_{29} + \frac{1}{s} R_{28} + \frac{1}{s} R_{27} + \frac{1}{s} R_{26} + \frac{1}{s} R_{25} + \frac{R_{24}}{s} \dots \right] \ddot{Y}_{m2}$$

The analog block diagram is shown in Figure 63.

We may dispense with the digital block diagram and write the appropriate equations directly from Figure 63.

$$\begin{aligned} 1) \quad Y &= W_8 - W_6 & 2) \quad \dot{W}_1 &= R_{24}Y & 3) \quad W_1 &= T/2 \frac{(3z - 1)}{z - 1} \dot{W}_1 \\ & & \dot{W}_2 &= R_{25}Y + W_1 & & i = 1, \dots, 8 \\ & & \dot{W}_3 &= R_{26}Y + W_2 & & \\ & & \dot{W}_4 &= R_{27}Y + W_3 & \text{or} & (350) \\ & & \dot{W}_5 &= R_{28}Y + W_4 & W_{1k} &= W_{1k-1} \\ & & \dot{W}_5 &= R_{28}Y + W_4 & & + 3T/2 \dot{W}_{1k} \\ & & \dot{W}_6 &= R_{29}Y + W_5 & & - T/2 \dot{W}_{1k-1} \\ & & \dot{W}_7 &= R_{22}R & & i=1, 2, \dots, 8 \\ & & \dot{W}_8 &= R_{23}R + W_7 & & \end{aligned}$$



R24=	0.001044050
R25=	0.033823400
R26=	0.554799228
R27=	2.086306452
R28=	3.685937200
R29=	3.209230000
R30=	1.000000000
R17=	0.266000000
R18=	1.000000000
R19=	1.569230000
R20=	1.000000000

Figure 63. A More Complex "Sway/Roll" Example

$G(z)$, for the no-delay case is readily computed and has the form

$$\frac{Y}{R} = \frac{R_{119}z^6 + R_{118}z^5 + R_{117}z^4 + R_{116}z^3 + R_{115}z^2 + R_{114}z + R_{113}}{R_{126}z^6 + R_{125}z^5 + R_{124}z^4 + R_{123}z^3 + R_{122}z^2 + R_{121}z + R_{120}} \quad (351)$$

and for the delay case

$$\frac{Y}{R} = \frac{R_{112}z^{12} + R_{111}z^{11} + R_{110}z^{10} + \dots + R_{100}}{R_{22}z^{12} + R_{21}z^{11} + R_{20}z^{10} + \dots + R_{10}} \quad (352)$$

The data are tabulated in Table 12 (again, $T = 0.04$ seconds).

Again, we found that the impulse responses of the twelfth-order analytical model agree exactly with the impulse response obtained directly from the computer code (not shown).

Some representative Bode plot data are given in Table 13.

Using the parameter values given us, we see that the filtering introduced by the order of call has actually improved the fidelity of the frequency response.

E. SUMMARY AND CONCLUSIONS

The encoding of an algorithm, where a definite sequence of call is given, can introduce filtering of which the designer of the algorithm is unaware. For the washout case study, we see that the filtering action was "benevolent" in that it actually improved the fidelity of the frequency response. The effect of updating the integrator states as the last event in a given frame time leads to an analytical model of the computer code which is twice the order of algorithm being encoded.

TABLE 12. COEFFICIENTS FOR 6th ORDER WASHOUT

DELAY CASE PARAMETERS		NO DELAY CASE PARAMETERS	
NUMERATOR	DENOMINATOR	NUMERATOR	DENOMINATOR
R100= 0.000000000	R10= 6.681920000-14	R113= 0.027531382	R120= 0.883439038
R101= 0.000000000	R11= 1.070321344-10	R114= -0.221926594	R121= -5.412024152
R102= 0.000000000	R12= 0.000000007	R115= 0.700013312	R122= 13.81359199
R103= 0.000000000	R13= 0.000015459	R116= -1.131414950	R123= -18.80302025
R104= 0.001010584	R14= 0.001281063	R117= 1.000460185	R124= 14.39616595
R105= 0.022094159	R15= 0.050372041	R118= -0.462284093	R125= -5.878152572
R106= -0.218187219	R16= 0.541785006	R119= 0.087620757	R126= 1.000000000
R107= 0.728195607	R17= -4.504607365		
R108= -1.208163855	R18= 12.54729624		
R109= 1.084555467	R19= -17.81501210		
R110= -0.506104743	R20= 13.98631577		
R111= 0.096600000	R21= -5.807446200		
R112= 0.000000000	R22= 1.000000000		

TABLE 13. FREQUENCY RESPONSE DATA, 6th ORDER WASHOUT

MAG
4
freq.

CONT	DISCRETE, NO DELAY	DISCRETE DELAY
1.833472489	-2.614690348	1.948711343
4.026912923	36.32463432	14.36929036
1.000000000	1.000000000	1.000000000
-2.405029014	-3.026181390	-2.412522944
-42.92847068	-38.25338109	-42.44121200
2.000000000	2.000000000	2.000000000
-5.633216300	-6.144060048	-5.576132340
-58.65023633	-52.10560145	301.5580652
3.000000000	3.000000000	3.000000000
-8.031772688	-8.504798812	-7.938527142
-66.49678734	-57.69456014	293.7055865
4.000000000	4.000000000	4.000000000
-9.924000906	-10.34754451	-9.778310534
-71.20086176	-60.12882875	289.0036661
5.000000000	5.000000000	5.000000000
-11.48275868	-11.84540095	-11.27354613
-74.33561069	298.9727785	-74.15427992
6.000000000	6.000000000	6.000000000
-12.80673528	-13.09802451	-12.52335630
-76.57418687	298.9268998	-76.44184967
7.000000000	7.000000000	7.000000000
-13.95687896	-14.16724547	-13.58926581
-78.25287151	299.4021514	-78.20508987
8.000000000	8.000000000	8.000000000
-14.97328861	-15.09375872	-14.51203844
-79.55838679	300.2095026	-79.63326613
9.000000000	9.000000000	9.000000000
15.88369136	-15.90583247	-15.31989859
-80.60272779	301.2347408	-80.84148715
10.00000000	10.00000000	10.00000000

APPENDIX A

EXAMPLES DEMONSTRATING THE SETUP OF THE GENERALIZED SKIP-SAMPLING THEOREM

This appendix contains several exercises on the setup procedure for the generalized skip-sampling theorem. The situation is reviewed in Fig. A-1 and Eqs. A-1 and A-2.

$$C^{T/M} = [G R^{T/N}]^{T/M} \equiv [G^{T/NK} R^{T/N}]^{T/M} \quad (A-1)$$

In Eq. A-1, M and N are rational numbers and K is an integer. If $z = e^{sT/NK}$, then NK/M must be an integer. Equation A-1 can be evaluated using Eq. A-2:

$$C^{T/M} = \frac{1}{2\pi j} \int_{\Gamma} G(p) R(p^K) \frac{z}{z - p^{NK/M}} \frac{dp}{p}, \quad p = e^{sT/NK} \quad (A-2)$$

$$= \sum \text{residues of } \frac{G(p) R(p^K)}{p}$$

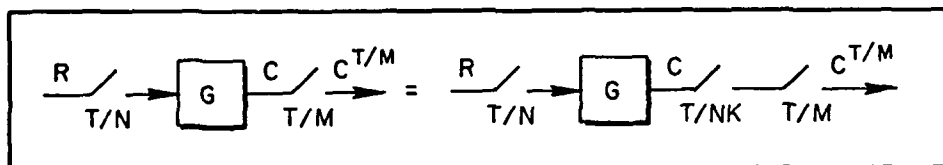
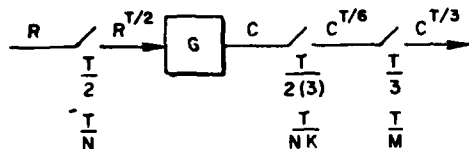


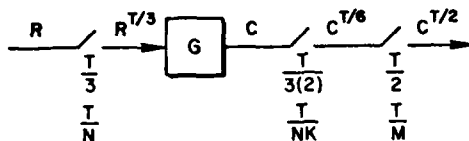
Figure A-1. A Phantom Sample Formulation of a
T/N, T/M Sampling Format

Ex. A-1



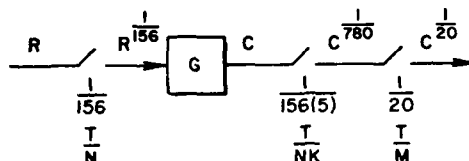
$$C^{T/3} = \frac{1}{2\pi j} \int_{\Gamma} \frac{G(p) R(p^3) Z}{Z - p^2} \frac{dp}{p}$$

Ex. A-2



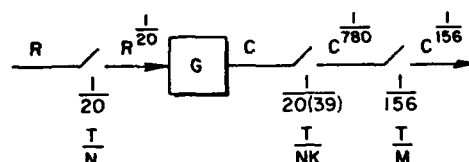
$$C^{T/2} = \frac{1}{2\pi j} \int_{\Gamma} \frac{G(p) R(p^2) Z}{Z - p^3} \frac{dp}{p}$$

Ex. A-3



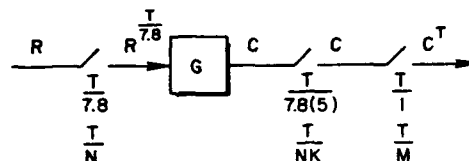
$$C^{1/20} = \frac{1}{2\pi j} \int_{\Gamma} \frac{G(p) R(p^5) Z}{Z - p^{39}} \frac{dp}{p}$$

Ex. A-4



$$C^{1/156} = \frac{1}{2\pi j} \int_{\Gamma} \frac{G(p) R(p^{39}) Z}{Z - p^5} \frac{dp}{p}$$

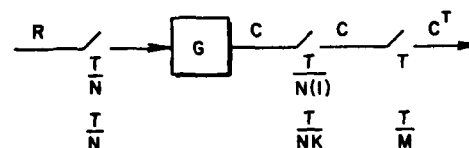
Ex. A-5



$$C^T = \frac{1}{2\pi j} \int_{\Gamma} \frac{G(p) R(p^5) Z}{Z - p^{39}} \frac{dp}{p}$$

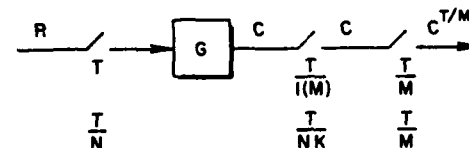
LIMITING FORMS

Ex. A-6



$$C^T = \frac{1}{2\pi j} \int_{\Gamma} \frac{G(p) R(p) Z}{Z - p^N} \frac{dp}{p}$$

Ex. A-7



$$C^{T/M} = \frac{1}{2\pi j} \int_{\Gamma} \frac{G(p) R(p^M) Z}{Z - p} \frac{dp}{p}$$

$$\hat{=} G^{T/M} R^T = G(z) R(z^M) Z = e^{sT/M}$$

APPENDIX B **SKIP-SAMPLING THEOREM**

When dealing with functions such as

$$[GR^{T/N}]^{T/M} \equiv [G^{T/MN}R^{T/N}]^{T/M} \quad (B-1)$$

there is the option of which poles to circle. That is, in

$$[GR^{T/N}]^{T/M} \equiv \frac{1}{2\pi j} \int_{\Gamma} G(p)R(p^N) \frac{z}{z - p^N} \frac{dp}{p} \quad (B-2)$$

the poles of $G(p)R(p^N)/p$ or the poles of $z/(z - p^N)$ may be enclosed. For the special case of $[R^{T/N}]^T$, the result of closing the contour around $z/(z - p^N)$ is known as Sklansky's identity (Ref. 6). The result, for arbitrary N , is

$$[R^{T/N}]^T = \frac{1}{N} \sum_{k=0}^{N-1} R(a_k z_N)$$

where

$$z_N = e^{sT/N}, \quad a_k = e^{j2\pi k/N} \quad (B-3)$$

$$k = 0, 1, \dots, N-1$$

Of particular interest is the case of $N = 2$, since only real numbers are involved:

$$a_k = \begin{cases} 1 & k=0 \\ e^{j\pi} & k=1 \end{cases} \Rightarrow a_k = \begin{cases} 1 & k=0 \\ -1 & k=1 \end{cases}, \quad z = e^{sT/2}$$

$$[R^{T/2}]^T = \frac{1}{2} [R(z) + R(-z)] \quad (B-4)$$

Therefore, collect terms and let $z^2 \rightarrow z$, since Eq. B-4 is by definition an even function of z .

For $N = 3$, the algebra is less attractive:

$$a_k = \begin{cases} 1 & k = 0 \\ e^{j2\pi/3} & k = 1 \\ e^{j4\pi/3} & k = 2 \end{cases}$$

$$[R^T/3]^T = \frac{1}{3} [R(z) + R(e^{j2\pi/3}z) + R(e^{-j2\pi/3}z)] \quad (B-5)$$

Thus, one may collect terms and let $z^3 \rightarrow z$. However, in general, it is laborious to solve Eq. B-3 literally in terms of T , although as a computer computation (for given R and T) it is straightforward.

The derivation of Eq. B-3 will not be given, but the general technique involved will be demonstrated for the easily followed case of $N = 2$. Consider

$$c^T = [R^T/2]^T = \frac{1}{2\pi j} \int_{\Gamma} P(p) \frac{z}{z - p^2} \frac{dp}{p} \quad (B-6)$$

Let $z \rightarrow z_1^2$ and enclose the poles of $z_1^2 - p^2$. That is, enclose the poles which are exterior to the unit circle, keeping in mind that this forces a "reverse" in direction of the contour of Γ , hence a change of sign. However, the change of sign will be cancelled by the minus sign necessary to place $z - p^2$ in the proper form for residue evaluations (e.g., $p^2 - z = 0$).

$$\begin{aligned} R^T &= \frac{-1}{2\pi j} \int_{\Gamma} \frac{R(p)}{p} \frac{z_1^2}{(p - z_1)(p + z_1)} dp = -\text{res}|_{p=z_1} - \text{res}|_{p=-z_1} \\ &= \frac{R(z_1)}{z_1} \cdot \frac{z_1^2}{2z_1} + \frac{R(-z_1)z_1^2}{-z_1(-2z_1)} \\ &= \frac{1}{2} [R(z_1) + R(-z_1)] \end{aligned} \quad (B-7)$$

The usefulness of Sklansky's identity for frame time ratios which are powers of 2 is clear. For example, if

$$c^T = [R^{T/16}]^T = \left[\left[\left[[R^{T/16}]^{T/8} \right]^{T/4} \right]^{T/2} \right]^T \quad (B-8)$$

This problem can be solved, using only real numbers, by applying Sklansky's identity four times ($2^4 = 16$).

APPENDIX C

A DIMENSIONALITY PROBLEM

The use of the high-to-low rate transfer often introduces a dimensionality problem. For example, if

$$C^{T/3} = \left[M_2^{T/6} G^{T/2} \right]^{T/3} = \left[\frac{z^2 + z + 1}{z^2} G(z^3) \right]_{z=e^{sT/6}}^{T/3} \quad (C-1)$$

and $G(z)$ is, for example, a seventh-order transfer function, $G(z^3)$ is 21st-order and therefore

$$[\cdot] = \frac{z^2 + z + 1}{z^2} G(z^3)$$

is 23rd. This dimensionality is of little concern if one chooses to implement the algorithm of Section IV; however, the occurrence of shifting between time frames ratioed by powers of 2 is common enough to make a technique for using Sklansky's identity, in a more efficient manner, attractive.

Suppose we replace z^3 by x in $G(z^3)$ and find the high-to-low rate transform, with a ratio of 2. That is,

$$[G(x)]^{T/2} = W(x)$$

Using Sklansky's identity, we may write:

$$C^{T/3} = \frac{1}{2} \left[\frac{z^2 + z + 1}{z^2} G(z^3) + \frac{z^2 - z + 1}{z^2} G(-z^3) \right] \quad (C-2)$$

$$= \frac{z^2 + 1}{z^2} \left[\frac{G(z^3) + G(-z^3)}{2} \right] + \frac{1}{z} \left[\frac{G(z^3) - G(-z^3)}{2} \right] \quad (C-3)$$

$$= \frac{z^2 + 1}{z^2} W(z^6) + \frac{1}{z} \left[\frac{G(z^3) - G(-z^3)}{2} \right] \quad (C-4)$$

The reader may find it puzzling that a z^6 argument is placed on W . To see this, recognize that the use of Sklansky's identity,

$$\left[G^{T/2}(z) \right]^T = W(z^2) \Big|_{z=e^{sT/2}} = W(z) \Big|_{z=e^{sT}} \quad (C-5)$$

generates a function of z^2 . That is, when one evaluates equations like Eq. C-5, we are dealing with a function of z^2 ($z = e^{sT/2}$) and it is convenient to switch directly over to a function of z wherein $z = e^{sT}$. However, in Eq. C-5, recognize that the algorithm automatically makes the substitution for us. That is, it does not yield $W(x^2)$ in the $T/2$ time frame; rather it gives $W(x)$ in a T time frame. Since $(z^2 + 1)/z^2$ is still in a $T/6$ time frame, one must insure that the arguments are compatible. Clearly, $W(x^2)$ is the desired format. Since $x = z^3$, we have $W(z^6)$.

Next, suppose

$$\frac{G(z^3) - G(-z^3)}{2} = H(z^3) \quad (C-6)$$

and apply the definitions to find out what H is, in terms of G and W.
Since

$$\frac{G - \bar{G}}{2} = H$$

$$\frac{G + \bar{G}}{2} = W$$

the sum gives

$$H + W = G \quad (C-7)$$

Using Eq. C-7, rewrite Eq. C-4 as

$$\left[\frac{z^2 + z + 1}{z^2} G(z^3) \right]^{T/3} = \left(\frac{z^2 - z + 1}{z^2} \right) W(z^6) + \frac{1}{z} G(z^3) \quad (C-8)$$

where

$$[G_{(x)}^{T/2}]^T = W$$

The use of Eq. C-8 is clear -- we may now use any convenient computer multiply option and add option to generate the 23rd-order $C^{T/3}$ with a minimum of dimensionality.

Alternatively, for frequency response purposes, we can evaluate $C^{T/3}$, for $z = l_4 bT/6$, rather easily:

$$\begin{aligned} C^{T/3} \Big|_{z=l_4 bT/6} &= \frac{z^2 - z + 1}{z} \Big|_{z=l_4 bT/6} W(z) \Big|_{z=l_4 bT} \\ &+ \frac{1}{z} \Big|_{z=l_4 bT/6} G(z) \Big|_{z=l_4 bT/2} \end{aligned} \quad (C-9)$$

APPENDIX D

s- AND z-DOMAIN A-10 TRANSFER FUNCTIONS

The s- and z-plane A-10 transfer functions used in the A-10 case study are tabulated in Table 14. The appropriate time frame used in the discretization of each transfer function is listed in the left-most column of the table.

TABLE 14. s- and z-PLANE A-10 TRANSFER FUNCTIONS

T	G	G(s)	G(z)
0.0625	G ₁	$\frac{50.6}{s^2 + 66s + 3025}$	$\frac{0.00129131z^2}{z^2 - 1.576113308z + 0.653311216}$
0.0625	G ₂	$\frac{25}{s + 25}$	$\frac{0.135135135}{z - 0.864864865}$
0.05	G ₃	$\frac{-s(4.78s + 4.1)}{s^2 + 2.1s + 3.51}$	$\frac{-(z - 1)(4.475769343z + 4.291710624)}{z^2 - 1.8899688z + 0.897847411}$
0.05	G _{4,5}	$\frac{1}{s}$	$\frac{0.05z}{z - 1}$
0.05	G ₇	$\frac{.55(s + 10)(s + 20)}{(s + 2)(s + 5)(s + 40)}$	$\frac{0.02z[z - 0.666666][z - 0.5]}{(z - 0.9090909)(z - 0.8)(z - 1/3)}$
0.05	G ₈	$\frac{50}{s^2 + 35s + 2500}$	$\frac{0.013888889z^2}{z^2 - 0.416666666z + 0.111111111}$
0.05	G ₁₀	$\frac{0.01745(0.56s^2 + 0.04s - 55)}{s^2 + 2.1s + 3.51}$	$\frac{0.01745[(z^2/3) - 1.007304795z + 0.50279455]}{z^2 - 1.8899688z + 0.897847411}$
$T/3 = 1/30$; $G_6 = e^{-.07s}$ or $M_3 e^{-.07s}$; $M_3 = (1 - e^{-sT/3})/s$			
$G_9 = .2792$, $G_{11} = 3.0$			

REFERENCES

1. Whitbeck, R. F., and L. G. Hofmann, Analysis of Digital Flight Control Systems with Flying Qualities Applications. Vol. II: Technical Report, AFFDL-TR-78-115, Sept. 1978.
2. Whitbeck, Richard F., and Dennis Didaleusky, Multi-Rate Digital Control Systems with Simulation Applications. Vol. I: Technical Report, AFWAL-TR-80-3101, Sept. 1980.
3. Kranc, G. M., "Input-Output Analysis of Multirate Feedback Systems," IRE Trans. on Automatic Control, Vol. PG AC-3, Nov. 1957, pp. 21-28.
4. Ragazzini, J. R., and G. F. Franklin, Sampled-Data Control Systems, New York, McGraw-Hill, 1958.
5. Harrington, W. W., and L. R. Maki, "LAMARS Motion Fidelity Study in the Heavy, Pitch, and Sway Degrees-of-Freedom Using an F-15 Airframe," AFFDL-TM-79-FGD, Sept. 1979.

LMED
-8